



National Library  
of Canada

Bibliothèque nationale  
du Canada

Canadian Theses Service

Service des thèses canadiennes

Ottawa, Canada  
K1A 0N4

## NOTICE

The quality of this microform is heavily dependent upon the quality of the original thesis submitted for microfilming. Every effort has been made to ensure the highest quality of reproduction possible.

If pages are missing, contact the university which granted the degree.

Some pages may have indistinct print especially if the original pages were typed with a poor typewriter ribbon or if the university sent us an inferior photocopy.

Reproduction in full or in part of this microform is governed by the Canadian Copyright Act, R.S.C. 1970, c. C-30, and subsequent amendments.

## AVIS

La qualité de cette microforme dépend grandement de la qualité de la thèse soumise au microfilmage. Nous avons tout fait pour assurer une qualité supérieure de reproduction.

S'il manque des pages, veuillez communiquer avec l'université qui a conféré le grade.

La qualité d'impression de certaines pages peut laisser à désirer, surtout si les pages originales ont été dactylographiées à l'aide d'un ruban usé ou si l'université nous a fait parvenir une photocopie de qualité inférieure.

La reproduction, même partielle, de cette microforme est soumise à la Loi canadienne sur le droit d'auteur, SRC 1970, c. C-30, et ses amendements subséquents.

THE UNIVERSITY OF ALBERTA

THERMODYNAMIC INVESTIGATIONS. 1. GASES AND VAPORS  
IN LIQUIDS; 2. CALORIMETRIC STUDIES

BY

Yuming Xu

A THESIS

SUBMITTED TO THE FACULTY OF GRADUATE STUDIES AND  
RESEARCH IN PARTIAL FULFILMENT OF THE REQUIREMENTS FOR  
THE DEGREE OF DOCTOR OF PHILOSOPHY

DEPARTMENT OF CHEMISTRY

EDMONTON, ALBERTA

SPRING, 1990



National Library  
of Canada

Bibliothèque nationale  
du Canada

Canadian Theses Service    Service des thèses canadiennes

Ottawa, Canada  
K1A 0N4

## NOTICE

The quality of this microform is heavily dependent upon the quality of the original thesis submitted for microfilming. Every effort has been made to ensure the highest quality of reproduction possible.

If pages are missing, contact the university which granted the degree.

Some pages may have indistinct print especially if the original pages were typed with a poor typewriter ribbon or if the university sent us an inferior photocopy.

Reproduction in full or in part of this microform is governed by the Canadian Copyright Act, R.S.C. 1970, c. C-30, and subsequent amendments.

## AVIS

La qualité de cette microforme dépend grandement de la qualité de la thèse soumise au microfilmage. Nous avons tout fait pour assurer une qualité supérieure de reproduction.

S'il manque des pages, veuillez communiquer avec l'université qui a conféré le grade.

La qualité d'impression de certaines pages peut laisser à désirer, surtout si les pages originales ont été dactylographiées à l'aide d'un ruban usé ou si l'université nous a fait parvenir une photocopie de qualité inférieure.

La reproduction, même partielle, de cette microforme est soumise à la Loi canadienne sur le droit d'auteur, SRC 1970, c. C-30, et ses amendements subséquents.

ISBN 0-315-60235-X

THE UNIVERSITY OF ALBERTA

RELEASE FORM

NAME OF AUTHOR: Yuming Xu

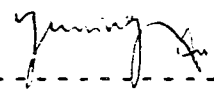
TITLE OF THESIS: THERMODYNAMIC INVESTIGATIONS: (1) GASES  
AND VAPORS IN LIQUIDS; (2) CALORIMETRIC  
STUDIES

DEGREE: Doctor of Philosophy

YEAR THIS DEGREE GRANTED: SPRING, 1990

Permission is hereby granted to THE UNIVERSITY OF ALBERTA  
LIBRARY to reproduce single copies of this thesis and to lend or sell such copies  
for private, scholarly or scientific research purposes only.

The author reserves other publication rights, and neither the thesis nor  
extensive extracts from it may be printed or otherwise reproduced without the  
author's written permission.

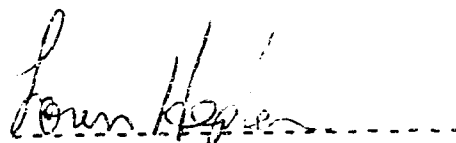
  
-----  
c/o Dr. Loren Hepler  
Dept. of Chemistry  
University of Alberta  
Edmonton Alberta T6G 2G2

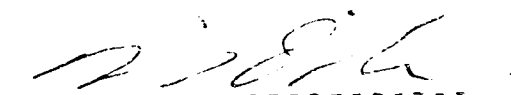
Date: March 26 1990  
-----

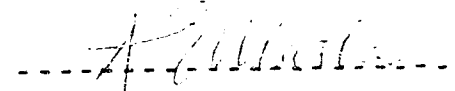


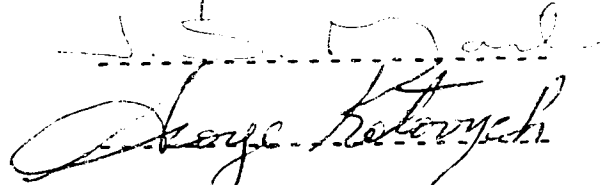
THE UNIVERSITY OF ALBERTA  
FACULTY OF GRADUATE STUDIES AND RESEARCH

The undersigned certify that they have read, and recommend to the Faculty of Graduate Studies and Research for acceptance, a thesis entitled **"Thermodynamic Investigations: 1. Gases and Vapors in Liquids, 2. Calorimetric Studies"** submitted by Yuming Xu in partial fulfilment of the requirements for the degree of DOCTOR OF PHILOSOPHY.

  
(Supervisor)





  
Robert M. Stolzberg  
(External Examiner)

Date: March 12, 1992

**TO LILI and VICKI**

## Abstract

Solubilities (expressed as Henry's law constants) for 13 gases and vapors (carbon dioxide, alkanes from ethane to n-octane, benzene, toluene, m-xylene, dichloromethane, and methanol) in two Alberta bitumens (Athabasca and Wolf Lake) and three acidic gases (carbon dioxide, sulfur dioxide and hydrogen sulfide) in four physical solvents (propylene carbonate, methyl cyanoacetate, N-formyl morpholine and Selexol) have been measured using gas-liquid chromatography over the temperature range from 25 to 150°C. The results of these measurements have been used for thermodynamic calculations of enthalpies of solution ( $\Delta H_s$ ), entropies of solution ( $\Delta S^\circ$ ) and infinite dilution activity coefficients based on Raoult's law. Results obtained for moderately soluble gases and vapors over a temperature range are accurate enough to permit the evaluation of heat capacity changes ( $\Delta C_p^\circ$ ) associated with dissolution.

Partial molar volumes of acidic gases in physical solvents have been measured, using a dilatometer. The results of these measurements in combination with Henry's law constants allow the estimation of the solubilities of gases in liquids at higher pressures.

A Tian-Calvet heat flow calorimeter has been used for thermodynamic investigation of calcium nitrate tetrahydrate,  $\text{Ca}(\text{NO}_3)_2 \cdot 4\text{H}_2\text{O}$ . The calorimeter

was calibrated and tested using synthetic sapphire ( $\alpha\text{-Al}_2\text{O}_3$ ) as a standard material. The accuracy of heat capacity measurement was found to be 1%.

The heat capacities for two phase systems (liquid + vapor) of water and deuterium oxide were measured from 30°C to 275°C and the results were used to calculate the heat capacities of saturated liquid and heat capacities at constant saturation pressures.

Heat capacities of crystalline, molten and supercooled liquid  $\text{Ca}(\text{NO}_3)_2 \cdot 4\text{H}_2\text{O}$  were obtained. Specific heat capacities of very concentrated  $\text{Ca}(\text{NO}_3)_2$  solution were measured over concentration range 3 to 14 mol kg<sup>-1</sup> solvent. The results were then used for calculation of partial molar heat capacities of  $\text{Ca}(\text{NO}_3)_2$  and  $\text{H}_2\text{O}$ . Melting temperature and enthalpy of  $\text{Ca}(\text{NO}_3)_2 \cdot 4\text{H}_2\text{O}$  were also measured and compared with literature data. Finally, the heats of solution of sodium chloride (NaCl) and potassium nitrate ( $\text{KNO}_3$ ) in molten  $\text{Ca}(\text{NO}_3)_2 \cdot 4\text{H}_2\text{O}$  were measured, which gives information on interactions of ions in very concentrated electrolyte solutions.

## **Acknowledgements**

I am in great debt to my supervisor, Dr. Loren G. Hepler, for his encouragement, patience and guidance throughout the course of this work and with whom it has been a great pleasure to work.

I am grateful to Dr. Alan E. Mather of the Department of Chemical Engineering for his helpful discussion, providing his unpublished experimental data and donating some of the samples of physical solvents used in the work described in Chapters 5 and 6.

I acknowledge Dr. Kim L. Kasperski for her helpful discussion about the research in the first part of this work, advice on GLC measurements and reading over and editing the first section of this thesis.

I acknowledge Dr. Andrew W. Hakin for his great help and fruitful discussion on calorimetric measurements. I thank Dr. Jamey K. Hovey for his useful discussion and advice about this work and also Dr. John F. Smith for his help with dilatometric measurements described in Chapter 6. The assistance of R. P. Schutte in making some of the GLC measurements reported in Chapters 4 and 5 is very much appreciated.

Special thanks are given to my wife, Lili Li, for all kinds of support over the last years.

Finally, financial support from the Alberta Oil Sands Technology and Research Authority and Natural Sciences and Engineering Research Council is acknowledged.

## TABLE OF CONTENTS

CHAPTER		PAGE
1.	Introduction.....	1
2.	Equilibrium Constants From Gas-Liquid Chromatography	
	Retention Time Measurements.....	4
	Principle of Measurement.....	4
	Partition Coefficient.....	5
	Specific Retention Volume.....	7
	Determination of Dead Time.....	10
	Relation between Specific Retention Volume and	
	Partition Coefficient.....	14
	Thermodynamic Equilibrium Constant K.....	17
	Criteria for Obtaining a Meaningful Equilibrium	
	Constant from $V_g^\circ$ .....	20
3.	Obtaining Thermodynamic Quantities from Equilibrium Constants ...	25
	Obtaining $\Delta G^\circ$ , $\Delta H^\circ$ , $\Delta S^\circ$ and $\Delta C_p^\circ$ .....	25
	Infinite Dilution Activity Coefficient, $\gamma_2^\infty$ .....	39
	Solubility: Henry's Law Constant $K_H$ .....	44
4.	Solubilities and Thermodynamic Properties of Gases and	
	Vapors in Bitumens.....	46
	Introduction.....	46
	Experimental.....	48

## TABLE OF CONTENTS (continued)

CHAPTER	PAGE
4. continued	
Materials.....	48
Apparatus.....	49
Columns.....	51
Retention Time Measurements.....	52
Results and Calculations.....	64
Specific Retention Volumes.....	64
Henry's Law Constants.....	64
Infinite Dilution Activity Coefficients.....	65
Calculation of $\Delta G^\circ$ , $\Delta H^\circ$ , $\Delta S^\circ$ and $\Delta C_p^\circ$ .....	65
Discussion.....	85
Comparison of Henry's Law Constants.....	85
Comparison of Enthalpies of Solution.....	86
Solubility of Methane in Bitumens.....	89
Variation of Activity Coefficient with Carbon Number of Solute Alkanes.....	93
5. Solubilities of Carbon Dioxide, Hydrogen Sulfide and Sulfur Dioxide in Physical Solvents.....	96
Introduction.....	96
Experimental.....	99
Results and Discussion.....	101

## TABLE OF CONTENTS (continued)

CHAPTER	PAGE
6. Partial Molar Volumes of Acidic Gases in Physical Solvents.....	113
Introduction.....	113
Experimental.....	117
Principles of the Dilatometer.....	117
Apparatus.....	118
Measurement Procedure.....	120
Results and Discussion.....	122
7. Calibrating and Testing the C-80 Heat-Flow Calorimeter.....	127
Principles of Heat-Flow Calorimetry.....	127
Apparatus.....	133
Calibration of the Platinum Resistance Probe PT1.....	138
Sensitivity Calibration.....	143
Heat Capacity Measurements.....	151
Testing on Heat Capacities of Synthetic Sapphire ( $\alpha$ -Al <sub>2</sub> O <sub>3</sub> ).....	153
8. Heat Capacities of Saturated Water and Deuterium Oxide.....	162
Introduction.....	162
Heat Capacities of Saturated Two Phase System.....	163
Heat Capacities of Saturated Liquid.....	165
Heat Capacities of Liquid at Constant Saturation Pressures.....	169



## TABLE OF CONTENTS (continued)

CHAPTER	PAGE
9. Calorimetric Investigation on Thermodynamics of	
Calcium Nitrate Tetrahydrate $\text{Ca}(\text{NO}_3)_2 \cdot 4\text{H}_2\text{O}$ .....	171
Introduction.....	171
Heat Capacities.....	172
Composition Dependence of Heat Capacity: Partial Molar	
Heat Capacities of $\text{Ca}(\text{NO}_3)_2 \cdot 4\text{H}_2\text{O}$ in Concentrated	
Aqueous Solution.....	179
Melting Temperature, Enthalpy and Entropy.....	188
Prediction of the Glass Phase Transition Temperature.....	194
10. Heats of Solution of Sodium Chloride and Potassium	
Nitrate in Molten Calcium Nitrate Tetrahydrate.....	200
Introduction.....	200
Experimental.....	201
Reversal Mixing Cell.....	201
Procedure.....	203
Materials.....	204
Results and Discussion.....	207
11. Philosophy and Some Conclusions .....	220
References.....	225

**TABLE OF CONTENTS (continued)**

CHAPTER	PAGE
Appendix A .....	238
Appendix B .....	242

## LIST OF TABLES

TABLE	DESCRIPTION	PAGE
4-1	Temperatures of the GC oven.....	50
4-2	Liquid loadings in Athabasca and Wolf Lake bitumen columns.....	63
4-3	Specific retention volumes ( $\text{cm}^3 \text{g}^{-1}$ ) for solutes in Athabasca bitumen.....	67
4-4	Specific retention volumes ( $\text{cm}^3 \text{g}^{-1}$ ) for solutes in Wolf Lake bitumen.....	68
4-5	Henry's Law constants (atm) for solutes in Athabasca bitumen.....	69
4-6	Henry's Law constants (atm) for solutes in Wolf Lake bitumen.....	70
4-7	Equations for vapor pressure calculations.....	71
4-8	Infinite dilution activity coefficients for solutes in Athabasca bitumen.....	73
4-9	Infinite dilution activity coefficients for solutes in Wolf Lake bitumen.....	74
4-10	Average enthalpies $\Delta H^\circ$ ( $\text{kJ mol}^{-1}$ ) of solution of gases and vapors in bitumens.....	75
4-11	$\Delta H_\theta^\circ$ , $\Delta G_\theta^\circ$ , $\Delta S_\theta^\circ$ and $\Delta C_p^\circ$ for dissolving gases/ vapors in bitumens.....	76

## LIST OF TABLES (continued)

TABLE	DESCRIPTION	PAGE
4-12	Enthalpies of solution ( $\text{kJ mol}^{-1}$ ) for solutes in selected alkane solvents and in paraffin and bitumen .....	88
5-1	Principal differences between physical and chemical solvents...	98
5-2	Properties of physical solvents.....	102
5-3	Henry's Law constants (atm) for acid gases in four physical solvents.....	103
5-4	Average enthalpies and entropies of solution for acid gases in four physical solvents.....	104
5-5	Comparison of Henry's Law constants for $\text{CO}_2$ , $\text{H}_2\text{S}$ and $\text{SO}_2$ in propylene carbonate and $\text{CO}_2$ in N-formyl morpholine (NFM)..	107
6-1	Partial molar volumes ( $\text{cm}^3 \text{mol}^{-1}$ ) of acidic gases in physical solvents at $25^\circ\text{C}$ .....	125
6-2	Predicted (Krichevsky-Kasarnovsky equation) solubilities ( $X_2$ , mole fraction) of $\text{CO}_2$ at higher pressures at $25^\circ\text{C}$ .....	126
7-1	Calorimetric block temperature calibration (PT1).....	140
7-2	Constants for Equation (7-13).....	141
7-3	Sensitivities of C-80 calorimeter.....	148
7-4	Sensitivity calibration equation constants.....	149
7-5	Heat capacities of synthetic sapphire ( $\alpha\text{-Al}_2\text{O}_3$ ).....	155

### LIST OF TABLES (continued)

TABLE	DESCRIPTION	PAGE
8-1	Saturation two phase heat capacities of $\text{H}_2\text{O}$ and $\text{D}_2\text{O}$ .....	166
8-2	Saturated liquid heat capacities and heat capacities of liquid at constant saturation pressures ( $\text{J K}^{-1} \text{ mol}^{-1}$ ) for water and deuterium oxide.....	170
9-1	Heat capacities of crystalline and liquid $\text{Ca}(\text{NO}_3)_2 \cdot 4\text{H}_2\text{O}$ .....	176
9-2	Specific heat capacities of $\text{Ca}(\text{NO}_3)_2$ solution at different concentrations ( $\text{mol kg}^{-1}$ ) and temperatures.....	181
9-3	Heat capacities for solutions with a constant amount of solvent (1000 grams $\text{H}_2\text{O}$ ) and m moles $\text{Ca}(\text{NO}_3)_2$ .....	183
9-4	Experimental determination of $t_m$ , $\Delta H_m$ and $\Delta S_m$ .....	192
10-1	Heats of solution of $\text{NaCl}$ in water at $40^\circ\text{C}$ .....	210
10-2	Heats of solution of $\text{NaCl}$ in $\text{Ca}(\text{NO}_3)_2 \cdot 4\text{H}_2\text{O}$ .....	211
10-3	Heats of solution of $\text{KNO}_3$ in $\text{Ca}(\text{NO}_3)_2 \cdot 4\text{H}_2\text{O}$ .....	212
10-4	Equations for calculating $\Delta H_s^\infty$ , $\Delta C_p^\circ$ and $C_{p2}^\circ$ of $\text{NaCl}$ and $\text{KNO}_3$ in $\text{Ca}(\text{NO}_3)_2 \cdot 4\text{H}_2\text{O}$ .....	219

## LIST OF FIGURES

FIGURE	DESCRIPTION	PAGE
3-1	Illustration of Raoult's law and Henry's law .....	40
4-1	A graph of plate height against linear velocity of carrier gas for the determination of optimum flow rate.....	55
4-2A	Graphs of specific retention volume against sample size for pentane and hexane in Athabasca bitumen.....	58
4-2B	Graphs of specific retention volume against sample size for heptane and octane in Athabasca bitumen.....	59
4-3	Graphs of specific retention volume of benzene, toluene and xylene against sample size in Athabasca bitumen.....	60
4-4	Graphs of specific retention volume of dichloromethane in Athabasca bitumen against sample size showing the dependence of retention volume on sample size.....	61
4-5	Graphs of specific retention volume of methanol in Athabasca bitumen against sample sizes showing the strong dependence of retention volume on sample size.....	62
4-6	Graphs of $\ln V_g^\circ$ against $1/T$ for $\text{CO}_2$ and n-alkanes from ethane to octane in Athabasca bitumen. Slopes from linear fitting lead to average enthalpies over the temperature range.....	77
4-7	A graph of $\ln V_g^\circ$ against $1/T$ for benzene, toluene, and xylene in Athabasca bitumen.....	78

## LIST OF FIGURES (continued)

FIGURE	DESCRIPTION	PAGE
4-8	A graph of $\ln V_g^\circ$ against $1/T$ for dichloromethane and methanol in Athabasca bitumen.....	79
4-9	A graph of $\ln V_g^\circ$ against $1/T$ for carbon dioxide and alkanes from ethane to octane in Wolf Lake bitumen.....	80
4-10	A graph of $\ln V_g^\circ$ against $1/T$ for benzene, toluene, xylene in Wolf Lake bitumen.....	81
4-11	A graph of $\ln V_g^\circ$ against $1/T$ for dichloromethane and methanol in Wolf Lake bitumen.....	82
4-12	Residuals from fitting $\ln V_g^\circ$ to linear function of $1/T$ , showing an obvious temperature dependence.....	83
4-13	Residuals from fitting $\ln V_g^\circ$ to Equation (3-34), showing randomly scattered residuals.....	84
4-14	A graph of enthalpies of solution against carbon numbers for alkane solutes (ethane to octane) in Athabasca bitumen.....	91
4-15	A graph of $\ln K_H$ for alkane solutes (ethane to octane) in Athabasca bitumen at 40°C and 60°C against carbon numbers...	92
5-1	Henry's law constants for $\text{CO}_2$ in physical solvents as a function of temperature.....	110

## LIST OF FIGURES (continued)

FIGURE	DESCRIPTION	PAGE
5-2	Henry's law constants for H <sub>2</sub> S in physical solvents as a function of temperature.....	111
5-3	Henry's law constants for SO <sub>2</sub> in physical solvents as a function of temperature.....	112
6-1	Diagram of dilatometer.....	119
7-1	Illustration of the principle of a heat-flux meter.....	129
7-2	Block diagram of C-80 calorimeter.....	134
7-3	A cross-sectional diagram of the C-80 calorimeter.....	135
7-4	A graph showing the calibration calorimetric block temperature...	142
7-5	Joule effect calibration signal for the C-80 calorimeter.....	146
7-6	Sensitivity curve for the C-80 calorimeter.....	150
7-7a	Heat capacities of $\alpha$ -Al <sub>2</sub> O <sub>3</sub> in the temperature range 300 K to 550 K measured with the C-80 calorimeter in comparison with the data of Mraw and Naas.....	157
7-7b	Heat capacities of $\alpha$ -Al <sub>2</sub> O <sub>3</sub> in the temperature range 300 K to 550 K measured with the C-80 calorimeter in comparison with the data of Ginnings and Furukawa .....	158



## LIST OF FIGURES (continued)

FIGURE	DESCRIPTION	PAGE
7-7c	Heat capacities of $\alpha\text{-Al}_2\text{O}_3$ in the temperature range 300 K to 550 K measured with the C-80 calorimeter in comparison with the data of Ditmars.....	159
7-7d	Heat capacities of $\alpha\text{-Al}_2\text{O}_3$ in the temperature range 300 K to 550 K measured with the C-80 calorimeter in comparison with the data of Inaba.....	160
7-8	Deviations of heat capacity data for $\alpha\text{-Al}_2\text{O}_3$ from the fitted results of Equation (7-22).....	161
8-1	Saturation two phase heat capacities for water and deuterium oxide as a function of temperature.....	167
9-1	Heat capacities of crystalline and liquid $\text{Ca}(\text{NO}_3)_2 \cdot 4\text{H}_2\text{O}$ as a function of temperature.....	177
9-2	Heat capacities of crystalline and liquid $\text{ZnCl}_2$ as a function of temperature.....	178
9-3	Heat capacities of concentrated $\text{Ca}(\text{NO}_3)_2 \cdot 4\text{H}_2\text{O}$ solution as a function of molality at 331.6 K.....	186
9-4	Partial molar heat capacities for $\text{Ca}(\text{NO}_3)_2$ and $\text{H}_2\text{O}$ in concentrated aqueous solution at 331.6 K .....	187
9-5	A typical heat flux meter signal for melting of $\text{Ca}(\text{NO}_3)_2 \cdot 4\text{H}_2\text{O}$ .....	190

### LIST OF FIGURES (continued)

FIGURE	DESCRIPTION	PAGE
10-1	Illustration of reversal mixing cell.....	205
10-2	Illustration of two different arrangements for mixing components in reversal mixing cell .....	206
10-3	Heats of solution of NaCl in H <sub>2</sub> O as a function of molality.....	212
10-4	Heats of solution at infinite dilution for NaCl and KNO <sub>3</sub> in molten Ca(NO <sub>3</sub> ) <sub>2</sub> ·4H <sub>2</sub> O as a function of temperature.....	219

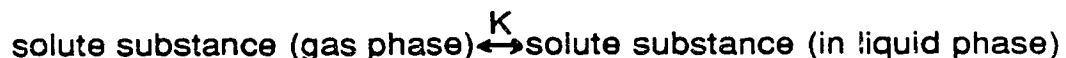
## Chapter 1

### Introduction

This thesis consists of two different kinds of thermodynamic studies: gas liquid chromatographic investigations and calorimetric investigations.

Gas-liquid chromatography (GLC) has been developed as a versatile analytical method. However, it has also become a useful tool for physicochemical studies. In the first part of this work, we employed the gas-liquid chromatographic technique to study the thermodynamics of gases and vapors in liquids.

The equilibrium process for the gas or vapor dissolving in liquid can be described as



in which  $K$  represents the equilibrium constant.

In Chapter 2, a brief summary of the basic principles of the GLC method for thermodynamic investigations is given. A detailed derivation and discussion on the approach to obtain the thermodynamic equilibrium constant  $K$  from GLC retention time measurements (specific retention volumes  $V_g^0$ ) is provided.

Chapter 3 describes how to obtain the thermodynamic quantities such as equilibrium solubility of a gas or vapor in a liquid (Henry's law constant,  $K_H$ ), enthalpy of solution ( $\Delta H_s$ ), entropy of solution ( $\Delta S_s$ ), and activity coefficient from the equilibrium constants or specific retention volumes. A critical review of

methods for calculating  $\Delta H_s$  from  $K$  is also presented in this chapter.

Because of the practical importance of the solubilities and thermodynamic properties of gases and vapors in bitumen, which relates to enhanced oil recovery, we used Athabasca and Wolf lake bitumen as the stationary phase and measured the retention times of 13 gases and vapors in these bitumens at several temperatures. The results are used for further calculations to obtain related thermodynamic quantities. The experimental details along with the measured and calculated results are presented in Chapter 4.

In Chapter 5, we report on the use of GLC to obtain the solubilities and enthalpies of solution for acidic gases (carbon dioxide, hydrogen sulfide and sulfur dioxide) in four physical solvents.

The solubilities obtained from GLC measurements are at low pressures. However, the solubilities at higher pressures are usually more important in industry. The Krichevsky-Kasarnovsky equation can be used to predict solubilities at higher pressures. To make this prediction, the partial molar volume of solute in liquid is required. Therefore, we measured the partial molar volumes of acidic gases in physical solvents, using a dilatometric method. The experimental procedures and results are presented in Chapter 6.

The second part of this thesis involves thermodynamic investigations with the Tian-Calvet heat flow calorimeter. An outline on the basic principles of the heat flow calorimeter and a description of our apparatus are given in Chapter 7. Calibration and testing of the calorimeter with synthetic sapphire ( $\alpha\text{-Al}_2\text{O}_3$ ) are also described in this chapter.

In Chapter 8, the heat capacities of liquid in equilibrium with its saturated vapor system (two phase) are measured for water and deuterium oxide. An equation for calculating heat capacity of saturated liquid from measured heat capacity of two phases is derived and calculated results are presented.

Calcium nitrate tetrahydrate is chosen as a further substance for our calorimetric investigations. Chapter 9 describes thermodynamic studies on heat capacities of both crystalline and molten  $\text{Ca}(\text{NO}_3)_2 \cdot 4\text{H}_2\text{O}$  and partial molar heat capacities for  $\text{Ca}(\text{NO}_3)_2$  and  $\text{H}_2\text{O}$  in concentrated aqueous solution. Properties such as melting temperature, enthalpy and entropy of melting are also investigated in this chapter. In Chapter 10, molten  $\text{Ca}(\text{NO}_3)_2 \cdot 4\text{H}_2\text{O}$  is used as a solvent for studying ion interactions in very concentrated electrolyte solution. Heats of solution of sodium chloride ( $\text{NaCl}$ ) and potassium nitrate ( $\text{KNO}_3$ ) in molten  $\text{Ca}(\text{NO}_3)_2 \cdot 4\text{H}_2\text{O}$  are measured and discussed in Chapter 10.

## **Chapter 2**

### **Equilibrium Constants from Gas-Liquid Chromatography**

#### **Retention Time Measurements**

##### **Principles of Measurement**

Gas-liquid chromatography (GLC) as a probe for studying the physico-chemical properties of gases in liquids is based on the equilibrium distribution of a solute between the gas and liquid phases. In this chapter a brief summary of GLC basic principles is given. For more detailed descriptions several excellent books should be consulted.<sup>1-5</sup>

The heart of a gas-liquid chromatograph is the chromatographic column. The chromatographic system is composed of two phases: gas (mobile) and liquid (stationary). The stationary phase is a liquid or a mixture of liquids that a gas or vapor solute in the gas phase will dissolve in. The stationary phase can be held in the column in any of several ways. For a packed column, the stationary phase is usually coated on an inert solid support. In the elution technique (the commonest technique of gas chromatography) a stream of carrier gas (inert gas, such as nitrogen or helium) passes continually through the column. The sample to be studied (a pure compound or a mixture of compounds in either gas or volatile liquid state) is introduced at the beginning of the column. After a sample is introduced it is swept by the carrier gas onto the column (if the sample is introduced as a liquid, it evaporates to form a vapor first). When it enters the column and reaches the packing, the sample partly

dissolves in the stationary phase and partly remains in the carrier gas stream and an equilibrium is set up. The portion remaining in the stream is carried a little further along the column by the carrier gas and equilibrates again with fresh stationary phase. At the same time, sample already dissolved in the stationary phase re-enters the gas phase so that a new equilibrium with fresh carrier gas is set up. Thus a zone of solute vapor is formed and moves down the column along with the carrier gas.

The speed at which the vapor zone moves depends mainly on two factors, the flow rate of carrier gas and the equilibration rate. The faster the stream of carrier gas moves, the faster the zone moves; and the slower equilibrium is attained, the slower the zone moves. When two or more components are present in the sample, each of them usually behaves independently of the others, so that for a given carrier gas flow rate, the speed of movement of the zone for each component will depend only on the extent to which it is dissolved. Since different substances dissolve to different extents in the same liquid, they therefore form different zones and move at different speeds. If the column is long enough, they can be separated and elute at the end of the column at different times. Therefore, the retention time of a sample provides information about the solubility of the sample in the stationary liquid.

### **Partition Coefficient**

The process carried out in the GLC column is a distribution process. The

distribution equilibrium of a component  $i$  between a stationary phase and a mobile phase can be expressed as

$$i(g) \stackrel{k}{=} i(L) \quad (2-1)$$

in which  $g$  indicates gas phase and  $L$  indicates liquid phase while  $k$  is called the partition or distribution coefficient.

Traditionally,  $k$  is defined as the ratio of concentration of  $i$  in the liquid phase to that in the gas phase,

$$k = C_{i,L} / C_{i,g} \quad (2-2)$$

Units used for  $C_{i,L}$  and  $C_{i,g}$  will be discussed later.

Another commonly used parameter to describe the equilibrium distribution is  $k'$ , called the partition ratio (defined by Littlewood<sup>1</sup>), or capacity factor or mass distribution coefficient.  $k'$  is the ratio of the moles of vapor  $i$  dissolved in the stationary phase to the moles of  $i$  in the gas phase:

$$k' = n_{i,L} / n_{i,g} \quad (2-3)$$

If the vapor does not dissolve at all in the stationary phase ( $k$  or  $k' = 0$ ), its retention time ( $t_R$ ) will be the time taken for the gas or vapor to travel through the gas volume of the column, and is called the unretention or dead time,  $t_m$ . In another case, if a molecule which dissolves in stationary phase spends time  $t_m$  in gas phase, it must spend  $k'$  times  $t_m$  in the stationary phase. The total retention time in both gas phase and liquid phase,  $t_R$ , is given by

$$t_R = t_m (1 + k') \quad (2-4)$$



Rearrangement of Equation (2-4) gives

$$k' = \frac{t_R - t_m}{t_m} \quad (2-5)$$

in which  $t_R$  and  $t_m$  are the retention time of a solute and unretention time (dead time) of the column, respectively, both obtained directly from measurements.

### Specific Retention Volume

The quantities measured in GLC are the retention time (the time required for a small sample of solute to pass through the column at a given flow rate of carrier gas) and the unretention or dead time. The product of the retention time and the flow rate of carrier gas is the volume of carrier gas swept through the column as the solute passes through, called the retention volume  $V_R$ . The same calculation for  $t_m$  gives the unretention or dead volume of the column,  $V_m$ :

$$V_R = t_R F_{out} \quad (2-6)$$

$$V_m = t_m F_{out} \quad (2-7)$$

Here  $F_{out}$  is the flow rate at the column outlet, measured with a soap bubble flow meter. Because this flow rate is measured at room temperature and atmospheric pressure and the gas is saturated with water vapor, while the flow rate in the column is at oven temperature and a higher pressure, it must be corrected to column conditions in order to obtain the desired average flow rate.

#### 1. Temperature Correction

Since the flow rate is measured at room temperature,  $T_{room}$ , according to

Charles's law the flow rate at column temperature,  $T_{col}$ , is obtained by

$$F_{col} = F_{out} \frac{T_{col}}{T_{room}} \quad (2-8)$$

## 2. Water Vapor Pressure Correction

Levy<sup>6</sup> has pointed out that for accurate work a correction must be made for the water vapor pressure. This correction can be made by multiplying the flow rate with a correction term,  $(P_{out} - P_w)/P_{out}$ , in which  $P_w$  is the saturated water vapor pressure at room temperature and  $P_{out}$  is the column outlet pressure (i.e., atmospheric pressure).

## 3. Pressure Gradient Correction

Since the pressure at the inlet of the column is higher than the pressure at the outlet, there exists a pressure gradient along the column. As a consequence of this pressure gradient a velocity gradient is produced, which leads to different volume flow rates along the column. The retention volume obtained from Equation (2-6) is therefore greater than the real retention volume. To correct for this effect, James and Martin<sup>7</sup> proposed a pressure gradient correction factor (compression factor),  $j$ , to calculate an average flow rate in the column from the flow rate measured. The derivation of  $j$  is given in the original paper<sup>7</sup> or several text books.<sup>1-2</sup> Here we only cite the final expression for  $j$ :

$$j = \frac{3}{2} \frac{\left[\left(\frac{P_{in}}{P_{out}}\right)^2 - 1\right]}{\left[\left(\frac{P_{in}}{P_{out}}\right)^3 - 1\right]} \quad (2-9)$$

Considering these corrections, the retention volume and unretention volume are calculated by

$$V_R^o = t_R F_{out} j \frac{T_{col}}{T_{room}} \left(1 - \frac{P_w}{P_{out}}\right) \quad (2-10)$$

and

$$V_m^o = t_m F_{out} j \frac{T_{col}}{T_{room}} \left(1 - \frac{P_w}{P_{out}}\right) \quad (2-11)$$

in which  $V_R^o$  is the "corrected retention volume" and  $V_m^o$  the "corrected void volume". The difference between  $V_m^o$  and  $V_R^o$  is the net retention volume,  $V_N$ . This net retention volume can be used in calculating equilibrium thermodynamic functions.  $V_N$  varies with experimental conditions such as flow rate or the weight of stationary phase and so we can not compare  $V_N$  values from different experiments. However, the specific retention volume  $V_g^o$  as given by Littlewood *et al.*<sup>8</sup> permits inter-comparisons.  $V_g^o$  is defined as the net retention volume of a solute at 0°C per unit weight of stationary phase and is calculated by

$$V_g^o = \frac{V_N}{w_{1,L}} \frac{273.15}{T_{col}} \quad (2-12)$$

in which  $w_{1,L}$  is the weight of stationary phase in the column. More generally, specific retention volume is defined as the volume of carrier gas at 0 °C and mean column pressure that elutes one half the solute from a column which

contains 1 gram of liquid stationary phase and with no pressure gradient. Specific retention volume can be calculated from common experimental parameters (retention time, flow rate, temperature and pressure) by the equation

$$V_g^o = \frac{t_R - t_m}{W_{1,L}} F_j \frac{273}{T_{room}} \left(1 - \frac{P_w}{P_{out}}\right) \quad (2-13)$$

The specific retention volume is characteristic of a particular solute, stationary phase and carrier gas. It makes it possible to compare retention properties of a given solute in columns which contain different amount of the same stationary phase at the given column temperature. The specific retention volume  $V_g^o$  calculated with Equation (2-12) or (2-13) can be used to obtain many thermodynamic properties such as partition coefficients, equilibrium constants, Henry's law constants, infinite dilution activity coefficients and enthalpies of solution. In this chapter, we only derive the equations for the calculations of partition coefficients and thermodynamic equilibrium constants from specific retention volumes.

### **Determination of Dead Time**

Examination of Equation (2-13) shows that specific retention volume is calculated from the net retention time, flow rate and weight of stationary phase, of which the net retention time is an especially important factor. The accuracy of the determination of net retention time depends on the difference between retention time of a solute and the dead time of the column. If the retention time  $t_r$  is much greater than the dead time  $t_m$ , the measurement of the dead time will not

affect the net retention time significantly. However, if the retention time of a gas solute is very close to the dead time of the column, the accurate evaluation of the dead time  $t_m$  becomes critical. A small uncertainty in the dead time measurement produces a significant error in specific retention volume and thermodynamic quantities. Several methods have been proposed to determine the dead time of a column and there have been several publications<sup>19-27</sup> regarding their merits. In this section, we briefly discuss only the methods that have been commonly used.

### **1. Direct measurement of $t_m$ .**

In an ideal GLC system the dead time is considered as the time a small amount of unretained gas (not dissolved in the stationary phase and not adsorbed by the packing) takes to pass through the chromatographic system under identical conditions to that under which samples are tested. James and Martin<sup>7</sup> designated the air peak as the dead time. Since then, air has been widely used as an unretained gas for measuring the dead time. Other inert gases such as nitrogen, neon, argon have also been chosen by some investigators for determining the non-retention time, of which neon has been used the most. Controversy developed with the advent of the flame ionization detector (FID) regarding the best substance to use for dead time measurement, as the FID does not respond to air or other inert gases. Methane has been suggested as a substitute for use with flame ionization detectors. Many authors have supported the use of air and inert gases as an indication of dead time for the thermal conductivity detector (TCD) and methane for the FID.

Riedo *et al.*<sup>28</sup> investigated a series of inert gases and light hydrocarbons over a wide temperature range and found that neon had the smallest retention time. Parcher and Johnson<sup>26</sup> compared dead times obtained from four inert gases with those calculated by a mathematical linearization scheme (which will be discussed later) using C<sub>1</sub>-C<sub>5</sub> hydrocarbons. They confirmed that neon had the lowest retention time.

However, the use of air or methane for  $t_m$  determinations has been questioned. Some authors<sup>21-23</sup> have shown that both air and methane are retained by some stationary phases. Thus, some other procedures have been suggested.

## 2. Mathematical dead time

A mathematical method of dead-time evaluation was developed initially by Peterson and Hirsch<sup>29</sup> and modified by many other authors,<sup>27,30-34</sup> because of the controversy about the direct measurement of  $t_m$ . This method requires the measurement of the retention time of three homologous compounds (usually alkanes). The dead time  $t_m$  is calculated by

$$t_m = \frac{t_{(n)} t_{(n+2)} - t_{(n+1)}^2}{t_{(n)} + t_{(n+2)} - 2 t_{(n+1)}} \quad (2-14)$$

which is derived from the fact that the relationship between the logarithm of the net retention time and the number of carbon atoms for the homologous series is linear, i.e.,  $\log(t_r - t_m) = bn + c$ , in which  $n$  is carbon number and  $b$  and  $c$  are constants. This method has been criticized by many authors. Sharples and

Vernon<sup>25</sup> did some sample calculations showing that small errors in measurement of retention times of the members of the homologous series produce surprisingly large variation in  $t_m$ . Wainwright *et al.*<sup>22</sup> have shown that different choices of the homologous compounds lead to different calculated  $t_m$ .

Similar linearization schemes have been applied to the retention times of a series of inert gases<sup>26,35-37</sup> when the detection system responds to air and inert gases (such as a thermal conductivity detector). In this method, the physical properties or energy parameters such as Lennard-Jones, Buckingham, Kirkwood-Muller, or London are used as the linearization parameters. Nakahara *et al.*<sup>36</sup> have shown that modified Buckingham parameters are the best. The linearization schemes use the equation

$$\ln \{(t_r - t_m) \sqrt{M_i}\} = A + B\psi_i \quad (2-15)$$

in which  $M_i$  is the molecular weight of an inert gas  $i$ , and  $\psi_i$  is the modified Buckingham potential of the gas. Lin and Parcher<sup>37</sup> claimed that the linearization scheme with inert gases is the most accurate method for the determination of column dead time.

Other methods have been proposed but are not commonly used. Smith *et al.*<sup>19</sup> wrote a very extensive, critical review in which they summarized and compared all these methods. Here we quote from their conclusions: "The only method which was shown to lead to accurate results under a wide variety of conditions was the use of neon, or possibly helium, together with the appropriate

treatment of data. In fact, the use of multiple analyses using neon is, in our opinion, the most reliable and accurate method of determining system dead time and is the method of choice when determining absolute data such as Henry's law values or other thermodynamic data." Therefore, they recommended that when retention data are to be used to calculate some properties of the column or stationary phase, such as Henry's law constants, the dead time should be determined experimentally using an inert gas such as neon.

### **Relation between Specific Retention Volume and Partition Coefficient**

As was mentioned before, a common measure of distribution of a solute between gas phase and stationary phase is the partition coefficient. However, the numerical values of a partition coefficient vary with the choice of solute concentration unit in both phases.

The commonly used units for concentration of solute in the gas phase are moles of solute per unit volume of carrier gas or partial pressure of the solute and for solute in the liquid phase the choices are usually either molarities, molalities or mole fractions.

The different choices of concentration units lead to different expressions that connect the partition coefficient or equilibrium constant to specific retention volume  $V_g^\circ$ .

1. If we choose the unit of  $C_{i,L}$  as moles of solute per unit volume of stationary phase, the general expression for the partition coefficient (Equation



2-2) becomes

$$k = \frac{n_{2,L} / V_{1,L}}{n_{2,g} / V_m^o} = \frac{n_{2,L}}{n_{2,g}} \frac{V_m^o}{V_{1,L}} \quad (2-16)$$

in which  $n_{2,L}$  and  $n_{2,g}$  represent numbers of moles of solute in liquid and gas phase, respectively.  $V_{1,L}$  represents the volume of stationary phase, and  $V_m^o$  is the corrected void volume of the column.

Substitution of Equation (2-3) into (2-16) gives

$$k = k' \frac{V_m^o}{V_{1,L}} \quad (2-17)$$

Comparing Equation (2-5) with Equations (2-10) and (2-11) gives

$$k' = \frac{V_R^o - V_m^o}{V_m^o} = \frac{V_N}{V_m^o} \quad (2-18)$$

Further combination of Equation (2-18) with Equation (2-17) yields

$$k = V_N / V_{1,L} \quad (2-19)$$

Substituting Equation (2-12) into (2-19), we obtain

$$k = \frac{V_g^o w_{1,L} T_{col}}{273.15 V_{1,L}} \quad (2-20)$$

Note that the ratio  $w_{1,L} / V_{1,L}$  is the density ( $\rho$ ) of stationary phase at column temperature. Therefore, Equation (2-20) becomes

$$k = \frac{V_g^o \rho T_{col}}{273.15} \quad (2-21)$$

2. When the concentration unit of solute in liquid phase is chosen as moles

of solute per unit weight of liquid phase, the partition coefficient is written as

$$k = \frac{n_{2,L} / w_{1,L}}{n_{2,g} / V_m^0} \quad (2-22)$$

Using a derivation similar to that of Equation (2-21), we obtain

$$k = \frac{V_g^0 T_{col}}{273.15} \quad (2-23)$$

3. When the concentration unit for solute in the liquid phase is chosen as mole fraction,  $X_2$ , and that in the gas phase as partial pressure of the solute,  $P_2$ , then Equation (2-2) becomes

$$k = \frac{C_{2,L}}{C_{2,g}} = \frac{X_2}{P_2} \quad (2-24)$$

The mole fraction of solute,  $X_2$ , can be expressed by

$$X_2 = \frac{n_{2,L}}{n_{1,L} + n_{2,L}} \approx \frac{n_{2,L}}{n_{1,L}} = \frac{n_{2,L} M_{1,L}}{w_{1,L}} \quad (2-25)$$

Because the gas pressure is very low in the GLC column, we use the ideal gas equation for  $P_2$ :

$$P_2 = \frac{n_{2,g} RT_{col}}{V_m^0} \quad (2-26)$$

Combination of Equations (2-25) and (2-26) with Equation (2-24) gives

$$k = \frac{n_{2,L}}{n_{2,g}} \frac{V_m^0 M_{1,L}}{w_{1,L} RT} \quad (2-27)$$

Substitution of Equations (2-3) and (2-18) into Equation (2-27) leads to

$$k = \frac{V_N M_{1,L}}{w_{1,L} RT} \quad (2-28)$$

Combination of Equation (2-12) with Equation (2-28) yields

$$k = \frac{V_g^0 M_{1,L}}{R 273.15} \quad (2-29)$$

Equations (2-21), (2-23) and (2-29) are basic equations which relate the partition coefficient to the specific retention volume. These equations are all correct, but Equations (2-23) and (2-29) are most convenient to use. Equation (2-21) requires the density of the stationary phase at column temperature, which is not always available. Furthermore, when we apply the partition coefficient in thermodynamic calculations, such as that of the enthalpy of solution, the thermal expansion coefficient of the stationary phase,  $d \ln \rho / dT$ , appears in the equations related to Equation (2-21). This thermal expansion coefficient is sometimes difficult to obtain and it also makes the thermodynamic calculations more complicated. These problems can be avoided by using Equations (2-23) and (2-29).

### **Thermodynamic Equilibrium Constant K**

The partition coefficient has been used by many investigators to describe the equilibrium distribution. Some investigators have also used the partition coefficient as an equilibrium constant in calculations of thermodynamic properties. However, from a rigorous thermodynamic point of view, the partition coefficient cannot be used directly in thermodynamic calculations. Thermodynamic properties relate directly only to the thermodynamic equilibrium constant  $K$  that is defined<sup>5</sup> by

$$K = a_{2,L} / a_{2,g} \quad (2-30)$$

in which  $a_{2,L}$  and  $a_{2,g}$  represent activities of solute substance in the stationary phase and gas phase, respectively.

To obtain values of the thermodynamic equilibrium constant  $K$  from experimental data, it is first necessary to choose the standard states<sup>9-11</sup> that define the activities in terms of fugacities,  $f$ , as in

$$a = f / f^\circ \quad (2-31)$$

in which  $f^\circ$  is the fugacity corresponding to the chosen standard state. It is customary and convenient to choose a standard state for the solute based on Henry's law for most investigations of dilute solutions, which means that the activity coefficient for the solute in a sufficiently dilute solution (Henry's law region) is unity. Values of these activity coefficients for the solute in less dilute solutions provide a measure of deviation of real properties from the limiting Henry's law. Alternatively, many investigators who have used GLC have chosen a standard state based on Raoult's law. This common choice, which we regard as awkward for our purposes, provides limiting activity coefficients for the solute in dilute solution ( $\gamma_2^\infty$ ) that may be considerably different from unity.

Our reference state for the substance of interest in the gas phase is the ideal gas, and the standard state is the ideal gas at  $P = 1.0$  atm. The fugacity of solute in gas phase is calculated by  $f_{2,g} = P_2 \phi_2$  in which  $\phi_2$  is the fugacity coefficient. From Equation (2-31) the activity of solute in the gas phase is then calculated by

$$a_{2,g} = \frac{f_{2,g}}{f_2^o} = \frac{P_2 \phi}{1 \text{ atm}} \quad (2-32)$$

A reference state based on Henry's law is chosen for the liquid solution that results from dissolving solute (2) in solvent (1):

$$P_2 = K_H X_2 \quad (2-33)$$

The standard state is now the hypothetical state based on extrapolation of Henry's law to  $X_2 = 1.0$ . Thus we have  $f_2^o = K_H$  and  $f_{2,L} = K_H X_2 \gamma_2$  in which  $\gamma_2$  is the activity coefficient based on Henry's law. Therefore the activity of a solute in the liquid phase,  $a_2$ , can be obtained from

$$a_{2,L} = X_2 \gamma_2 \quad (2-34)$$

Using the reference states, standard states, and activities summarized above, we now obtain

$$K = \frac{a_{2,L}}{a_{2,g}} = \frac{X_2 \gamma_2}{P_2 \phi_2 / 1 \text{ atm}} = \frac{X_2 \gamma_2 (1 \text{ atm})}{P_2 \phi_2} \quad (2-35)$$

Therefore, we have

$$K = \frac{\gamma_2 (1 \text{ atm})}{K_H \phi_2} \quad (2-36)$$

Equation (2-36) is a general equation that can be applied to all gas-liquid equilibrium processes. For our GLC system all gas pressures are quite low and we have  $\phi_2 = 1.0$ . The concentrations of solutes in liquids in our GLC system are very dilute; therefore we have  $\gamma_2 = 1.0$ . Then Equation (2-36) reduces to give

the simple expression.

$$K = 1 \text{ atm} / K_H \quad (2-37)$$

Note that the thermodynamic equilibrium constant defined above is dimensionless (as it should be), with the pressure and Henry's law constant expressed in units consistent with our standard state for the gas phase (atm).

Combination of Equation (2-24) with Equation (2-33) leads us to

$$K_H = \frac{1}{k} = \frac{R 273.15}{V_g^\circ M_{1,L}} \quad (2-38)$$

Therefore, when the gas phase pressure is very low and the concentration of the solute in the liquid phase approaches infinite dilution (this is the case for most GLC systems) the thermodynamic equilibrium constant can be calculated from the partition coefficient  $k$  as follows

$$K = k (1 \text{ atm}) = \frac{V_g^\circ M_{1,L} (1 \text{ atm})}{R 273.15} \quad (2-39)$$

Equation (2-39) is the equation used for calculating the thermodynamic equilibrium constant from GLC retention measurements. It indicates that the equilibrium constant is directly proportional to the specific retention volume. For some further thermodynamic calculations, the equilibrium constant can be replaced by the specific retention volume. This illustrates why the specific retention volume is the most fundamental quantity in GLC measurements.

### **Criteria for Obtaining a Meaningful Equilibrium Constant from $V_g^\circ$**

Equation (2-39) reveals the direct relation between equilibrium constant  $K$

and specific retention volume  $V_g^\circ$ . However, it should be realized that the  $V_g^\circ$  value should be independent of any operational variables of the column other than the temperature. There are several factors that might cause the specific retention volume to differ from the relationship given in Equation (2-39). Martire<sup>12,13</sup> has described many factors, of which non-equilibrium between two phases, non-linear isotherms and liquid and/or solid surface adsorption of solutes are primary factors that should be eliminated in order to obtain a significant and meaningful equilibrium constant. Thus several conditions must be met to permit evaluation of equilibrium constants (and subsequently, further thermodynamic properties) from GLC retention times:

(1) There must be equilibrium between the liquid and gas phases. To achieve equilibrium between the two phases, the flow rate of carrier gas must be suitably slow. According to Parcher *et al.*,<sup>14</sup> the non-equilibrium effects can be minimized by using a flow rate which corresponds to the "optimum flow rate". The method for obtaining the optimum flow rate is described in Chapter 4. In practice, the optimum flow rate is first determined for each system by a series of measurements at different flow rates. All subsequent measurements leading to retention times to be used in thermodynamic calculations are then done at a flow rate slightly slower than this optimum flow rate.

(2) The concentration of the solute in the liquid phase must be small enough that Henry's law is applicable (linear isotherm range), or measurements must be made over an appropriate range of concentrations so that it is possible to extrapolate to infinite dilution.<sup>14</sup> This condition can be met by using very small

sample sizes so that  $K$  is a constant. But in practice the question is how small a sample size is necessary. This can be determined by testing that  $V_g^\circ$  is independent of sample size. If  $V_g^\circ$  is independent of sample size then these sample sizes are considered to be in the linear isotherm region. In other cases, if  $V_g^\circ$  varies with small sample sizes, a series of measurements at different sample sizes should be made so that extrapolated specific retention volumes (or retention times) to zero sample size can be made. This extrapolated specific retention volume (at zero sample size, or infinite dilution) is then used in thermodynamic calculations such as in Equation (2-39).

(3) Adsorption of gas/vapor solute on the surfaces of the liquid and/or the solid support must be negligible in comparison with the amount of gas / vapor dissolved in the liquid. If the adsorption is detectable, an appropriate correction must be made.<sup>15-18</sup> The adsorption phenomena can be detected from elution peak shape and the variation of  $V_g^\circ$  with stationary phase loading (the ratio of stationary phase to solid support). To minimize the adsorption of solute onto the solid support surfaces, the solid support material should be pre-treated.<sup>1,4-5</sup> Common pre-treatments include alkali-washing, acid-washing, and silanization.

The surfaces of solid supports such as firebrick and chromosorb contain adsorption sites which consist of Si-OH, Al-OH and Fe-OH groups. The Si-OH groups can either react with basic molecules (based on acid-base reaction) or form hydrogen bonds with polar compounds that contain electron donor groups, while Al-OH and Fe-OH groups are acidic sites which can also form hydrogen



bonds. These active sites can react with both stationary phase and sample molecules. The acid and alkali washes are used to remove these active sites and so reduce the adsorption of sample onto the support. Silanization of the solid support ensures further removal or blocking of the active hydroxyl groups. The solid support is silanized by treating it with dimethylchlorosilane (DMCS). The active hydroxyl groups are replaced by siloxane and silyl ether groups which have a much smaller adsorption capacity. These pre-treatments can reduce the number or activity of the adsorption sites but can not remove all active sites completely. Thus for a system containing a non-polar stationary phase and polar solute compounds, adsorption of solute onto solid surfaces can still be observed if liquid loading is not high enough.

The adsorption of solute molecules onto liquid surface was first observed by Martin<sup>15</sup> in 1961 and then confirmed by Pecsok *et al.*<sup>17</sup> and Martire<sup>16</sup> as well as Meyer and Fllefson.<sup>18</sup> Martin observed that the elution order of solutes from gas-chromatographic columns containing a polar stationary phase changed with the liquid loading and with the surface area of exposed liquid. He attributed these changes to adsorption of solutes at the gas-liquid interface and developed a new retention equation

$$V_{Rg}^o = K_s V_L + K_a A_L \quad (2-40)$$

to account for this adsorption effect. In Equation (2-40)  $V_{Rg}^o$  represents the corrected net retention volume per gram of packing,  $K_s$  is the gas-liquid partition coefficient as previously defined,  $V_L$  is the volume of liquid phase per gram of

packing,  $K_a$  represents the adsorption coefficient (the value of  $K_a$  depends on the extent of the adsorption of solute onto the particular liquid surfaces) and  $A_L$  is the exposed surface area of the liquid per gram of packing.

Equation (2-40) indicates that retention time of a solute depends upon dissolution of the solute into bulk liquid as well as upon adsorption at the liquid surface. It was reported<sup>16</sup> that when the liquid phase is highly polar and the solute is nonpolar, with a high surface area and a low liquid loading, the adsorption on the liquid surface is significant. If the adsorption is not negligible, the specific retention volume,  $V_g^o$ , calculated by Equation (2-13) includes both dissolution and adsorption contributions and therefore calculated thermodynamic quantities that refer to the process of dissolving solute into liquid phase become meaningless. Therefore, the contribution to specific retention volume by adsorption onto the liquid surface must be eliminated in order to obtain meaningful thermodynamic quantities. Using Equation (2-40),  $K_s$  and  $K_a$  can be evaluated from retention times, surface area and volume of liquid phase in the following way. Rearrangement of Equation (2-40) gives

$$\frac{V_{Rg}^o}{A_L} = K_s \frac{V_L}{A_L} + K_a \quad (2-41)$$

A plot of  $V_{Rg}^o/A_L$  against  $V_L/A_L$  gives a straight line with slope  $K_s$  and intercept  $K_a$ . After  $K_s$  is obtained, a new  $V_g^o$ , referring only to the solution process, can be obtained from Equation (2-23) using  $k_s$  in place of  $k$ . Thermodynamic properties are then calculated using this new  $V_g^o$ .

## Chapter 3

### Obtaining Thermodynamic Quantities from Equilibrium Constants

Applications of thermodynamics to a wide variety of physical and/or chemical equilibrium processes involve calculations of equilibrium constants at various temperatures from the thermodynamic quantities  $\Delta H^\circ$ ,  $\Delta S^\circ$  and  $\Delta C_p^\circ$ . Correspondingly, it is also possible to obtain the same thermodynamic properties from knowledge of equilibrium constants at several temperatures. We have discussed the determination of equilibrium constants from GLC retention times in Chapter 2. In this chapter, a detailed derivation of the evaluation of thermodynamic functions from the equilibrium constant will be presented, together with a short review of earlier work.

#### Obtaining $\Delta G^\circ$ , $\Delta H^\circ$ , $\Delta S^\circ$ and $\Delta C_p^\circ$

We begin by considering the standard Gibbs energy (free energy) change for an equilibrium

$$\Delta G^\circ = -RT \ln K \quad (3-1)$$

Combining Equation (3-1) with the fundamental thermodynamic relation

$$\Delta G^\circ = \Delta H^\circ - T\Delta S^\circ \quad (3-2)$$

gives

$$\ln K = -\frac{\Delta H^\circ}{RT} + \frac{\Delta S^\circ}{R} \quad (3-3)$$

We also have thermodynamic equations for the temperature dependence of  $\Delta H^\circ$  and  $\Delta S^\circ$ :

$$d\Delta H^\circ / dT = \Delta C_p^\circ \quad (3-4)$$

$$d\Delta S^\circ / dT = \Delta C_p^\circ / T \quad (3-5)$$

As a first approximation we choose  $\Delta C_p^\circ = 0$  so that both  $\Delta H^\circ$  and  $\Delta S^\circ$  are independent of temperature. In this special case we then see from Equation (3-3) that a graph of  $\ln K$  against  $1/T$  should be a straight line having slope equal to  $-\Delta H^\circ/R$  and intercept equal to  $\Delta S^\circ/R$ .

Another way to deduce this same linear dependence of  $\ln K$  on  $1/T$  is based on the van't Hoff equation:

$$d \ln K / dT = \Delta H^\circ / RT^2 \quad (3-6)$$

Again choosing  $\Delta C_p^\circ = 0$  so that  $\Delta H^\circ$  is independent of temperature, integration of Equation (3-6) leads to

$$\ln K = -\frac{\Delta H^\circ}{RT} + I \quad (3-7)$$

in which  $I$  is a constant of integration. Comparison of Equations (3-7) and (3-3) shows that the integration constant is equal to  $\Delta S^\circ/R$ . Again Equation (3-7) shows a linear relationship between  $\ln K$  and  $1/T$  and the values of  $\Delta H^\circ$  and  $\Delta S^\circ$  can be obtained from the slope and intercept.

The equations above, based on  $\Delta C_p^\circ = 0$ , are adequate for a short temperature range or with equilibrium constants of low accuracy. However, for

many equilibrium systems plots of  $\ln K$  against  $1/T$  show significant curvature that indicates  $\Delta C_p^\circ \neq 0$  for these systems. Calorimetric investigations have verified the dependence of  $\Delta H^\circ$  on temperature ( $\Delta C_p^\circ \neq 0$ ). It is therefore necessary to consider more complicated treatments with non-zero  $\Delta C_p^\circ$  and temperature dependent  $\Delta H^\circ$ .

To obtain thermodynamic functions such as  $\Delta H^\circ$ ,  $\Delta S^\circ$  and  $\Delta C_p^\circ$  from equilibrium constants, it is customary to fit some reasonable and convenient functions to experimental data of  $\ln K$  and temperature and then do the appropriate differentiation. Many methods and equations have been developed for this kind of calculation. One widely used empirical equation developed by Harned and Robinson<sup>38</sup> is in the form of

$$\log K = A + B/T + CT \quad (3-8)$$

It was based on the experimental observation that the electromotive forces of hydrogen, silver-silver chloride cells used in their investigations of ionization of acids could be expressed as a quadratic function of temperature. This led them to suggest that  $\Delta G^\circ$  should also be a quadratic function of temperature, leading to Equation (3-8). Differentiation of this equation leads to a  $\Delta H^\circ$  and  $\Delta C_p^\circ$  that depend on temperature as  $\Delta H^\circ = D + ET^2$  and  $\Delta C_p^\circ = FT$  in which  $D$ ,  $E$  and  $F$  are constants. Although this equation has been widely used we will choose another approach because the Harned-Robinson expression is inconsistent with a principle established by Clarke and Glew<sup>39</sup> that is discussed later in this chapter.

Ives<sup>40-41</sup> and colleagues have used various expressions containing  $T$ ,  $1/T$ ,  $T^n$ , and  $\ln T$ , to describe the dependence of  $\ln K$  on temperature. Many of them are inconsistent with the principle proposed by Clarke and Glew.<sup>39</sup> Ives and Moseley<sup>42</sup> have shown that many of these equations are unnecessarily complicated and lead to unjustified conclusions about the temperature dependence of  $\Delta C_p^\circ$ .

Pitzer<sup>43</sup> chose  $\Delta C_p^\circ$  to be a constant and then used Equations (3-4) and (3-5) to obtain

$$\Delta H^\circ = \Delta H_\theta^\circ + \Delta C_p^\circ T \quad (3-9)$$

and

$$\Delta S^\circ = \Delta S_\theta^\circ + \Delta C_p^\circ \ln T \quad (3-10)$$

in which  $\Delta H_\theta^\circ$  and  $\Delta S_\theta^\circ$  are constants of integration. These equations then lead to

$$\Delta G^\circ = \Delta H_\theta^\circ - T\Delta S_\theta^\circ + \Delta C_p^\circ (T - T \ln T) \quad (3-11)$$

and

$$\ln K = \frac{\Delta S_\theta^\circ - \Delta C_p^\circ}{R} - \frac{\Delta H_\theta^\circ}{RT} + \frac{\Delta C_p^\circ}{R} \ln T \quad (3-12)$$

An important use of Equation (3-12) is in thermodynamic analysis of equilibrium constants that have been determined at several temperatures. The aim is to evaluate the three initially unknown quantities represented by  $\Delta S_\theta^\circ$ ,  $\Delta H_\theta^\circ$  and  $\Delta C_p^\circ$ , and then to use these quantities in Equations (3-9) and (3-10) to obtain the values of  $\Delta H^\circ$  and  $\Delta S^\circ$  at the temperatures of interest.

Everett and Wynne-Jones<sup>44</sup> have rewritten Equation (3-12) as a general expression:

$$\ln K = A + B/T + C \ln T \quad (3-13)$$

in which  $A = (\Delta S_{\theta}^{\circ} - \Delta C_p^{\circ}) / R$ ,  $B = -\Delta H_{\theta}^{\circ} / R$  and  $C = \Delta C_p^{\circ} / R$

Although modern digital computers allow convenient fitting of Equations (3-12) and (3-13) to experimental results in terms of the desired A, B and C or  $\Delta S_{\theta}^{\circ}$ ,  $\Delta H_{\theta}^{\circ}$  and  $\Delta C_p^{\circ}$ , it is also useful to consider another procedure that was first developed by Everett and Wynne-Jones.<sup>44</sup>

Equation (3-12) can be rearranged in terms of  $T_1$  and  $K_1$  as

$$T_1 \ln K = (T_1/R) (\Delta S_{\theta}^{\circ} - \Delta C_p^{\circ}) - (\Delta H_{\theta}^{\circ}/R) + (\Delta C_p^{\circ}/R) (T_1 \ln T_1) \quad (3-14)$$

Similarly we can write this equation again in terms of  $T_2$  and  $K_2$ .

Subtraction of this other equation from Equation (3-14) and rearranging gives

$$\frac{T_1 \ln K_1 - T_2 \ln K_2}{T_1 - T_2} = \frac{\Delta C_p^{\circ}}{R} \left[ \frac{T_1 \ln T_1 - T_2 \ln T_2}{T_1 - T_2} \right] + \frac{\Delta S_{\theta}^{\circ} - \Delta C_p^{\circ}}{R} \quad (3-15)$$

A graph of  $(T_1 \ln K_1 - T_2 \ln K_2) / (T_1 - T_2)$  against  $(T_1 \ln T_1 - T_2 \ln T_2) / (T_1 - T_2)$  leads to a straight line with slope equal to  $\Delta C_p^{\circ}/R$  and intercept equal to  $(\Delta S_{\theta}^{\circ} - \Delta C_p^{\circ})/R$ .

Having obtained  $\Delta C_p^{\circ}$  as just described, Everett and Wynne-Jones<sup>(44)</sup> used the "sigma-plot" method for analyzing equilibrium constants at several temperatures. This method is based on Equation (3-12) in a different form:

$$\ln K - \left( \frac{\Delta C_p^{\circ}}{R} \right) \ln T = \Sigma = - \frac{\Delta H_{\theta}^{\circ}}{RT} + \frac{\Delta S_{\theta}^{\circ} - \Delta C_p^{\circ}}{R} \quad (3-16)$$

A graph of  $\Sigma$  against  $1/T$  leads to a straight line with slope equal to  $-\Delta H_{\theta}^{\circ}/R$  and intercept equal to  $(\Delta S_{\theta}^{\circ} - \Delta C_p^{\circ})/R$ , from which  $\Delta H_{\theta}^{\circ}$  and  $\Delta S_{\theta}^{\circ}$  can be evaluated when  $\Delta C_p^{\circ}$  is known. Use of  $\Delta H_{\theta}^{\circ}$ ,  $\Delta S_{\theta}^{\circ}$  and  $\Delta C_p^{\circ}$  in Equations (3-9) and (3-10) then gives values of  $\Delta H^{\circ}$  and  $\Delta S^{\circ}$  at any temperature within the range of validity of constant  $\Delta C_p^{\circ}$ .

Ives and Moseley<sup>42</sup> have made a useful modification of the earlier procedure of Everett and Wynne-Jones that we have just described. They developed a method known as the "difference table-sigma plot" method. Ramette<sup>45</sup> has also described and illustrated this method. In this method a "difference table" is first built. The first column in the difference table consists of the standard free energies  $\Delta G^{\circ}$  at equally spaced intervals of temperature. "First differences" are entered in the second column, named  $\Delta 1$ , and "second differences",  $\Delta 2$ , in the next column, etc. The first differences in the "difference table" are related to entropies by way of

$$d\Delta G^{\circ} / dT = -\Delta S^{\circ} \quad (3-17)$$

and second differences are related to heat capacity by way of Equations (3-17) and (3-5).

In a difference table one sooner or later reaches a column in which the entries are random numbers and all physical significance has been lost. This is because the experimental values of  $\Delta G^{\circ}$  are subject to random errors and are therefore not properly regarded as a strictly continuous function of the independent variable  $T$ . Ives and Moseley<sup>42</sup> concluded from the analysis of the



difference table for ionization of cyanoacetic acid at 5 to 45°C that the random errors in the experimental results limited them to considering  $\Delta C_p^\circ$  of ionization to be a temperature independent constant.

Ives and Moseley<sup>42</sup> constructed a graph of the entropies of ionization obtained from difference table as  $-(\Delta 1)/\Delta T$  against the logarithms of the corresponding mean temperatures. On the basis of the temperature independent  $\Delta C_p^\circ$  and Equation (3-10), they then obtained the mean and temperature independent  $\Delta C_p^\circ$  of ionization from the slope of the resulting straight line, and finally obtained  $\Delta H_\theta^\circ$  and  $\Delta S_\theta^\circ$  using the sigma-plot method based on the fundamental equation

$$\Delta G^\circ = \Delta H_\theta^\circ - T\Delta S_\theta^\circ + \int \Delta C_p^\circ dT - T \int \frac{\Delta C_p^\circ}{T} dT \quad (3-18)$$

which is used as

$$\Delta G^\circ + T \Delta C_p^\circ \ln T = \Sigma = \Delta H_\theta^\circ + (\Delta C_p^\circ - \Delta S_\theta^\circ) T \quad (3-19)$$

Consequently, they obtained the values of  $\Delta H^\circ$  and  $\Delta S^\circ$  at any temperature from  $\Delta H_\theta^\circ$ ,  $\Delta S_\theta^\circ$  and  $\Delta C_p^\circ$  using the same procedure as discussed earlier.

It is also possible to apply the difference table-sigma plot method to  $\ln K$  values by way of the van't Hoff equation as Ives and Moseley<sup>42</sup> have pointed out and as illustrated by Ramette.<sup>45</sup> In a difference table in terms of  $\ln K$ , the first differences relate to  $\Delta H^\circ$  by

$$\Delta H^\circ = RT_1 T_2 \Delta 1 / \Delta T \quad (3-20)$$

$\Delta C_p^\circ$  can be obtained by using Equation (3-4) in the form

$$\Delta C_p^\circ = \Delta(\Delta H^\circ) / \Delta T \quad (3-21)$$

Applying Equation (3-21) to the successive values of  $\Delta H^\circ$  obtained from (3-20) leads to a series of  $\Delta C_p^\circ$  whose average value is taken to be the desired  $\Delta C_p^\circ$ . Once  $\Delta C_p^\circ$  is obtained  $\Delta H_\theta^\circ$  and  $\Delta S_\theta^\circ$  are evaluated from the slope and intercept of a sigma plot based on Equation (3-16).

Ives and Moseley<sup>42</sup> observed in their difference table that  $\Delta 1$  values are distinctly different from zero and also increase significantly with increasing temperature; the  $\Delta 2$  values are all non-zero and significantly positive; the values of  $\Delta 3$  and  $\Delta 4$  have alternating signs with mean values that are not significantly different from zero. They therefore concluded that the second differences are temperature independent and the first differences vary linearly with temperature. However, they also noted that significant non-zero third differences would represent a term in  $\Delta C_p^\circ$  that contains  $T$  and non-zero fourth differences would represent a term that contains  $T^2$ . On this basis, they wrote  $\Delta C_p^\circ$  as

$$\Delta C_p^\circ = a + bT + cT^2 \quad (3-22)$$

and carried out an extension of the sigma-plot method. In this extended sigma-plot method, Equation (3-19) becomes

$$\Delta G^\circ + aT \ln T + \frac{b}{2}T^2 + \frac{c}{6}T^3 = \Sigma = \Delta H_\theta^\circ + T(a - \Delta S_\theta^\circ) \quad (3-23)$$

The methods and equations discussed above are either empirical equations or based on some assumptions. Although these equations are used by many investigators, a more general method is still needed. Clarke and Glew<sup>39</sup> have developed a general method of calculating thermodynamic

function values from equilibrium data. In this procedure the essential idea is that the various thermodynamic functions ( $K$ ,  $\Delta G^\circ$ ,  $\Delta H^\circ$ ,  $\Delta S^\circ$  and  $\Delta C_p^\circ$ ) are considered to be continuous, well-behaved (differentiable) functions of temperature. To apply this idea, a reference temperature  $\theta$  is chosen for which it is desired to calculate the values of various thermodynamic functions that we represent by  $\Delta G_\theta^\circ$ ,  $\Delta S_\theta^\circ$ ,  $\Delta H_\theta^\circ$ ,  $\Delta C_{p\theta}^\circ$ ,  $(d\Delta C_p^\circ/dT)_\theta$ ,  $(d^2\Delta C_p^\circ/dT^2)_\theta$  and  $(d^3\Delta C_p^\circ/dT^3)_\theta$ . On the basis of the stated assumption that  $\Delta C_p^\circ$  is a well-behaved function of temperature Clarke and Glew expressed  $\Delta C_p^\circ$  at any temperature as a perturbation of the value at the reference temperature  $\theta$  using a Taylor series expansion:

$$\Delta C_p^\circ = \Delta C_{p\theta}^\circ + (d\Delta C_p^\circ/dT)_\theta (T - \theta) + \frac{1}{2}(d^2\Delta C_p^\circ/dT^2)_\theta (T - \theta)^2 + \frac{1}{6}(d^3\Delta C_p^\circ/dT^3)_\theta (T - \theta)^3 + \dots \quad (3-24)$$

Using this general expression for  $\Delta C_p^\circ$  in Equations (3-5) and (3-6) then gives

$$\Delta H^\circ = \Delta H_\theta^\circ + \Delta C_{p\theta}^\circ (T - \theta) + \frac{1}{2}(d\Delta C_p^\circ/dT)_\theta (T - \theta)^2 + \frac{1}{6}(d^2\Delta C_p^\circ/dT^2)_\theta (T - \theta)^3 + \frac{1}{24}(d^3\Delta C_p^\circ/dT^3)_\theta (T - \theta)^4 + \dots \quad (3-25)$$

and

$$\begin{aligned} \Delta S^\circ = & \Delta S_\theta^\circ + \Delta C_{p\theta}^\circ \ln(T/\theta) + (d\Delta C_p^\circ/dT)_\theta [T - \theta - \theta \ln(T/\theta)] + \frac{1}{2}(d^2\Delta C_p^\circ/dT^2)_\theta \\ & \left[ \frac{T^2 - \theta^2}{2} - 2\theta(T - \theta) + \theta \ln(T/\theta) \right] + \frac{1}{6}(d^3\Delta C_p^\circ/dT^3)_\theta \left[ \frac{T^3 - \theta^3}{3} - \frac{3\theta}{2}(T^2 - \theta^2) + \right. \\ & \left. 3\theta^2(T - \theta) - \theta^3 \ln(T/\theta) \right] + \dots \end{aligned} \quad (3-26)$$

Substitution of Equations (3-25) and (3-26) into Equation (3-3) led Clarke and Glew to obtain an equation of the form

$$\begin{aligned}
 R \ln K = & -\frac{\Delta G^\circ}{\theta} + \Delta H^\circ_\theta \left[ \frac{1}{\theta} - \frac{1}{T} \right] + \Delta C_{p\theta}^\circ \left[ \left( \frac{\theta}{T} \right) - 1 + \ln \left( \frac{T}{\theta} \right) \right] + \frac{\theta}{2} (d\Delta C_p^\circ / dT)_\theta \left[ \right. \\
 & \left. \left( \frac{T}{\theta} \right) - \left( \frac{\theta}{T} \right) - 2 \ln \left( \frac{T}{\theta} \right) \right] + \frac{\theta^2}{12} (d^2 \Delta C_p^\circ / dT^2)_\theta \left[ \left( \frac{T}{\theta} \right)^2 - 6 \left( \frac{T}{\theta} \right) + 3 + 2 \left( \frac{\theta}{T} \right) + \right. \\
 & \left. 6 \ln \left( \frac{T}{\theta} \right) \right] + \frac{\theta^3}{72} (d^3 \Delta C_p^\circ / dT^3)_\theta \left[ \left( \frac{T}{\theta} \right)^3 - 6 \left( \frac{T}{\theta} \right)^2 + 18 \left( \frac{T}{\theta} \right) - 10 \right. \\
 & \left. - 3 \left( \frac{\theta}{T} \right) - 12 \ln \left( \frac{T}{\theta} \right) \right] + \dots \dots \dots
 \end{aligned} \tag{3-27}$$

Equation (3-27) is customarily expressed in a simple form as

$$R \ln K = A + B/T + C \ln T + DT + ET^2 + FT^3 + \dots \tag{3-28}$$

in which the constant F relates to  $d^3 \Delta C_p^\circ / dT^3$ ; E relates to  $d^2 \Delta C_p^\circ / dT^2$  and  $d^3 \Delta C_p^\circ / dT^3$ ; D to  $d\Delta C_p^\circ / dT$ ,  $d^2 \Delta C_p^\circ / dT^2$  and  $d^3 \Delta C_p^\circ / dT^3$ ; C to four terms ( $\Delta C_p^\circ$  to  $d^3 \Delta C_p^\circ / dT^3$ ); B to five terms ( $\Delta H^\circ$  to  $d^3 \Delta C_p^\circ / dT^3$ ); and A to all six terms ( $\Delta G^\circ$  to  $d^3 \Delta C_p^\circ / dT^3$ ).

Equations (3-27) and (3-28) are general expressions for the representation of  $\ln K$  as a function of  $T$ . The termination of a Taylor series expansion depends on calculation requirements and the accuracy of experimental measurements. Equations (3-27) and (3-28) can be either reduced or extended. As Clarke and Glew<sup>39</sup> pointed out, the termination of a Taylor series expansion on  $\Delta C_p^\circ$  at  $d^3 \Delta C_p^\circ / dT^3$ , which leads to five parameters in Equations (3-27) and (3-28), is sufficient for most accurate sets of equilibrium measurements.

Equations (3-27) and (3-28) can be reduced to a simpler form when

where  $\theta$  represents the reference temperature, which they chose to be 298.15K. Although Halliwell and Strong<sup>48</sup> obtained Equation (3-29) in a different way, Equation (3-29) is essentially the same as the five constant Clarke and Glew equation (Equation 3-27) after combining the constants  $K_1$  to  $K_4$  with Equation (3-29) and rearranging the combined equation as a function of variable  $T$ .

It can now be seen that Equation (3-13) proposed by Everett and Wynne-Jones<sup>44</sup> is a simplified form of Equation (3-28) with  $\Delta C_p^\circ$  reduced to only the  $\Delta C_{p\theta}^\circ$  term. Equation (3-8) is unsatisfactory because the constants in Equation (3-8) are a combination of (A,B,D) from Equation (3-28), which is contrary to the principles first explained by Clarke and Glew.

We now apply the principles and procedures discussed above to obtain thermodynamic functions from gas-liquid chromatographic equilibrium constants. We start by specifying the equilibrium to which  $K$  (Equation 2-24) refers:



As the first step in deriving thermodynamic quantities for the equilibrium represented by Equation (3-30), the enthalpy of solution is considered to be temperature independent and is obtained from the slope of the plot of  $\ln K$  against  $1/T$ . Equation (2-32) shows that the equilibrium constant is directly proportional to specific retention volume  $V_g^\circ$ . Therefore, a plot of  $\ln V_g^\circ$  against  $1/T$  should give the same slope as that of  $\ln K$  versus  $1/T$  and the same value of  $\Delta H^\circ$ . Therefore,  $V_g^\circ$  has been widely used in place of  $K$  and Equation (3-6) has

been rewritten as

$$\Delta H^\circ = -R \, d \ln V_g^\circ / d(1/T) \quad (3-31)$$

It should be noted that  $\Delta H^\circ$  calculated by Equation (3-31) is actually an average  $\Delta H^\circ$  over the temperature range studied and so is justified only for small temperature ranges or for experimental results of low accuracy. For a large temperature range and for data of good accuracy, the temperature dependence of  $\Delta H^\circ$  should be taken into account.

The standard Gibbs energy (free energy) change is calculated by

$$\Delta G^\circ = -RT \ln K = -RT \ln (V_g^\circ M_{1,L} / R 273.15) \quad (3-32)$$

and the  $\Delta S^\circ$  for dissolution is then obtained from the basic thermodynamic relation represented by Equation (3-2)

The quantities  $\Delta H^\circ$ ,  $\Delta G^\circ$  and  $\Delta S^\circ$  refer to the equilibrium process presented by Equation (3-30) where the standard state for solute in solution is the hypothetical solute state obtained by extrapolating Henry's law to  $f_1 = 1.0$ .

Thermodynamic properties for many gas/liquid or vapor/liquid systems have been studied. Most investigators have assumed the enthalpy of solution to be temperature independent ( $\Delta C_p^\circ = 0$ ) in spite of the fact that for many systems the graphs of  $\ln K$  against  $1/T$  show observable curvature. Therefore, in the next step we consider the temperature dependence of enthalpies of solution in GLC.

Previously, most investigators stopped at the first step, taking  $\log K$  or  $\log V_g^\circ$  against  $1/T$  to be linear. Only a few have tried to fit a non-linear equation to  $\ln K$  obtained from GLC to account for temperature dependence of  $\Delta H^\circ$  and obtain

the value of  $\Delta C_p^\circ$ . Meyer and Baiocchi<sup>49-50</sup> made accurate measurements of specific retention volumes for n-octane and cycloheptane in n-C<sub>36</sub>H<sub>74</sub>. They observed the curvature in plots of  $\ln V_g$  against  $1/T$  and corrected these curvatures by fitting a quadratic equation in  $V_g^\circ = A + B/T + C/T^2$  to the values of  $\ln V_g^\circ$  and  $1/T$ . They also fitted the data with other two functions:  $\ln V_g^\circ = A + B/(C+T)$  and  $\ln V_g^\circ = A + B/T + C \ln T$ , of which the second equation is actually a simplified form of Equation (3-28). From these fits they obtained the values of heat capacity  $\Delta C_p^\circ$ .

It is possible, in principle, to treat the temperature dependence of  $\Delta H^\circ$  in a general way, that is, by applying the procedure suggested by Clarke and Glew<sup>42</sup> in which they consider a temperature dependence of  $\Delta C_p^\circ$  (Equation 3-24). However, previous experience and a preliminary assessment of accuracy of our experimental data have suggested that it will be sufficient to consider  $\Delta C_p^\circ$  to be a temperature independent constant, so we simplify Equation (3-24) to  $\Delta C_p^\circ = \Delta C_{p\theta}^\circ$ . Then Equation (3-25) reduces to

$$\Delta H^\circ = \Delta H_\theta^\circ + (T - \theta) \Delta C_p^\circ \quad (3-33)$$

Considering a constant  $\Delta C_p^\circ$  and using  $V_g^\circ$  to replace  $K$ , Equation (3-27) becomes

$$\ln V_g^\circ = \ln V_{g,\theta}^\circ + \frac{\Delta H_\theta^\circ}{R} \left[ \frac{1}{\theta} - \frac{1}{T} \right] + \frac{\Delta C_p^\circ}{R} \left[ \ln \left( \frac{T}{\theta} \right) + \frac{\theta}{T} - 1 \right] \quad (3-34)$$

By fitting Equation (3-34) to the specific retention volume data, we obtain  $\Delta H_{\theta}^{\circ}$  and  $\Delta C_p^{\circ}$ .  $\Delta H^{\circ}$  can then be calculated at any temperature using Equation (3-33).

The reference temperature  $\theta$  might be chosen as any temperature. Many authors prefer to choose 25°C because the thermodynamic functions are commonly reported at 25°C. But the best results are obtained by choosing  $\theta$  to be in the middle of the experimental temperature range.

### **Infinite Dilution Activity Coefficient, $\gamma_2^{\infty}$**

Many investigators have chosen to describe the results of thermodynamic investigations using GLC in terms of "infinite dilution activity coefficients" for the solute, with activities and activity coefficients based upon a Raoult's law reference state with the vapor pressure of the pure liquid solute substance as a standard state. In order to derive an equation which enables us to obtain the infinitely dilute activity coefficients,  $\gamma_2^{\infty}$ , from specific retention volumes, we first consider the standard state of solute in relation to Fig. 3-1. In Fig. 3-1 the solid line illustrates the vapor pressure of a typical substance (2) that we call the solute. The dashed line represents Henry's law that is especially useful for the solute in dilute solutions and the dotted line represents Raoult's law. When we choose a standard state (indicated by  $K_H$  in the figure) for the solute based on Henry's law, the solute activity coefficients are unity for the Henry's law (very



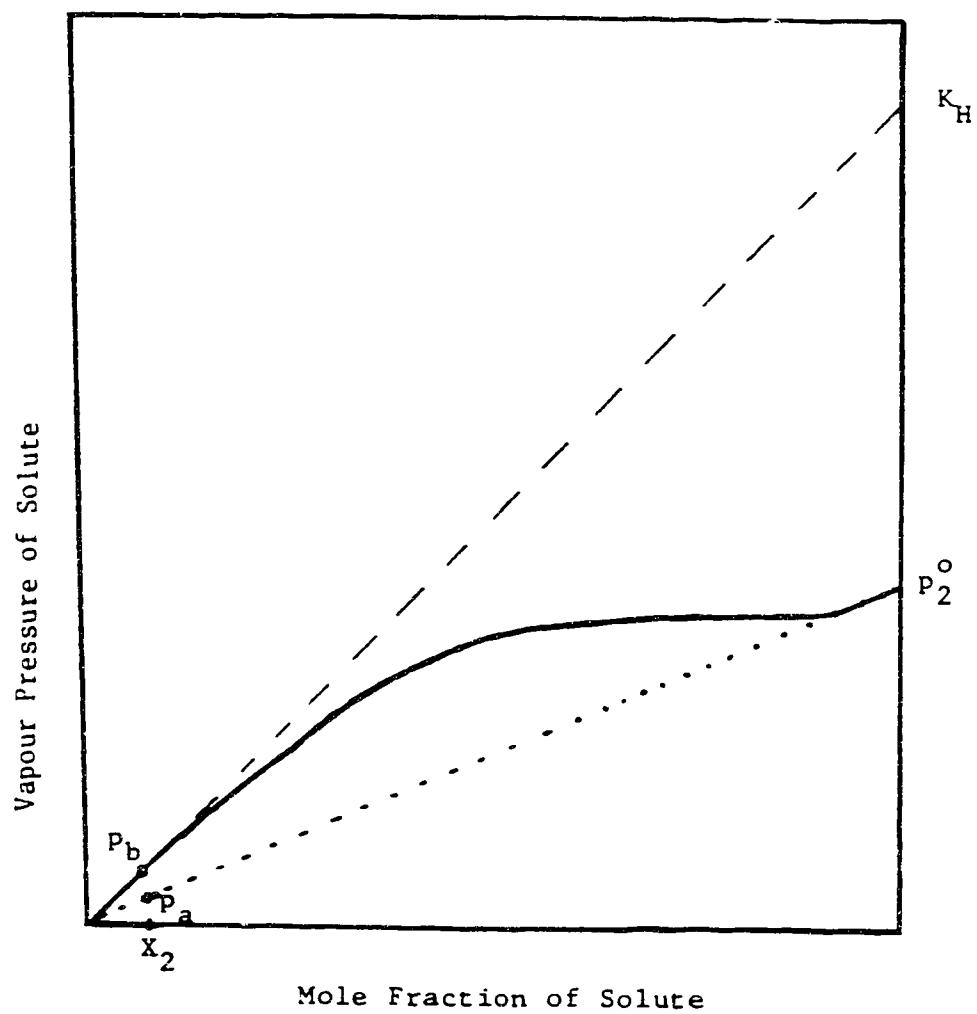


Figure 3-1 Illustration of Raoult's Law and Henry's Law

dilute) region and are close to unity in other dilute solutions. We regard this choice as the most convenient and therefore preferable for GLC investigations. However, it is permitted to choose a standard state based on the solute in the pure liquid state (provided that the experimental temperature is below the critical temperature for the solute) with the standard state denoted by  $P_2^\circ$  in the figure. In this case, solute activity coefficients for very dilute solution (Henry's law region) are usually substantially different from unity. This infinite dilution activity coefficient is a measure of the deviation of a dilute solute from the ideal property represented by Raoult's law.

We now consider a very dilute solution corresponding to  $X_2$  in Fig. 3-1.

From the definition of activity coefficient, we have

$$\gamma_2^\infty = \frac{a_2}{X_2} \quad (3-35)$$

in which  $a_2$  is the activity of solute, which has been given by Equation (2-25) as  $a_2 = f_2 / f_2^\circ$ . Now since we have focussed on Raoult's law and chosen  $P_2^\circ$  as our standard state, we rewrite Equation (3-35) as

$$\gamma_2^\infty = \frac{f_2 / P_2^\circ}{X_2} \quad (3-36)$$

Because of the low pressure in the GLC column, we have  $f_2 = P_2$ , which is represented in Figure 3-1 by  $P_b$ . The product of  $P_2^\circ$  and  $X_2$  in Equation (3-36) is expressed by  $P_a$  in Figure 3-1. Therefore we obtain

$$\gamma_2^\infty = \frac{P_b}{P_a} \quad (3-37)$$

for the infinite dilution activity coefficient. Combination of Equation (3-37) with Henry's law and Raoult's law then leads to

$$\gamma_2^\infty = K_H / P_2^\circ \quad (3-38)$$

Further combination of Equations (2-38) and (3-38) gives the commonly used equation for  $\gamma_2^\infty$ , which directly relates to specific retention volumes,  $V_g^\circ$

$$\gamma_2^\infty = \frac{R \, 273.15}{V_g^\circ M_{1,L} P_2^\circ} \quad (3-39)$$

In Equation (3-39) the saturated vapor pressure of pure solute,  $P_2^\circ$ , can be obtained from the Antoine equation,  $\log P_2^\circ = A - B / (t + C)$ , in which  $t$  is the temperature in degrees Celsius and  $A$ ,  $B$  and  $C$  are Antoine constants that can be obtained from the literature.<sup>51</sup> When these Antoine constants are not available for the temperature range of interest, the vapor pressures can be calculated from other equations such as the Riedel equation, Vapres-2 equation or Wagner equation.<sup>52</sup> All these equations with their constants are given in reference 52.

The derivation of Equation (3-39) is based on several assumptions, most of which can be met experimentally by a careful choice of experimental conditions as has been discussed in Chapter 2. If some assumptions cannot be met experimentally, corrections are needed. In the derivation of  $\gamma_2^\infty$ , it is assumed that none of the following types of interactions exist in the vapor phase above

the solution: solute-solute, solute-carrier gas and carrier gas-carrier gas, which implies an ideal vapor phase. Martire<sup>12-13</sup> has pointed out that if the gas phase does not meet the ideal assumption a general equation should be used which allows for imperfections of the gas phase, in order to obtain a true activity coefficient. This general equation is written as

$$\ln \gamma_2^\infty = \ln \frac{273.15 R}{P_2^\circ V_g^\circ M_{1,L}} - \frac{P_2^\circ B_{22}}{RT} \quad (3-40)$$

in which  $B_{22}$  represents the second virial coefficient of the solute vapor. The values of virial coefficients for many solutes have been evaluated and are available in the literature.<sup>53</sup> If the values of  $B_{22}$  are not available, they can be estimated from the Berthelot equation<sup>54</sup> or from an equation based on the principle of corresponding states.<sup>55</sup> The Berthelot equation has been shown to be valid for a variety of vapors over a large range of temperatures. It is expressed as

$$B_{22} = \frac{9}{128} \frac{RT_c}{P_c} \left(1 - \frac{6T_c^2}{T^2}\right) \quad (3-41)$$

in which  $P_c$  and  $T_c$  represent critical pressure and temperature, respectively. An equation<sup>55</sup> based on the principle of corresponding states, which is valid only for n-alkanes, is

$$\frac{B}{V_c} = 0.430 - 0.886\left(\frac{T_c}{T}\right) - 0.694\left(\frac{T_c}{T}\right)^2 - 0.0375(n-1)\left(\frac{T_c}{T}\right)^{4.5} \quad (3-42)$$

in which  $n$  is the number of carbons in the n-alkane. Neither Equation (3-41) nor (3-42) is applicable to polar compounds. If the  $B_{22}$  values are not available, we

are then unable to apply Equation (3-40).

Previous work<sup>12</sup> has shown that the assumption of an ideal gas phase is valid when the carrier gas is helium or hydrogen under usual GLC conditions. Since we have used helium as the carrier gas in this work, we calculated activity coefficients by directly applying Equation (3-39) without considering corrections for non-ideality of gas phase.

### **Solubility: Henry's Law Constant $K_H$**

Solubility of gases in liquids can be expressed in many ways. In gas liquid chromatography we express the solubilities of gases in liquids in terms of Henry's law constants. The Henry's law constant can be related to the mole fraction of a gas in a liquid,  $X_2$ , which is most commonly used in other static methods, by way of Henry's law (Equation 2-33). Once the Henry's law constant is known for a gas-liquid equilibrium system, the mole fraction of gas dissolved in liquid can be calculated from

$$X_2 = P_2 / K_H \quad (3-43)$$

in which  $P_2$  is the equilibrium partial pressure of the solute above liquid.

It should be pointed out that Equation (3-43) is valid only for low partial pressure systems, in which the fugacity of solute gas is taken as the same as the partial pressure. If we tried to apply Equation (3-43) to a high pressure system, we would need to use the fugacity of solute rather than partial pressure, such as is used in the Krichevsky-Kasarnovsky equation or Krichevsky-Ilinskaya

equation. This will be discussed in detail in Chapter 6.

The equation for calculating Henry's constants from GLC retention volumes has been derived in Chapter 2 (Equation 2-38). The Henry's law constant calculated by this equation is expressed in terms of pressure. In order to use Equation (2-38) to calculate  $K_H$ , we need to know the molecular weight of the stationary phase. When the stationary phase is a pure chemical compound the molecular weight is known or can be measured. However, if the stationary phase is a polymer or a mixture with a complicated composition, such as heavy oil or bitumen, the molecular weight is not always available. In this case we might prefer to express the Henry's law based on molality,  $m$ , as

$$P_2 = K_H^m \cdot m \quad (3-44)$$

in which  $K_H^m$  represents Henry's law constant based on molality and  $m$  indicates the molality of the solute in stationary phase. Using a similar procedure as used in Chapter 2, we can derive

$$K_H^m = \frac{R273.15}{1000 V_g^o} \quad (3-45)$$

Note that in Equation (3-45) the molecular weight of stationary phase disappears and so one can obtain the Henry's law constant without a knowledge of the molecular weight. Equation (3-45) is very useful for engineering and industrial calculations.

## Chapter 4

### Solubilities and Thermodynamic Properties of Gases and Vapors in Bitumen

#### Introduction

The solubilities of gases and vapors in bitumen are important data for fundamental studies of enhanced oil recovery. For example, it has been proposed that various steam-based processes for in-situ production are improved by addition of light hydrocarbons to the injected steam. One of the processes used to enhance oil recovery is to pump a gas such as carbon dioxide or natural gas into the reservoir from an injection well. Most of the gas forms a front to push the oil bank toward the production well while part of the gas dissolves in the oil and bitumen, thus reducing the viscosity of heavy oil and bitumen. Another example of the need for solubility data is associated with the suggestion that bitumen can be recovered from mined oil sands by way of solvent extraction using dichloromethane or some other solvent. Design and assessment of these and other production processes should be based partly on solubility-pressure data for a range of temperatures. Similar data are also needed in connection with recovery of relatively expensive additives such as dichloromethane or light hydrocarbons from the produced bitumens.

---

1. A version of this chapter has been accepted for publication in the Canadian Journal of Chemical Engineering, 1990.

Previous experience has shown that it is difficult to measure the solubility of gases in bitumen because of the very high viscosity. To deal with these difficulties there are two new approaches that are applicable to this problem. In one approach other researchers in this laboratory have applied a conventional equilibrium method (PVT measurement) to measure solubilities of gases in bitumen that has been diluted with a solvent (toluene) to reduce the viscosity, and have attempted to obtain by suitable calculations the solubilities in un-diluted bitumen. Another approach, which is described here, has been to use gas-liquid chromatography (GLC) to obtain Henry's law constants for several gases and vapors in bitumen over a range of temperatures. The anticipated advantage of the GLC method is that the high viscosity of bitumen would not cause a problem in our measurement, because in this method the bitumen is spread in a thin layer on a solid support, which allows rapid equilibration. The anticipated disadvantage of the GLC method is that this method would not yield accurate results for the least soluble gases, although some of which are very important.

Because we have applied the GLC method to obtain retention volumes for several gases and vapors at several temperatures, it has been possible to use these results in thermodynamic calculations of enthalpies of solution and other quantities that have been discussed in detail in Chapters 2 and 3. Further thermodynamic analyses of the solubilities of gases and vapors in bitumen are also of interest to users of solubility data since the temperature dependence of the solubility is related to thermodynamic functions such as enthalpy of solution.



In practice, users of gas solubility data might need the data for many different temperatures and pressures, but it is not practical to measure all solubility data needed. Instead, we can carefully measure several solubilities over a range of temperatures and then develop an expression through the equation of state and some thermodynamic properties, which permits us to calculate other solubilities at different temperatures and pressures than those directly measured.

Another reason for thermodynamic analyses is that during the in-situ recovery process thermal effects occur that are associated with the dissolution of gases and vapors in bitumen. Although these effects might be measured calorimetrically, experience has shown that such measurements are very difficult because of the high viscosity of bitumen. Therefore GLC measurements will provide useful information about both solubilities and related thermodynamic quantities. In this chapter the experimental procedures for obtaining retention volumes will be presented, along with the experimental results and derived thermodynamic quantities.

## **Experimental**

### **Materials**

Samples of bitumen from Athabasca and Wolf Lake, Alberta, were provided by Syncrude Canada Ltd. and BP Canada Inc., respectively. The average molecular weights (in benzene) were obtained by way of measurements at 40°C with a vapor phase osmometer and were found to be 554 g mol<sup>-1</sup> (Athabasca) and 645 g mol<sup>-1</sup> (Wolf Lake). Carrier gas (helium, 99.995%) was obtained from

Linde (Union Carbide Canada Limited). Other gases ( $\text{Ne}$ ,  $\text{CO}_2$ ,  $\text{C}_2\text{H}_6$ ,  $\text{C}_3\text{H}_8$ ,  $\text{C}_4\text{H}_{10}$ ) were supplied in high purities by Matheson Gas Products Canada. Commercial samples of all liquids used as solute vapours and toluene used as diluent for loading bitumen on Chromosorb W were obtained in the best available purity and then further purified by distillation when necessary. Chromosorb W solid support was provided by Mandel Scientific Company Ltd.

### Apparatus

A Hewlett-Packard 5890A gas chromatograph, equipped with a model 3392A integrator, was used for obtaining retention times and peak areas. The gases were detected with a thermal conductivity detector (TCD). The retention times and peak areas were recorded by the integrator. The carrier gas (helium) was passed sequentially through a molecular sieve moisture trap and an oxygen trap before it entered the chromatographic column.

The temperature of the column (oven) was measured and displayed by a digital thermometer installed in the GC. The accuracy of the temperature measurements was determined using a platinum resistance thermometer, which was also used for room temperature measurement. The maximum temperature difference between that displayed by the GC and measured with the platinum thermometer was smaller than  $0.2\text{ }^{\circ}\text{C}$  over the entire range of temperature studied. Table 4-1 shows the temperature calibration.

The flow rate of carrier gas was controlled with a needle valve and measured at the outlet of the detector with a soap bubble flow meter. The time

Table 4-1                      Temperatures of the GC oven

---

Temp. displayed (°C)	Temp. measured with platinum resistance thermometer (°C)
<hr/>	
30	29.81
40	39.85
50	49.81
60	59.88
70	69.91
80	79.97
90	89.91
100	99.96
120	120.14
130	130.19
150	150.24

---

at which a soap bubble moved through 10 ml was measured with the stopwatch installed in the GC. The precision of the flow rate measurement was  $\pm 0.1 \text{ cm}^3 \text{ min}^{-1}$  in the flow rate range 20 to  $40 \text{ cm}^3 \text{ min}^{-1}$ . This precision was estimated based on the standard deviation of at least five separate measurements. The flow rate was also frequently checked between runs. If we found any slight change of flow rate before and after a series of runs, we took an average value for our calculations.

The column inlet pressure was measured with a pressure gauge installed in the GC (accurate to  $\pm 2 \text{ kPa}$ ). The outlet pressure (atmospheric pressure) was measured with a mercury barometer (accurate to  $\pm 0.01 \text{ cm Hg}$ ).

## Columns

Columns were stainless steel tubing, 2 meters long by 1/4 inch outer diameter. The column was first cleaned by sequentially flowing acetone, distilled water, concentrated nitric acid, distilled water, concentrated ammonium hydroxide, distilled water and acetone. The solid support was 60/80 mesh Chromosorb W which had been washed with acid and treated with DMCS (dimethylchlorosilane) by the manufacturer. Bitumen that was to be used as the stationary phase was dissolved in toluene, followed by addition of an appropriate amount of Chromosorb W. The toluene was then removed by evaporation in a rotary evaporator. The resulting Chromosorb W that was coated with bitumen was placed in an oven at  $90^\circ\text{C}$  with a nitrogen atmosphere for 2-3 hr to remove the last of the toluene, and was then used to fill a GLC

column. The bitumen loadings of various packings were determined by measuring the weight losses of several samples on heating for 8 hr in a muffle furnace at 800°C. Blank measurements were made to allow for correction for the mass of ash formed on heating bitumen and for the small mass loss associated with heating Chromosorb W. Standard deviations of bitumen loadings measured in this way ranged from 0.1 to 0.3%. Since the Chromosorb W particles are very easily fragmented, the particles must be handled with great care during the whole coating process and the evaporator must be operated at the lowest rotating speed.

One end of cleaned and dried tubing was filled with a small plug of silanized glass wool and then connected to a vacuum source. The prepared packing (Chromosorb W coated with bitumen) was then slowly poured into the other end through a small funnel. During the filling, the column was gently tapped. After the tubing was filled with packing, another small plug of glass wool was placed in the open end. The tubing was then coiled to fit in the GC oven and compression fittings were attached at both ends. The packed column was then connected to the GC.

### **Retention Time Measurements**

Each packed column was conditioned at 150°C with a carrier gas flow rate of approximately 20 cm<sup>3</sup> min<sup>-1</sup> for 10 h. Because some of the lower boiling-point constituents of bitumen might be lost during conditioning, columns were weighed before and after conditioning to permit correction for the very small

amount of stationary phase lost.

Small samples of each gas/vapor investigated were injected with a 10  $\mu\text{L}$  syringe along with neon, which was used to determine the dead or void time of the column. The total injected volume of gas/vapor plus neon was 2  $\mu\text{L}$  for most solutes. Since for most solute gases/vapors investigated in this work the retention times were independent of the size of sample injected, these solutes (with neon) were injected seven times in sequence, and an average retention time was obtained to be used in subsequent calculations. The retention time was found to depend on sample size for methanol at all temperatures, and dichloromethane at lower temperatures. These solutes were therefore investigated by injecting samples of different sizes, with resulting retention volumes being extrapolated to zero sample size to obtain the limiting retention volume that is related to the desired Henry's law constant. Since the retention times for some less soluble gases (ethane, propane, carbon dioxide) are close to the retention time of neon, the peaks cannot be separated. In this case, these gases were injected separately from neon.

As was discussed in Chapter 2, several precautions should be taken in order to obtain a "true" equilibrium constant from GLC retention time measurements. Now we illustrate how our experimental conditions meet the requirements presented in Chapter 2.

The optimum flow rate was first determined before any retention data were taken. The optimum flow rate is defined based on rate theory of column band broadening and obtained from a Van Deemter plot. In chromatography, peak

band broadening has several causes, such as eddy diffusion, longitudinal diffusion, and mass transfer resistance etc. An equation which relates the overall plate height to these terms and flow rate has been developed<sup>1-3</sup> and written as

$$H = A + \frac{B}{u} + Cu \quad (4-1)$$

in which A, B, C are parameters, u is the linear velocity of carrier gas, which can be obtained by dividing the column length L by the dead time of the column, and H is plate height (height equivalent to a theoretical plate) which is obtained by

$$H = L / N \quad (4-2)$$

in which N represents the plate number that can be calculated directly from the retention times and baseline peak width by the equation

$$N = 16 \left( \frac{t_R}{W_t} \right)^2 \quad (4-3)$$

in which  $W_t$  is the baseline peak width.

A plot of H against u shows a valley. The velocity at the minimum point is called the optimum flow rate  $U_{opt}$ , which corresponds to the smallest plate height and the best column efficiency.

To determine  $U_{opt}$ , a series of experiments was done at a wide range of flow rates at the temperature of interest. The flow rates ( $\text{cm}^3/\text{min}$ ) are converted to linear velocity u ( $\text{cm/s}$ ) and plate heights H are calculated using Equations (4-2) and (4-3). The optimum flow rate is then obtained from the plot of H against u (Van Deemter plot). Figure 4-1 shows a typical Van Deemter plot. The optimum flow rate obtained from this plot is about 3.5  $\text{cm/s}$ , which corresponds to

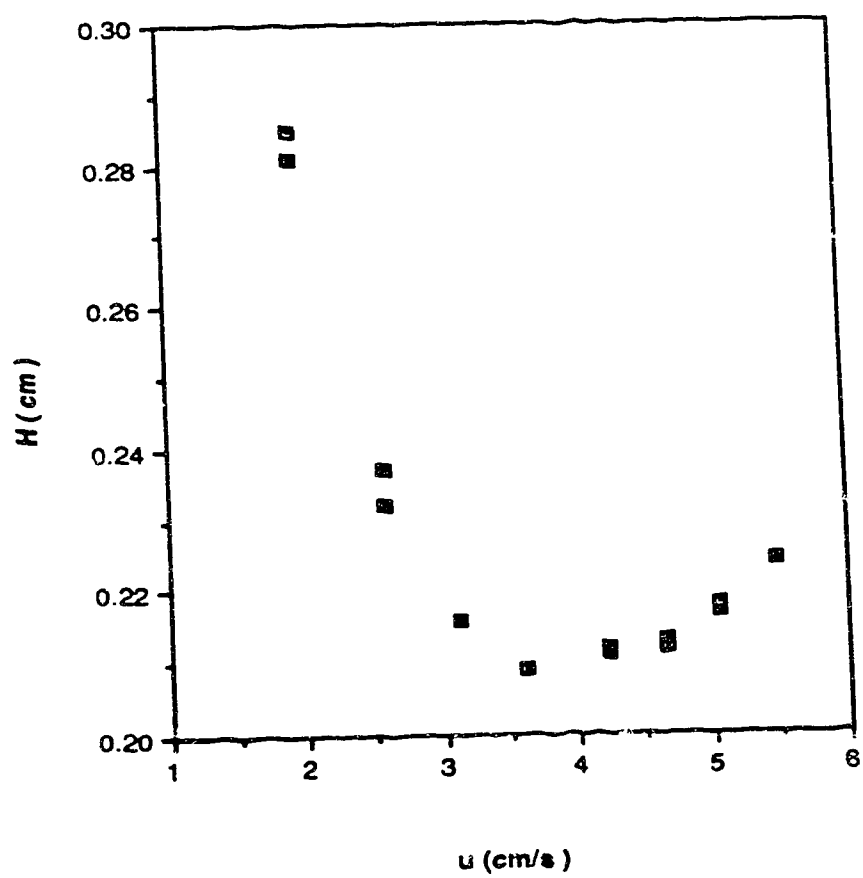


Figure 4-1 A graph of plate height against linear velocity of carrier gas for the determination of optimum flow rate



about 35 cm<sup>3</sup>/min.

Subsequent measurements were made at a flow rate slightly slower than this optimum flow rate. We had to sacrifice some column efficiency to ensure equilibrium between gas and liquid phases.

The solutes injected into bitumen columns included 4 gases and 9 vapors. They are carbon dioxide, normal alkanes from ethane to octane, benzene, toluene, m-xylene, dichloromethane, and methanol. Injected gas or vapor volumes less than 2  $\mu$ L gave retention times that were independent of sample sizes for most of these solutes, including carbon dioxide, alkanes and three aromatics, thus verifying that solute concentrations were in the desired linear isotherm or Henry's law region of concentration.

It was also found that the retention times depended on injected vapor volumes for dichloromethane at lower temperatures and methanol at all experimental temperatures, for all practical sample sizes. In these cases, different vapor volumes were injected and retention volumes against area percent of the solute peak were plotted and extrapolated to zero percent of sample to obtain the limiting retention volume that applies to the linear isotherm region. Examples of the relationship between retention volumes and sample sizes for the two cases mentioned above are given in Figures 4-2 to 4-5. Figure 4-2 represents the plots for the specific retention volumes of pentane, hexane, heptane and octane against area percent. Similarly, Figure 4-3 shows the graphs for benzene, toluene and m-xylene. These figures indicate that the specific retention volumes of these solutes are almost constant over the sample

size range studied. Figures 4-4 and 4-5 represent the same plots for dichloromethane and methanol, respectively.

To study and if necessary eliminate the effects of adsorption of solute on the liquid bitumen and solid support surfaces, several columns having different liquid loadings were studied. Specifically, measurements were made with five columns with 5-20% loadings of Athabasca bitumen and three columns with 5-15% loadings of Wolf Lake bitumen. The liquid loadings are presented in Table 4-2. If the retention volumes were found to change with the loading of bitumen, adsorption by the liquid surface existed. In this case one would measure the surface area of the packing and calculate the liquid phase volume to allow for the use of Equation (2-40) to eliminate adsorption contributions. However, because specific retention volumes obtained from our columns with different bitumen loadings showed no obvious trends, it was concluded that adsorption of gases/vapors on surfaces was negligible in comparison with solution in the bitumen. Therefore, the average specific retention volumes obtained from different columns was used for subsequent calculations of Henry's Law constants and thermodynamic functions.

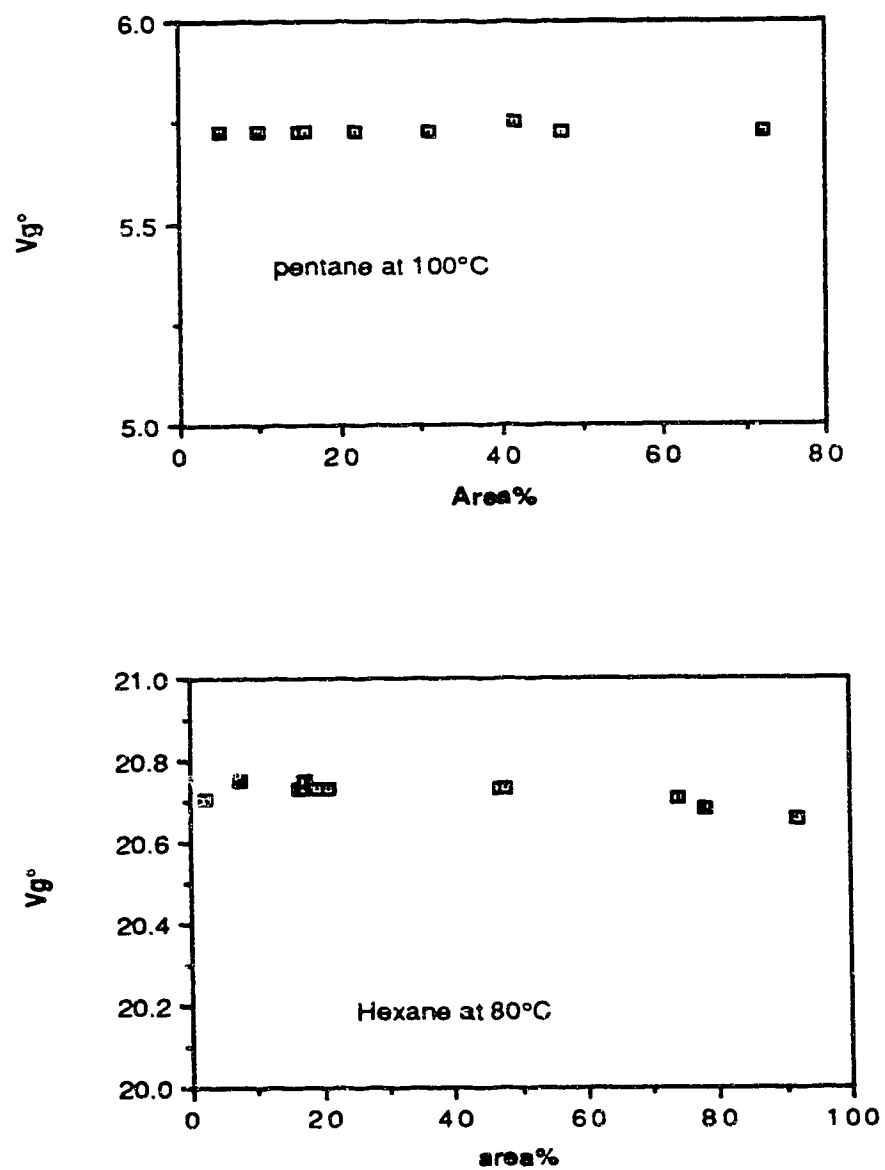


Figure 4-2A    Graphs of specific retention volume against sample size for pentane and hexane in Athabasca bitumen.

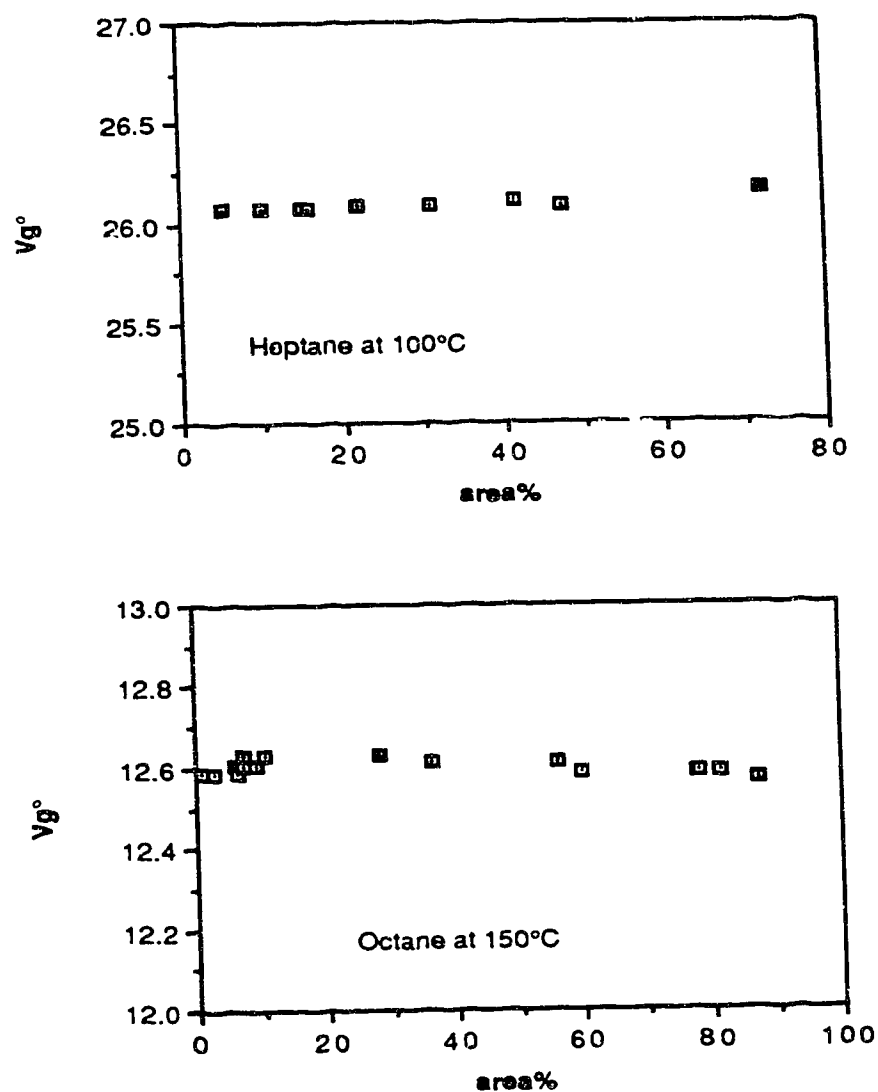
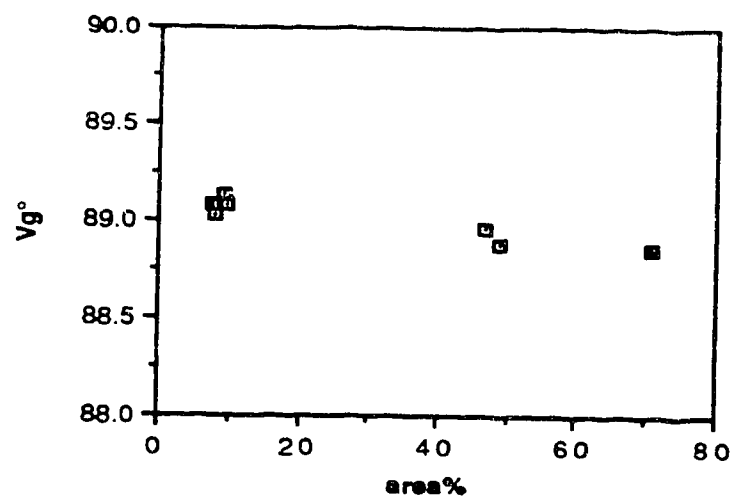
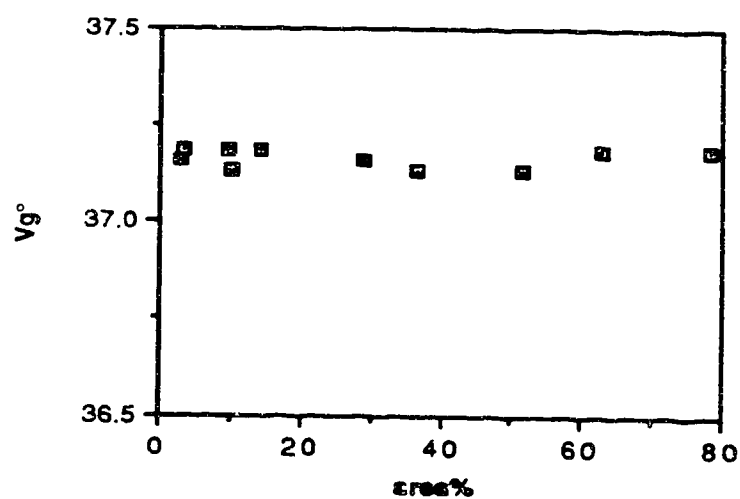


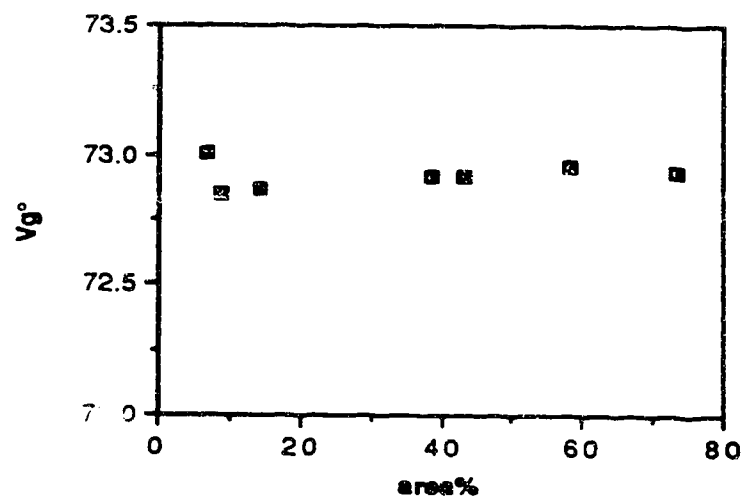
Figure 4-2B Graphs of specific retention volume against sample size for heptane and octane in Athabasca bitumen.



a) benzene at 60°C



b) toluene at 120°C



c) xylene at 120°C

Figure 4-3 Graphs of specific retention volume of benzene, toluene and xylene against sample size in Athabasca bitumen.

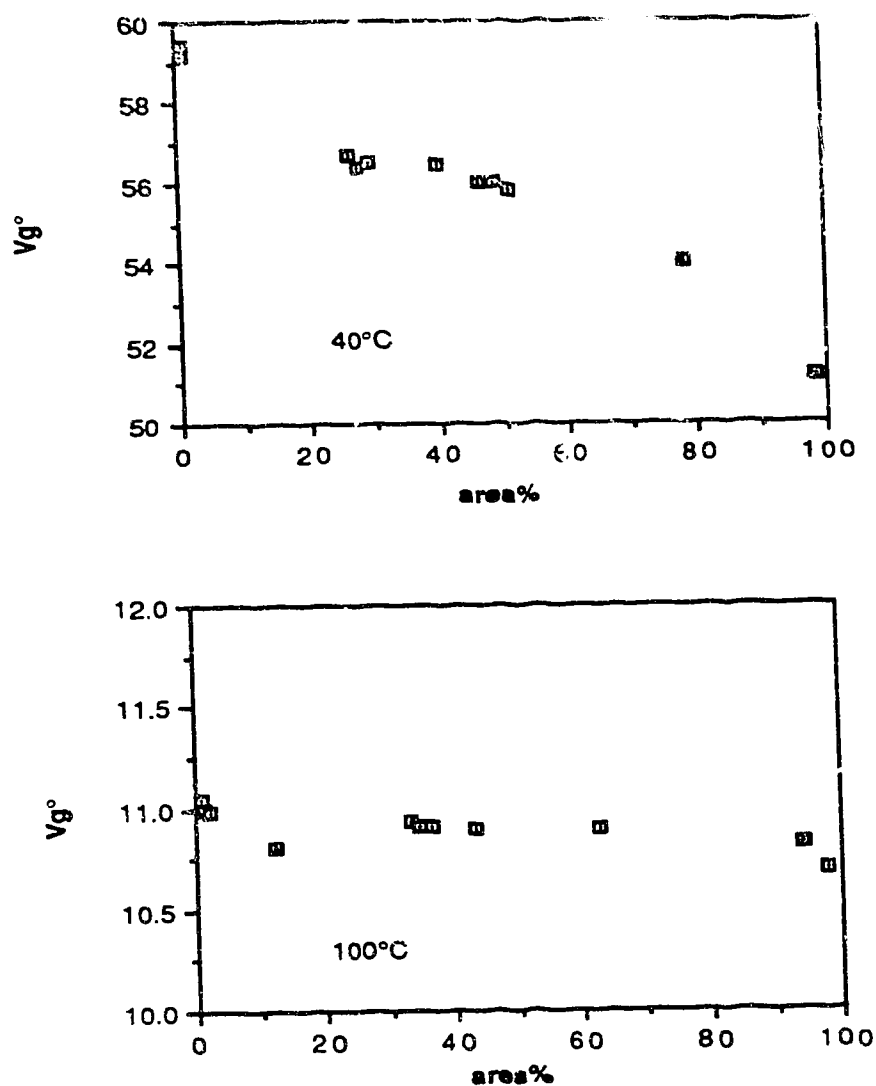


Figure 4-4 Graphs of specific retention volume of dichloromethane in Athabasca bitumen against sample size showing the dependence of retention volume on sample size

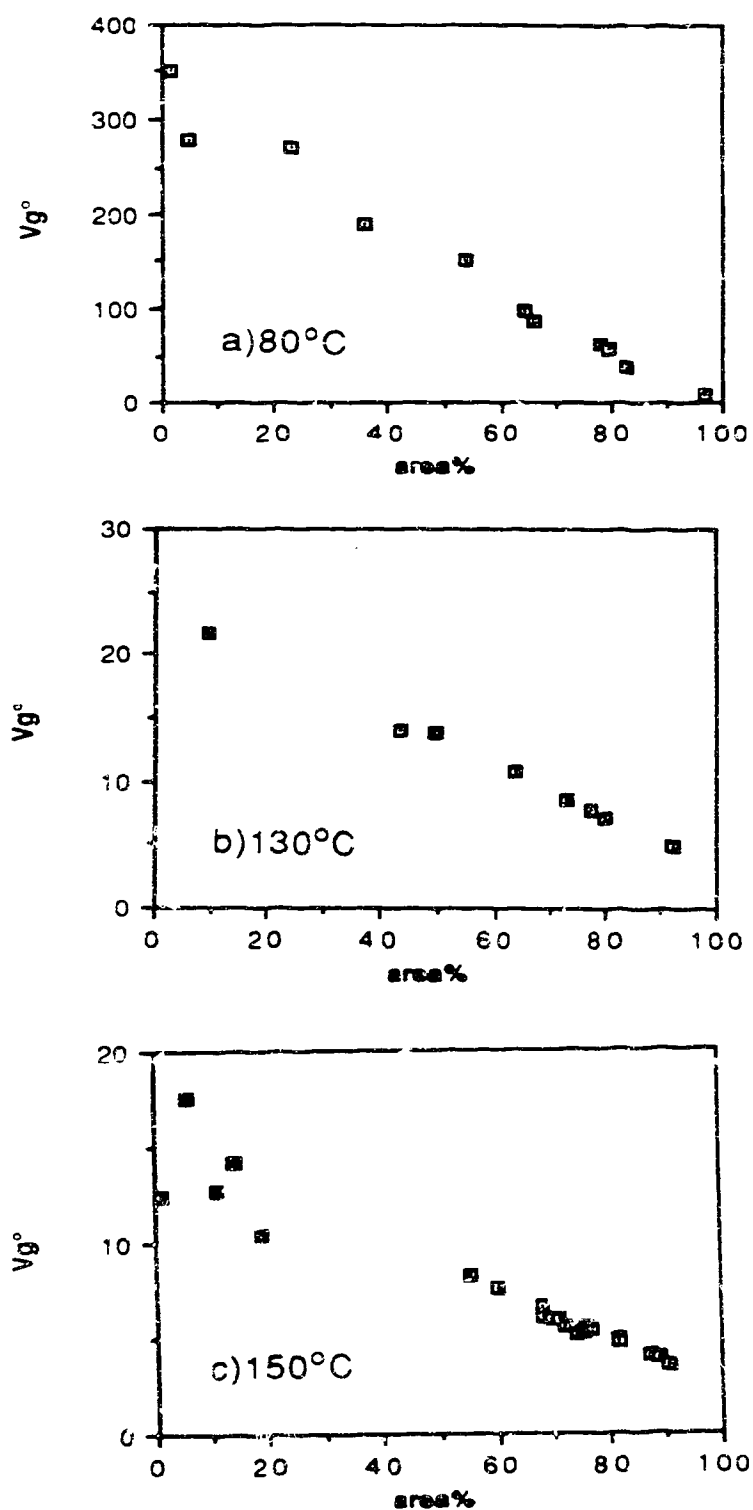


Figure 4-5 Graphs of specific retention volume of methanol in Athabasca bitumen against sample size showing the strong dependence of retention volume on sample size

Table 4-2 Liquid loadings in Athabasca and Wolf Lake bitumen columns

Column	Bitumen Loading (wt%)	
	Athabasca bitumen	Wolf Lake bitumen
column 1	8.38	11.31
column 2	7.97	13.97
column 3	18.66	5.17
column 4	12.37	
column 5	4.34	



## Results and Calculations

### Specific Retention Volumes

The specific retention volumes,  $V_g^\circ$ , were obtained directly from GLC retention time measurements using Equation (2-13). Table 4-3 presents the values for specific retention volumes of the solutes in Athabasca bitumen. Those for Wolf Lake bitumen are presented in Table 4-4. The specific retention volumes in Tables 4-3 and 4-4 are average values from five columns and three columns for Athabasca bitumen and Wolf Lake bitumen, respectively. These average specific retention volumes are used for further thermodynamic calculations.

### Henry's Law Constants

Henry's law constants,  $K_H$ , were obtained from specific retention volumes using Equation (2-38). The values of Henry's law constants for solutes in Athabasca and Wolf Lake bitumens are listed in Tables 4-5 and 4-6. Because the molecular weights of both bitumens were determined (the molecular weight for Athabasca bitumen is in agreement with the value measured and reported by Alberta Research Council<sup>58, 60</sup>), we can use Equation (2-38) to obtain the Henry's law constants. The Henry's law constants based on molality,  $K_H^m$  can also be calculated using Equation (3-45). These values are not presented in these tables, since they are easily obtained by multiplying  $K_H$  by  $M/1000$ .

### **Infinite Dilution Activity Coefficients.**

Vapor pressures of solutes at different temperatures that are needed for activity coefficient calculations in Equation (3-39) were calculated using Antoine or other equations. Table 4-7 lists the equations for the vapor pressure calculations along with the corresponding constants as well as the temperature ranges in which the equations apply. The infinite dilution activity coefficients were obtained using Equation (3-39). We present these values in Tables 4-8 and 4-9.

### **Calculation of $\Delta G^\circ$ , $\Delta H^\circ$ , $\Delta S^\circ$ and $\Delta C_p^\circ$ .**

First we choose  $\Delta H^\circ$  as temperature independent to obtain  $\Delta H^\circ$  values from the slopes of the lines in graphs of  $\ln V_g^\circ$  against  $1/T$  or by corresponding linear regression of  $\ln V_g^\circ$  against  $1/T$ . Figures 4-6 to 4-8 show these graphs for Athabasca bitumen and Figures 4-9 to 4-11 for Wolf Lake bitumen. Although lines in several of the graphs are not quite straight, we have calculated average slopes and thence the average (over the experimental temperature range)  $\Delta H^\circ$  values that are presented in Table 4-10.

It was observed that the curvature of lines in some graphs of  $\ln V_g^\circ$  against  $1/T$  was significant in relation to experimental uncertainties, which was confirmed by examination of the residuals of the linear fitting. Figure 4-12 is an example plot of residuals showing a definite curve, which illustrates that the enthalpy of solution is temperature dependent. Equation (3-34) was therefore

fitted to  $V_g^\circ$  values listed in Tables 4-3 and 4-4. Values of  $\Delta H_\theta^\circ$  and  $\Delta C_p^\circ$  were obtained from the non-linear least squares regression. Values of  $\Delta H_\theta^\circ$  and  $\Delta C_p^\circ$  are presented in Table 4-11. Note that  $\Delta H_\theta^\circ$  and  $\Delta C_p^\circ$  values are not reported for some solutes ( $\text{CO}_2$ ,  $\text{C}_2\text{-C}_4$ , and methanol) because experimental data for these substances are represented adequately by the simpler linear equation, which is equivalent to saying that some combinations of accuracy and temperature range are insufficient to permit evaluation of  $\Delta C_p^\circ$ . To evaluate the justification of the fit of Equation (3-34) the residuals were examined again and are given in Figure 4-13. The residuals from fitting of Equation (3-34) show random scatter, indicating that further consideration of possible temperature dependence of  $\Delta C_p^\circ$  expressed by Equation (3-24) is not justified.

The values of  $\Delta C_p^\circ$  can be used in combination with  $\Delta H_\theta^\circ$  to obtain  $\Delta H^\circ$  at any temperature through Equation (3-33). The  $\Delta C_p^\circ$  values are also related to the temperature dependence of entropy by Equation (3-10) that allows the calculation of  $\Delta S^\circ$  at any temperature from the knowledge of  $\Delta C_p^\circ$  and  $\Delta S_\theta^\circ$ . Values of  $\Delta G_\theta^\circ$  and  $\Delta S_\theta^\circ$  are also given in Table 4-11, as calculated using Equations (3-32) and (3-2), respectively.

TABLE 4-3 Specific retention volumes ( $\text{cm}^3 \text{g}^{-1}$ ) for solutes\* in Athabasca bitumen

t / °C	$V_g^o / \text{cm}^3 \text{g}^{-1}$											
	CO <sub>2</sub>	C <sub>2</sub>	C <sub>3</sub>	C <sub>4</sub>	C <sub>5</sub>	C <sub>6</sub>	C <sub>7</sub>	C <sub>8</sub>	Ben	Tol	Xyl	MeOH
30	0.789	0.951	3.08	11.0	35.0	106	-	-	-	-	-	82.8
40	0.632	0.843	2.64	8.80	25.1	73.0	201	550	-	-	-	55.5
50	0.480	0.734	2.24	6.96	18.7	-	-	-	-	-	-	38.4
60	0.386	0.649	1.88	5.56	14.3	37.1	92.1	233	91.7	245	618	29.0
70	-	0.578	-	4.56	11.2	-	-	-	-	-	-	20.9
80	-	-	-	-	8.86	20.7	46.7	108	49.5	120	284	16.6
90	-	-	-	-	7.20	16.3	34.4	76.9	36.9	-	-	218
100	-	-	-	-	5.86	12.6	26.3	56.4	29.6	66.2	141	10.4
110	-	-	-	-	-	-	-	-	22.9	49.1	102	103
120	-	-	-	-	3.87	8.04	15.8	31.1	18.5	38.1	76.7	51.2
130	-	-	-	-	-	-	-	-	15.2	30.3	57.6	28.0
150	-	-	-	-	-	4.57	8.26	14.5	10.2	19.1	34.7	15.3

\* Abbreviations for solutes are as follows: C<sub>3</sub>-C<sub>8</sub> (normal paraffanes, propane to octane); Ben (benzene); Tol (toluene); Xyl (xylene);

DCM (dichloromethane); MeOH (methanol)

TABLE 4-4 Specific retention volumes ( $\text{cm}^3 \text{g}^{-1}$ ) for solutes\* in Wolf Lake bitumen

t / °C	$V_g^o / \text{cm}^3 \text{g}^{-1}$										
	CO <sub>2</sub>	C <sub>2</sub>	C <sub>3</sub>	C <sub>4</sub>	C <sub>5</sub>	C <sub>6</sub>	C <sub>7</sub>	C <sub>8</sub>	Ben	Tol	Xyl
30	0.484	0.774	2.34	8.60	-	-	-	-	-	-	-
40	0.442	0.669	1.95	6.80	-	-	-	-	-	-	-
50	0.389	0.609	1.65	5.46	15.0	40.8	-	-	-	-	-
60	0.331	0.548	1.41	4.38	11.6	29.7	-	-	-	-	-
70	0.295	0.491	1.13	3.52	9.04	21.4	-	-	-	-	-
80	0.262	0.422	-	-	7.21	16.8	38.7	87.7	40.6	97.6	225
90	-	-	-	-	5.82	13.0	28.5	62.4	30.9	71.4	160
100	-	-	-	-	4.76	10.2	21.7	45.5	24.0	53.3	115
110	-	-	-	-	3.99	8.18	16.7	33.9	19.0	40.5	84.2
120	-	-	-	-	3.36	6.76	13.2	25.8	15.0	30.7	61.6
130	-	-	-	-	2.87	5.59	10.6	20.0	12.3	24.5	47.6
140	-	-	-	-	2.45	4.68	8.50	15.6	9.87	19.0	35.7
150	-	-	-	-	-	-	-	-	8.37	15.7	28.6

\* Abbreviations for solutes are the same as in Table 4-3

TABLE 4-5

Henry's Law constants (atm) for solutes\* in Athabasca bitumen

t / °C	K <sub>H</sub> / atm												
	CO <sub>2</sub>	C <sub>2</sub>	C <sub>3</sub>	C <sub>4</sub>	C <sub>5</sub>	C <sub>6</sub>	C <sub>7</sub>	C <sub>8</sub>	Ben	Tol	Xyl	DCM	MeOH
30	51.3	42.5	13.1	3.67	1.16	.382	-	-	-	-	-	0.490	-
40	64.0	48.0	15.3	4.59	1.61	.554	0.201	0.0737	-	-	-	0.729	-
50	84.3	55.1	18.1	5.82	2.16	-	-	-	-	-	-	1.05	-
60	105	62.3	21.5	7.28	2.83	1.09	0.440	0.174	0.441	0.166	0.0654	1.40	-
70	-	70.0	-	8.87	-	-	-	-	-	-	-	1.93	-
80	-	-	-	-	4.57	1.95	0.866	0.374	0.817	0.336	0.142	2.43	0.113
90	-	-	-	-	5.62	2.48	1.18	0.526	1.10	-	-	-	0.186
100	-	-	-	-	6.92	3.21	1.54	0.717	1.37	0.613	0.287	-	0.265
110	-	-	-	-	-	-	-	-	1.76	0.824	0.399	-	0.391
120	-	-	-	-	10.5	5.03	2.57	1.30	2.18	1.06	0.528	-	0.789
130	-	-	-	-	-	-	-	-	2.66	1.33	0.703	-	1.45
150	-	-	-	-	-	8.86	4.90	2.79	3.96	2.12	1.17	-	2.64

\* Abbreviations for solutes are the same as in Table 4.3

TABLE 4-6 Henry's Law constants (atm) for solutes\* in Wolf Lake bitumen

t/°C	K <sub>H</sub> /atm												
	CO <sub>2</sub>	C <sub>2</sub>	C <sub>3</sub>	C <sub>4</sub>	C <sub>5</sub>	C <sub>6</sub>	C <sub>7</sub>	C <sub>8</sub>	Ben	Tol	Xyl	DCM	MeOH
30	72.4	44.2	14.8	4.04	-	-	-	-	-	-	-	0.605	-
40	77.5	51.2	17.8	5.11	-	-	-	-	-	-	-	0.849	-
50	88.2	56.3	21.0	6.36	-	-	-	-	-	-	-	1.22	-
60	104	62.6	24.6	7.96	3.00	1.17	-	-	-	-	-	1.55	-
70	116	69.8	30.7	9.87	3.84	1.63	-	-	-	-	-	-	-
80	131	81.2	-	-	4.82	2.07	0.897	0.396	0.855	0.355	0.154	2.61	0.296
90	-	-	-	-	5.96	2.67	1.22	0.557	1.12	0.487	0.217	-	0.405
100	-	-	-	-	7.29	3.39	1.61	0.763	1.45	0.651	0.303	4.07	0.575
110	-	-	-	-	8.70	4.25	2.08	1.02	1.83	0.857	0.412	4.96	0.954
120	-	-	-	-	10.3	5.13	2.53	1.34	2.33	1.13	0.563	5.99	1.25
130	-	-	-	-	12.1	6.21	3.28	1.74	2.83	1.42	0.729	7.18	1.80
140	-	-	-	-	14.2	7.42	4.08	2.22	3.51	1.83	0.972	-	3.47
150	-	-	-	-	-	-	-	-	4.14	2.21	1.21	-	-

\* Abbreviations for solutes are the same as in Table 4-3

Table 4-7 Equations for vapor pressure calculations

Solute	Equation	Constant	Temperature Range
C <sub>3</sub>	Antoine Equation	A = 7.41188	4.40-87.7°C
	$\log P = A - B/(t+C)$	B = 1149.360	
	(t : °C, P: cmHg)	C = 298.050	
C <sub>4</sub>	Antoine Equation	A = 7.23086	-0.49-152 °C
		B = 1175.581	
		C = 271.079	
C <sub>5</sub>	Wagner Equation		144-469 K
	$\ln P = 1/T_r [A(1-T_r) +$	A = -7.2430	
	$B(1-T_r)^{1.5} +$	B = 1.44019	
	$C(1-T_r)^{2.5} +$	C = -2.89556	
	$D(1-T_r)^5]$	D = -2.086207	
	(T: K, P : kPa)		
C <sub>6</sub>	Riedel Equation	A = 533.3412	177-508 K
	$\ln P = A + B \ln T + C/T$	B = -5.593326	
	$+DT^6$	C = -5509.8512	
	(T: K, P: kPa)	D = 2.259624x10 <sup>-16</sup>	
C <sub>7</sub>	Riedel Equation	A = 62.808752	185-454 K
		B = -6.8926277	
		C = -6474.2355	
		D = 2.2179356x10 <sup>-17</sup>	
C <sub>8</sub>	Riedel Equation	A = 69.033523	216-484 K
		B = -7.7048846	



		C = -7315.5167 D = $1.754326 \times 10^{-17}$	
ben	Vapres-2 Equation $\ln P = A + B/T + CT + DT^2 + E \ln T$ (T: K, P: kPa)	A = 124.86728 B = -7564.7711 C = 0.024669095 D = $-4.0448273 \times 10^{-6}$ E = $-1.824444 \times 10^{-3}$	278-478 K
tol	Wagner Equation	A = -7.37328 B = 1.586866 C = -2.950635 D = -2.7393712	195-594 K
xyl	Antoine Equation	A = 7.01117 B = 1463.218 C = 215.159 A = 7.35037 B = 1749.900 C = 252.747	59.2-140.04 °C  146.85-326.85 °C
CH <sub>2</sub> Cl <sub>2</sub>	Wagner Equation	A = -5.82559 B = -1.09829 C = 0.65916530 D = -9.8170887	292-511 K
MeOH	Antoine Equation	A = 8.18811 B = 1676.569 C = 251.422	80-210 °C

---

TABLE 4-8

Infinite dilution activity coefficients for solutes\* in Athabasca bitumen

t / °C	$\gamma_2^\infty$										
	C <sub>3</sub>	C <sub>4</sub>	C <sub>5</sub>	C <sub>6</sub>	C <sub>7</sub>	C <sub>8</sub>	Ben	Tol	Xyl	DCM	MeOH
30	1.224	1.309	1.432	1.551	-	-	-	-	-	0.703	-
40	1.127	1.225	1.416	1.507	1.656	1.819	-	-	-	0.723	-
50	1.064	1.185	1.380	-	-	-	-	-	-	0.741	-
60	1.028	1.152	1.337	1.445	1.587	1.688	0.855	0.906	1.008	0.712	-
70	1.109	1.285	-	-	-	-	-	-	-	0.732	-
80	-	-	1.246	1.388	1.535	1.624	0.819	0.876	0.954	0.697	0.063
90	-	-	1.189	1.330	1.513	1.594	0.815	-	-	-	0.074
100	-	-	1.148	1.322	1.468	1.549	0.770	0.833	0.933	0.671	0.076
110	-	-	-	-	-	-	0.763	-	0.934	-	0.082
120	-	-	1.090	1.279	1.417	1.522	0.738	0.818	0.907	-	0.125
130	-	-	-	-	-	-	0.711	0.790	0.903	-	0.173
150	-	-	-	1.202	1.338	1.484	0.689	0.771	0.878	-	0.191

\* Abbreviations for solutes are the the same as in Table 4-3

TABLE 4-9

Infinite dilution activity coefficients for solutes\* in Wolf Lake bitumen

t / °C	$\gamma_2^\infty$										
	C <sub>3</sub>	C <sub>4</sub>	C <sub>5</sub>	C <sub>6</sub>	C <sub>7</sub>	C <sub>8</sub>	Bez	Tol	Xyl	DCM	MeOH
30	1.382	1.437	-	-	-	-	-	-	-	0.868	-
40	1.310	1.361	-	-	-	-	-	-	-	0.841	-
50	1.240	1.295	1.478	1.594	-	-	-	-	-	0.857	-
60	1.176	1.360	1.420	1.547	-	-	-	-	-	0.794	-
70	1.202	1.233	1.369	1.559	-	-	-	-	-	-	-
80	-	-	1.314	1.465	1.590	1.722	0.858	0.926	1.034	0.747	0.166
90	-	-	1.262	1.437	1.569	1.685	0.836	0.909	1.002	-	0.161
100	-	-	1.210	1.396	1.528	1.648	0.813	0.889	0.985	0.701	0.165
110	-	-	1.141	1.363	1.499	1.611	0.791	0.871	0.964	0.678	0.201
120	-	-	1.078	1.306	1.457	1.576	0.784	0.870	0.968	0.657	0.198
130	-	-	1.008	1.269	1.414	1.537	0.758	0.832	0.936	0.642	0.217
140	-	-	0.947	1.228	1.394	1.517	0.754	0.843	0.950	-	0.321
150	-	-	-	-	-	-	0.722	0.805	0.914	-	-

\* Abbreviations for solutes are the same as in Table 4-3

Table 4-10  
Average enthalpies  $\Delta H^\circ$  (kJ mol<sup>-1</sup>) of solution of gases/vapours in bitumens

Solutes	Athabasca Bitumen	Wolf Lake Bitumen
Carbon dioxide	-18	-11
Ethane	-12	-10
Propane	-17	-15
Butane	-16	-19
Pentane	-20	-22
Hexane	-23	-27
Heptane	-32	-31
Octane	-37	-35
Benzene	-28	-28
Toluene	-33	-33
Xylene	-38	-37
Dichloromethane	-28	-25
Methanol	-58	-48

Table 4-11

 $\Delta H_{\theta}^{\circ}$ ,  $\Delta G_{\theta}^{\circ}$ ,  $\Delta S_{\theta}^{\circ}$  and  $\Delta C_p^{\circ}$  for dissolving gases/vapours in bitumens

solute	$\theta$ (K)	$-\Delta H_{\theta}^{\circ}$ (kJ mol <sup>-1</sup> )	$\Delta G_{\theta}^{\circ}$ (kJ mol <sup>-1</sup> )	$-\Delta S_{\theta}^{\circ}$ (J K <sup>-1</sup> mol <sup>-1</sup> )	$\Delta C_p^{\circ}$ (J K <sup>-1</sup> mol <sup>-1</sup> )
Athabasca bitumen					
C5	353.15	23.8	4.46	80.0	17±10
C6	363.15	27.7	2.74	83.8	33±4
C7	353.15	32.4	-0.422	90.6	50±4
C8	373.15	36.1	-1.032	94.0	28±4
Ben	383.15	27.8	1.80	77.3	70±10
Tol	383.15	32.8	-0.617	84.0	40±10
Xyl	383.15	37.3	-2.93	89.7	32±7
DCM	333.15	28.0	0.932	86.8	115±20
Wolf Lake bitumen					
C5	373.15	22.0	6.16	75.5	35±4
C6	373.15	26.1	3.79	80.1	62±10
C7	383.15	30.4	2.33	85.4	58±14
C8	383.15	34.8	0.063	91.0	53±8
Ben	383.15	28.3	1.93	78.9	32±17
Tol	383.15	32.8	-0.942	84.3	39±10
Xyl	383.15	37.0	-2.82	89.2	21±8
DCM	353.15	24.7	2.82	77.9	48±13

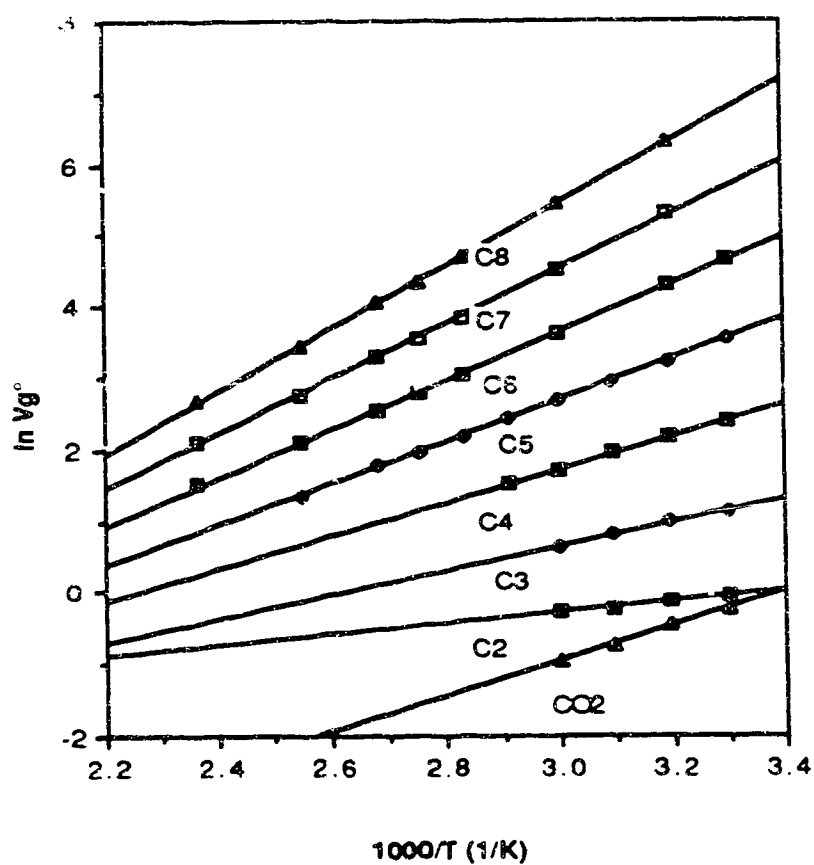


Figure 4-6 A graph of  $\ln V_g^\circ$  against  $1/T$  for carbon dioxide, and the alkanes from ethane to octane in Athabasca bitumen. Slopes from linear fittings lead to average enthalpies over the temperature range.

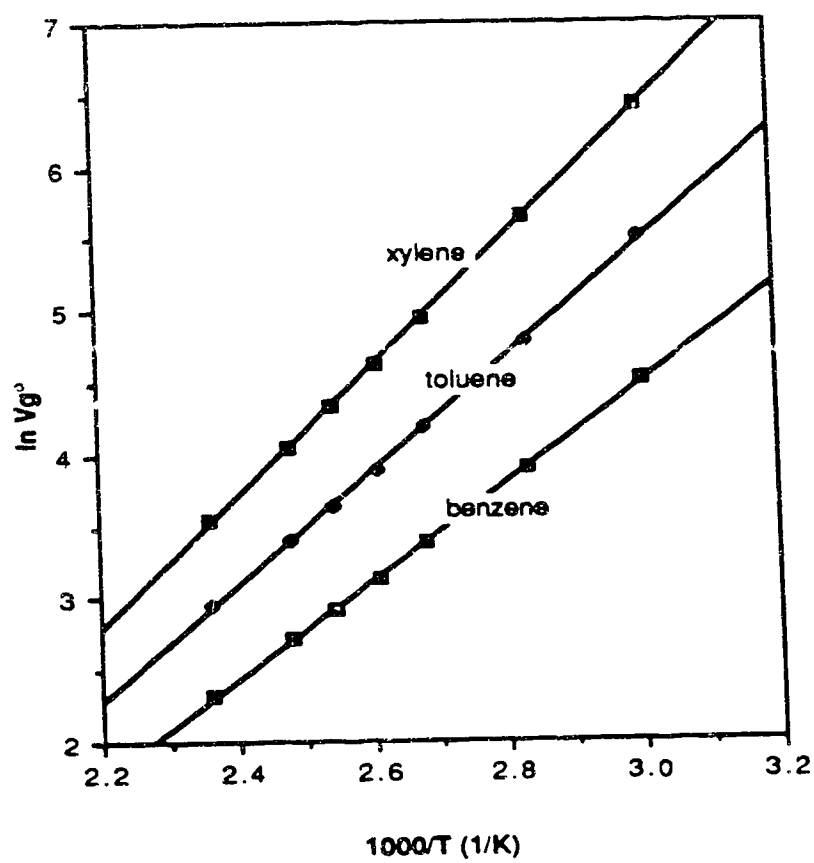


Figure 4-7 A graph of  $\ln V_g^\circ$  against  $1/T$  for benzene, toluene, and xylene in Athabasca bitumen

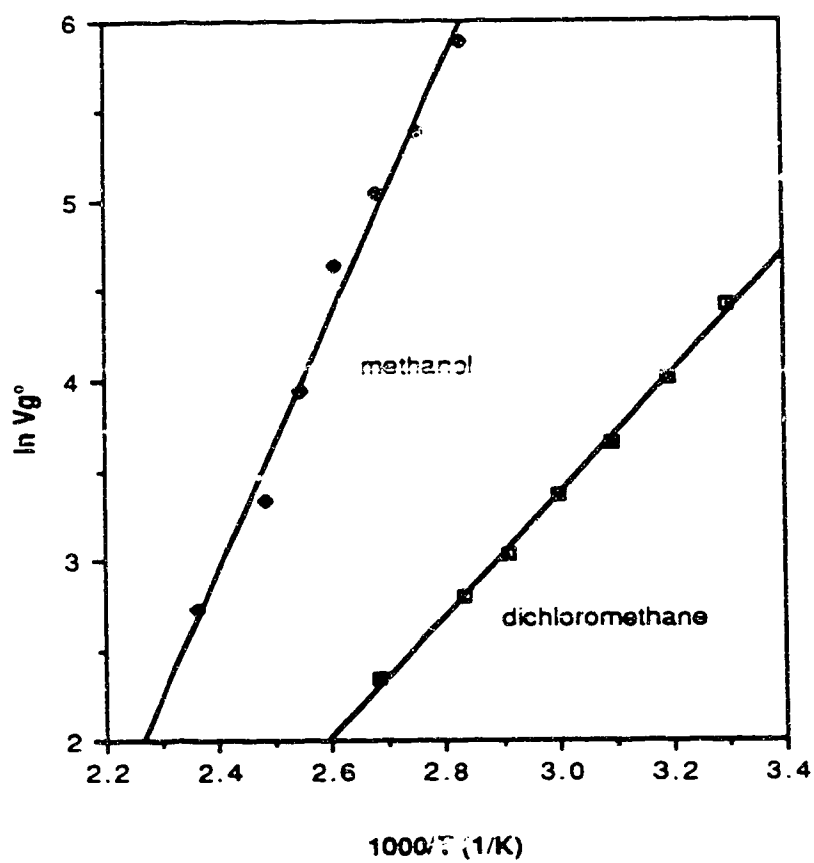


Figure 4-8 A graph of  $\ln V_g^\circ$  against  $1/T$  for dichloromethane and methanol in Athabasca bitumen



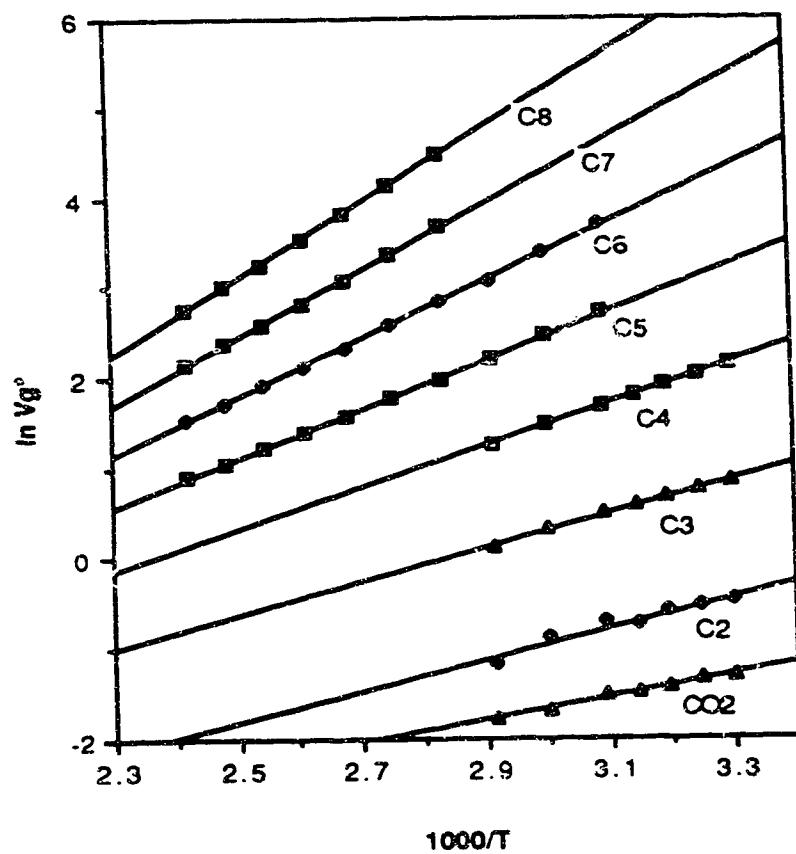


Figure 4-9 A graph of  $\ln V_g^\circ$  against  $1/T$  for carbon dioxide, and alkanes from ethane to octane in Wolf Lake bitumen.

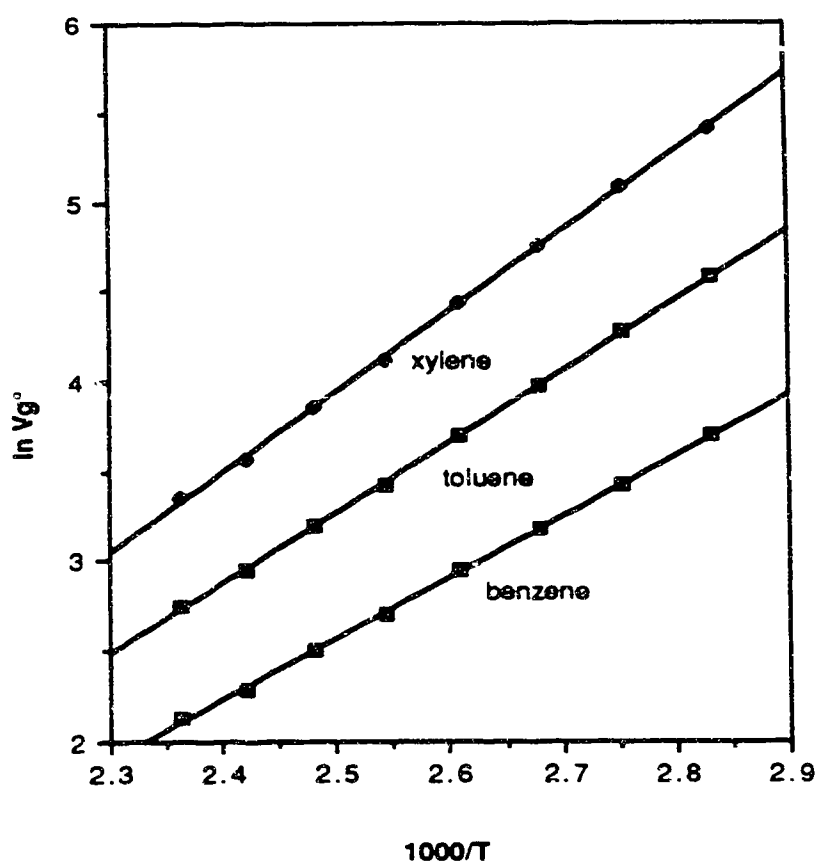


Figure 4-10 A graph of  $\ln V_g^\circ$  against  $1/T$  for benzene, toluene, xylene in Wolf Lake bitumen.

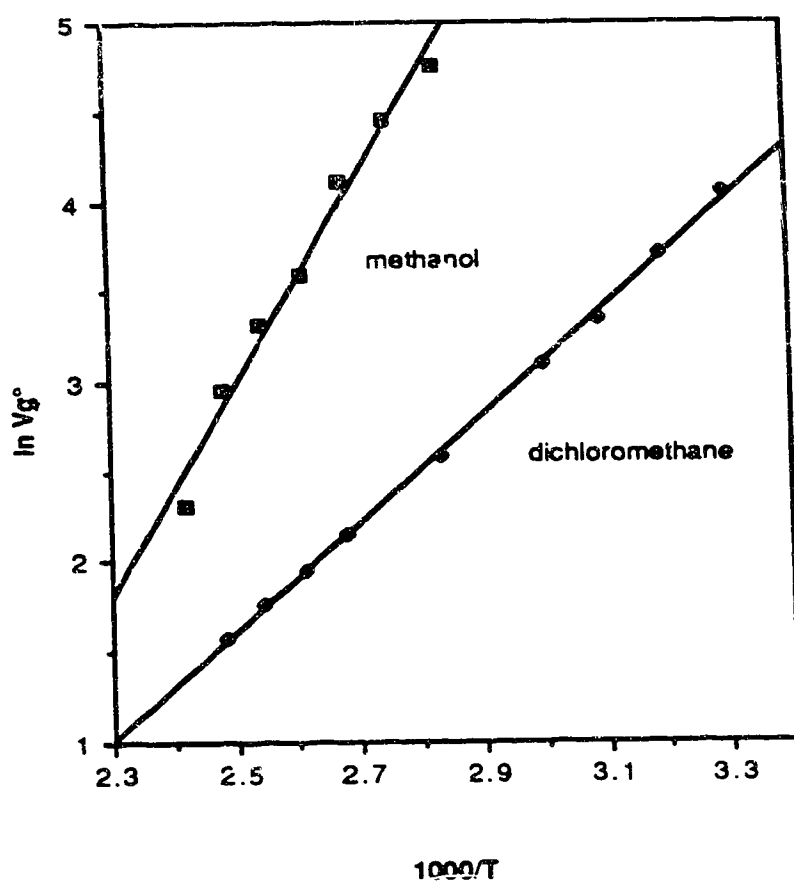


Figure 4-11 A graph of  $\ln V_g^\circ$  against  $1/T$  for dichloromethane and methanol in Wolf Lake bitumen.

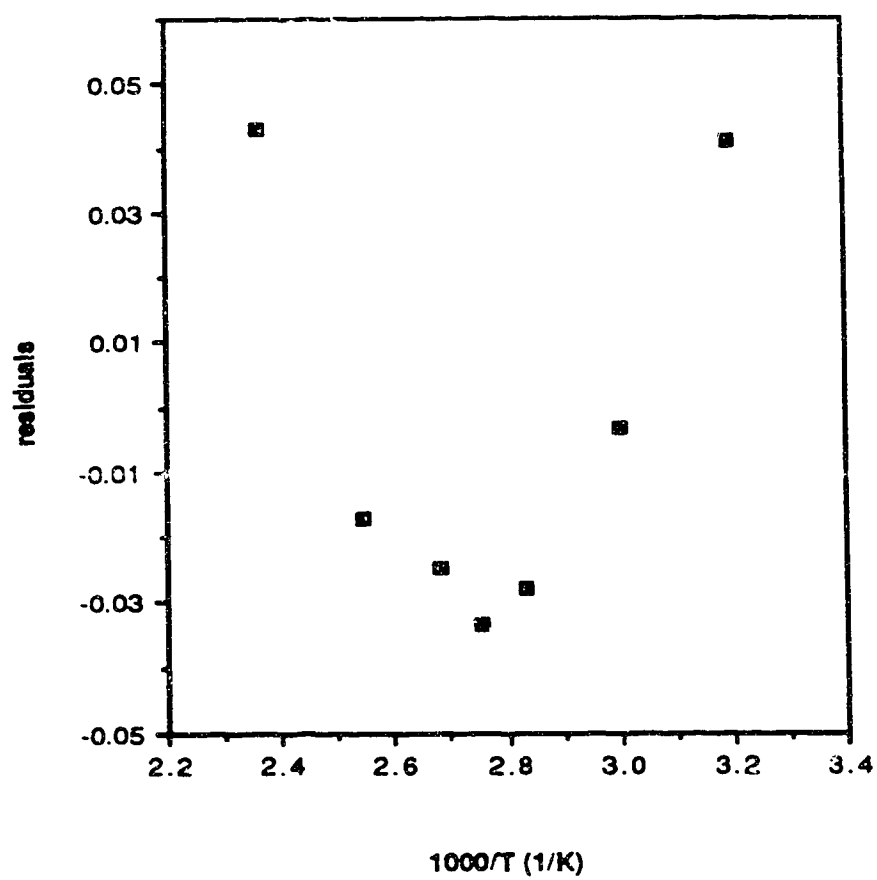


Figure 4-12 Residuals from fitting  $\ln V_g^\circ$  to linear function of  $1/T$ , showing an obvious temperature dependence.

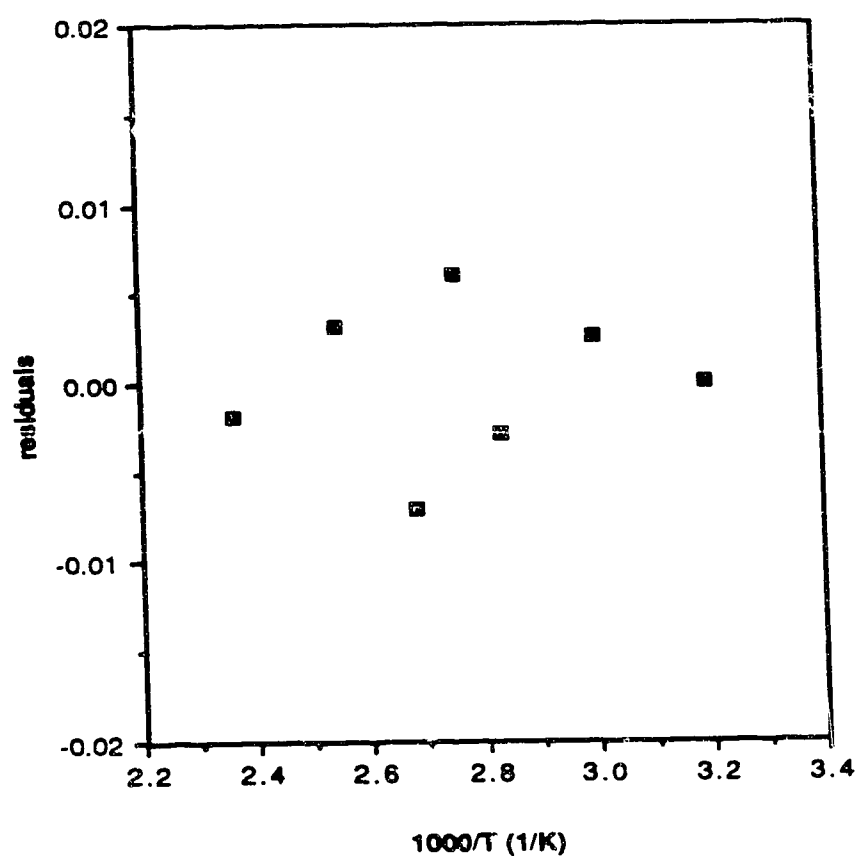


Figure 4-13 Residuals from fitting  $\ln V_g^\circ$  to Equation 3-34, showing randomly scattered residuals.

## Discussion

### Comparison of Henry's Law Constants

Most previous measurements of solubilities of gases in bitumen have been made at pressures of the order of 1 MPa (10 atm) or higher. Solubilities of gases at these pressures are of direct technological importance, but are not directly related to Henry's law constants that are useful for thermodynamic calculations. Some examples of complications associated with evaluation of Henry's law constants from such relatively high pressure solubility data have been discussed by Lu *et al.*<sup>56</sup> and by Bottomley *et al.*<sup>57</sup> Considering the experimental difficulties associated with conventional equilibrium measurements of solubilities of gases in bitumen (especially at lower temperatures where the bitumen has very high viscosities) and also the uncertainties in calculations of Henry's law constants from the high pressure solubility data, it is remarkable that there is reasonably good agreement between many of the independent results for carbon dioxide in Athabasca bitumen as summarized below.

We begin our comparisons by considering the results for the highest temperature, and proceed toward consideration of lower temperature results. The solubility results for carbon dioxide in Athabasca bitumen from Fu, *et al.*<sup>58</sup> lead us to  $K_H \approx 231$  atm for 100°C, which is in excellent agreement with our  $K_H = 229$  atm for this same temperature, obtained by extrapolation ( $\ln K_H$  vs  $1/T$ ) of

our results. Earlier results from Svrcek and Mehrotra<sup>59</sup> lead to  $K_H \approx 182$  atm for 97°C, which is in poor agreement with our  $K_H = 216$  atm for this same temperature. Mehrotra *et al.*<sup>60</sup> have reported results of comparative research done at the University of Calgary (78.7-80.4°C) and the Alberta Research Council (80.0°C). Their results lead to  $K_H \approx 138$  and 160 atm, respectively. The former result is in fair agreement with our  $K_H = 157$  atm, while the latter result is in excellent agreement with our value. Earlier results from Svrcek and Mehrotra<sup>59</sup> for 63°C lead us to  $K_H \approx 117$  atm, in good agreement with our  $K_H = 111$  atm for this same temperature. Other results from Svrcek and Mehrotra<sup>59</sup> for 42 and 24°C lead to  $K_H \approx 99$  and 82 atm, as compared with our  $K_H = 68$  and 44 atm, respectively, for these same temperatures.

### Comparison of Enthalpies of Solution

We have used the  $K_H$  values calculated from the solubility data of Svrcek and Mehrotra<sup>59</sup> and Mehrotra *et al.*<sup>60</sup> to estimate the enthalpy of solution of carbon dioxide in Athabasca bitumen as  $\Delta H^\circ \approx 9 \pm 4$  kJ mol<sup>-1</sup>. The difference between this value and our  $\Delta H^\circ = 18 \pm 3$  kJ mol<sup>-1</sup> is somewhat greater than the sum of estimated uncertainties. In the absence of a definitive enthalpy of solution from calorimetric measurements (very difficult because of high viscosity) or another  $\Delta H^\circ$  calculated from further solubility data, we are unable to categorize one value as "better" than the other.

Since enthalpies of solution for solutes in bitumens have not been determined previously we are unable to compare our enthalpies of solution with literature data. However, there are several literature data on the enthalpies of solution of these solutes in some high carbon number alkanes. Because bitumen is composed of many hydrocarbons, it is of interest to compare our data with those for the same solutes in pure alkane solvents as shown in Table 4-12. Although the data listed in Table 4-12 were obtained by different authors, they are remarkably constant for a solute in different alkane solvents. We note that  $\Delta H^\circ$  for solutes in paraffin and bitumen are very close. This is expected since both bitumen and paraffin are mixtures of high boiling-point hydrocarbons. In addition, the average  $\Delta H^\circ$  for a solute in all alkanes and liquid paraffin was calculated and listed in the same table. We note that  $\Delta H^\circ$  values for solutes in Athabasca bitumen are close to the averaged values, which might suggest to petroleum and bitumen researchers that a mixture of selected high boiling-point hydrocarbons could be used as an approximate model for bitumen.

Detailed examination of Tables 4-10 and 4-12 reveals that for alkane solutes, the enthalpies of solution show a linear relationship with the carbon numbers of solutes. Figure 4-14 shows a graph of average  $\Delta H^\circ$  of solution (Table 4-9) for normal alkanes from  $C_2$  to  $C_8$  in Athabasca bitumen, which gives a linear relation. Similar linear relationships have been found for other homologous series of solutes.<sup>1</sup> This can be explained qualitatively as follows.

The enthalpy of solution for a homologous series can be expressed in terms of two kinds of contributions: (1) methylene ( $-CH_2$ ) and methyl ( $-CH_3$ ) groups and



Table 4-12 Enthalpies of solution ( $\text{kJ mol}^{-1}$ ) for solutes in selected alkane solvents and in paraffin and bitumen

solvent	$\Delta H / \text{kJ mol}^{-1}$					
	n-C <sub>5</sub>	n-C <sub>6</sub>	n-C <sub>7</sub>	n-C <sub>8</sub>	CH <sub>2</sub> Cl <sub>2</sub>	methanol
n-C <sub>20</sub> <sup>a</sup>	24.9	29.6	34.4	39.2	23.0	
n-C <sub>22</sub> <sup>b</sup>	23.6	28.1	32.6	36.9		
n-C <sub>24</sub> <sup>b</sup>	24.4	28.6	33.1	37.9		
c	24.5	28.6	33.3	37.7		
d		28.9				
n-C <sub>28</sub> <sup>b</sup>	25.2	29.5	34.1	38.7		
n-C <sub>30</sub> <sup>b</sup>	24.4	28.9	33.5	38.0		
n-C <sub>32</sub> <sup>b</sup>	24.2	28.6	32.9	37.6		
n-C <sub>34</sub> <sup>b</sup>	24.1	28.6	33.0	37.6		
n-C <sub>36</sub> <sup>b</sup>	24.4	28.6	33.3	37.8		
liquid paraffin <sup>e</sup>	25.1	28.5	32.1		27	57
average	24.5±0.5	28.8±0.5	33.2±0.7	37.9±0.7		
Athabasca bitumen <sup>f</sup>	23±0.6	28±0.3	32±0.2	37±0.3	28±0.8	58±2

a: reference 61

b: reference 14

c: reference 62

d: reference 63

e: reference 64

f: present work

(2) non-methyl or methylene functional groups. This can be expressed by the equation

$$\Delta H^\circ = n\Delta H^\circ_{\text{CH}_2} + \Delta H^\circ_{\text{non-CH}_2} \quad (4-4)$$

in which  $\Delta H^\circ_{\text{CH}_2}$  is the contribution due to one methyl or methylene group,  $n$  is the number of methyl or methylene group in the solute molecules, and  $\Delta H^\circ_{\text{non-CH}_2}$  is the contribution due to the functional groups (non-methyl and non-methylene). Since methyl and methylene groups are non-polar, they contribute to the molecular interactions and, consequently, to  $\Delta H^\circ$  only by the London dispersion forces. As each methylene group is added to the molecules, the corresponding London dispersion forces increase proportionally. Therefore,  $\Delta H^\circ$  increases linearly with the carbon number of alkane solutes as shown in Figure 4-14. Non-methylene functional groups (such as -OH) are polar groups. They contribute to the enthalpy of solution by very strong molecular interactions such as hydrogen bonding, dipole-dipole interactions, and dipole-induced dipole interactions. These interactions are much stronger than London forces. Therefore enthalpies of solution are often large and less predictable for polar compounds. This explains why methanol and dichloromethane have exceptionally high enthalpies of solution compared to the alkanes as shown in Table 4-10.

### **Solubilities of Methane in Bitumens**

We have been unable to apply the gas-liquid chromatographic (GLC) method to determination of Henry's law constants for methane in bitumen

because the retention time for methane is very close to that for neon, which we have used for evaluation of the dead time for each column. Because of the technological importance of the solubility of methane in bitumen, it is worth considering estimation of the desired quantities on the basis of our results for heavier alkane solutes.

As shown in Figure 4-14, a linear relation between  $\Delta H^\circ$  and carbon numbers of alkane was obtained, which permits estimation of the desired  $\Delta H^\circ$  of solution of methane ( $C_1$ ) in Athabasca bitumen. The same procedure can be used for Wolf Lake bitumen.

Figure 4-15 shows a graph of  $\ln K_H$  (for 40 and 60°C) against carbon number for alkane solutes from  $C_2$  to  $C_8$  in Athabasca bitumen. Similar graphs with fewer points are obtained for other temperatures. Our results for the same solutes in Wolf Lake bitumen lead to similar graphs. Again the observed linear relationships between  $\ln K_H$  and carbon number permit estimation of  $\ln K_H$  for methane ( $C_1$ ) at each temperature.

Results of the estimation procedure described above lead to  $\Delta H^\circ \approx -5.9 \text{ kJ mol}^{-1}$  for methane in Athabasca bitumen and  $\Delta H^\circ \approx -6.9 \text{ kJ mol}^{-1}$  for methane in Wolf Lake bitumen. Corresponding estimates of Henry's law constants for methane in these bitumens are summarized by

$$\ln K_H = -(705/T) + 7.12 \quad (\text{methane in Athabasca bitumen}) \quad (4-5)$$

and

$$\ln K_H = -(829/T) + 7.61 \quad (\text{methane in Wolf Lake bitumen}) \quad (4-6)$$

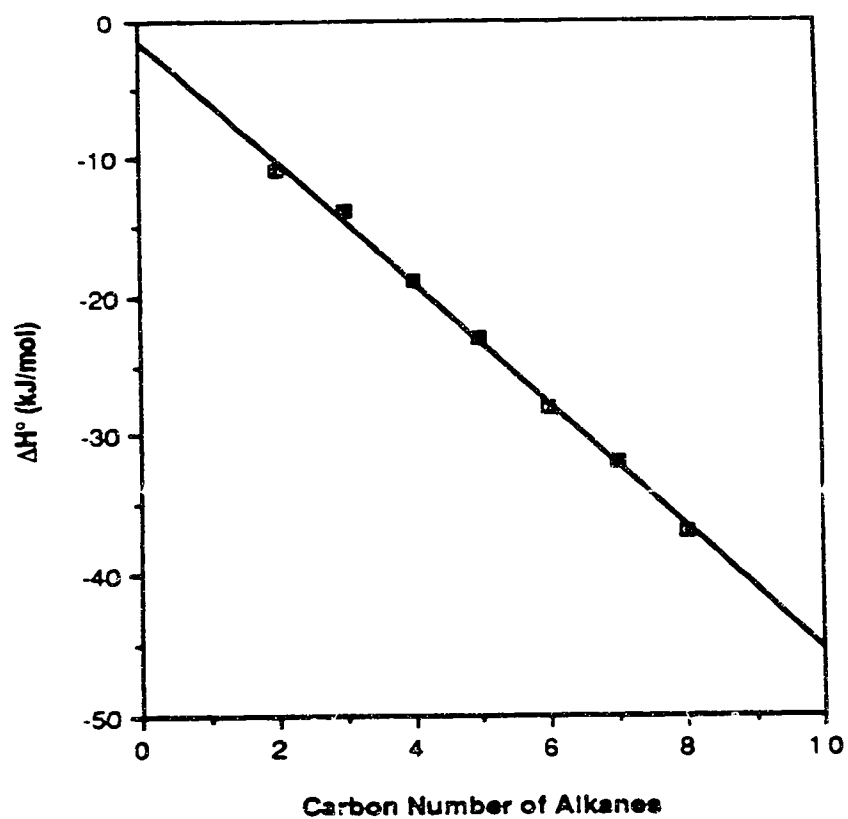


Figure 4-14 A graph of enthalpies of solution against carbon numbers for alkane solutes (ethane to octane) in Athabasca bitumen.

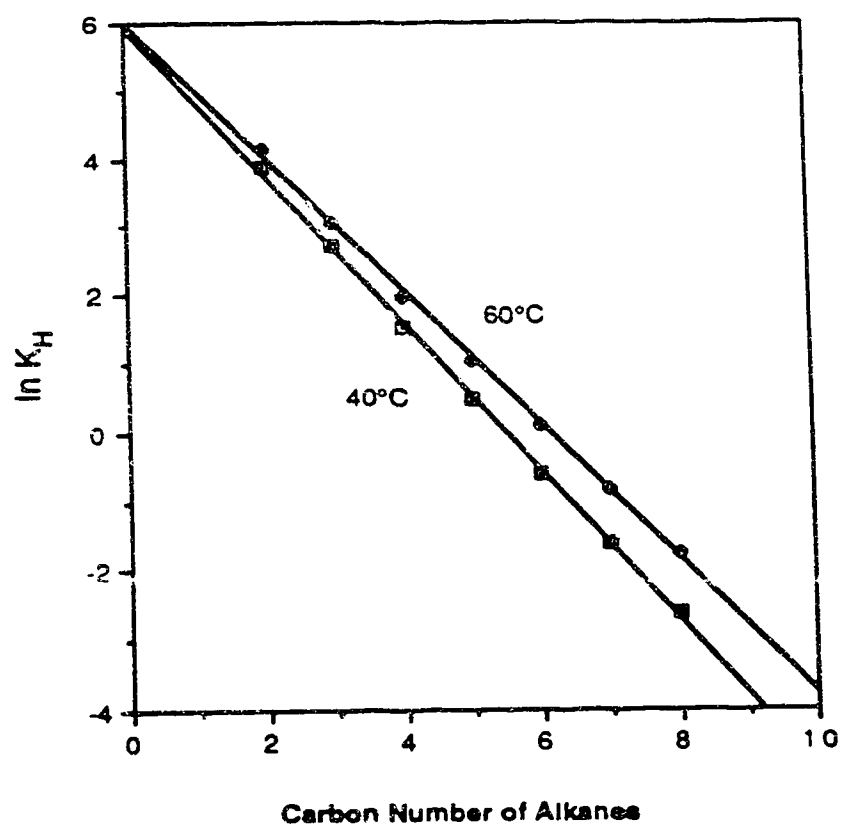


Figure 4-15 A graph of  $\ln K_H$  for alkane solutes (ethane to octane) in Athabasca bitumen at 40°C and 60°C against carbon numbers.

## Variation of Activity Coefficient with Carbon Number of Solute

### Alkanes

Infinite dilution activity coefficients measure the deviation of solute properties from Raoult's law. This activity coefficient is generally considered to be composed of two contributions called athermal activity coefficient ( $\gamma^{\text{ath}}$ ) and thermal activity coefficient ( $\gamma^{\text{th}}$ ). The athermal activity coefficient is independent of temperature and is associated with the statistical effects due to inequalities in the volumes of the molecules of the solutes and solvents. The thermal activity coefficient is dependent on temperature and is associated with the interaction energies between molecules. The athermal contribution is not important for some solutions, but it becomes significant for us since the molecular sizes of our solutes and solvents are quite different. The thermal factor is always present for non-ideal solutions.

Several theories have been developed to calculate and predict the activity coefficient and/or their contribution terms,  $\gamma^{\text{ath}}$  and  $\gamma^{\text{th}}$ .<sup>65-72</sup> These theories are based on the molecular sizes, molecular structures and some other molecular properties of both solute and solvent. Thus we can not apply these theories to our bitumen system quantitatively because bitumen is so complicated that we are unable to know about individual molecules and their structures. Instead, we can discuss our activity coefficients only qualitatively with the aid of the theories.

As mentioned previously, the activity coefficient can be expressed as two terms

$$\ln \gamma^{\infty} = \ln \gamma^{\text{ath}} + \ln \gamma^{\text{th}} \quad (4-7)$$

or 
$$\gamma^{\infty} = \gamma^{\text{ath}} \gamma^{\text{th}} \quad (4-8)$$

The athermal term  $\gamma^{\text{ath}}$  is related to the excess entropy of solution and can be evaluated by the approximate form of Flory and Huggins theory<sup>65-69</sup>

$$\ln \gamma^{\text{ath}} = \ln \frac{1}{r} + \left(1 - \frac{1}{r}\right) \quad (4-9)$$

In which  $r$  is the size ratio of molecules (stationary phase/solute). For our systems  $r$  is always greater than unity. Equation (4-9) leads us to the following conclusions: (a) When  $r$  is unity ( $r = 1$ ), it is equivalent to saying that when there is no size difference between solute and stationary phase,  $\ln \gamma^{\text{ath}} = 0$  and there is no entropy contribution; (b) When  $\ln \gamma^{\text{ath}}$  is negative it means that the entropy contribution leads the solution to deviate from Raoult's law negatively; (c) As the size ratio increases. The entropy contribution becomes more and more significant in  $\gamma^{\text{ath}}$  becomes more negative, and the total activity coefficient decreases.

The thermal term  $\gamma^{\text{th}}$  is related to the partial molar excess enthalpy  $\Delta H^E$ . Non-zero  $\Delta H^E$  can cause the solutions to have either a positive or negative deviation from Raoult's law.  $\gamma^{\text{th}}$  for a pure compound solute in a pure solvent can be estimated from molecular interaction theories such as Hildebrand-Scatchard solubility parameter theory.<sup>70-72</sup>

Now let us consider activity coefficients of  $C_3$  through  $C_8$  at a given temperature. The data in Tables 4-8 and 4-9 show that the activity coefficients

increase with increasing carbon number of the solutes. This can be explained qualitatively by the theory described above as follows. The effects of carbon number of solutes on both  $\gamma^{ath}$  and  $\gamma^{th}$  are two fold. First, the increase of carbon number of alkanes leads to increase in the molecular size of solute and the decrease of the size ratio between stationary phase and solute, which consequently leads to a larger  $\gamma^{ath}$  based on Equation (4-8). On the other hand, since the intermolecular forces between alkane solutes and bitumen are dominated by London dispersion forces, the increase of molecular sizes leads to an increase in the interaction forces (London forces) and  $\gamma^{th}$  increases as well. Therefore, the total activity coefficient,  $\gamma^\infty$ , increases with the solute molecular size.

The activity coefficients of methanol deviate further from unity than those of alkanes and aromatics at the same temperature as can be seen in Tables 4-8 and 4-9. This is because of the strong molecular interactions between methanol and bitumen. The intermolecular forces between methanol and bitumen are stronger than those between alkanes or aromatics and bitumen because of the polarity and hydrogen bonding of methanol, which interacts strongly with the polar compounds contained in the resin and asphaltene fractions of bitumen. This explanation can also be supported by the exceptionally large enthalpies of solution for methanol in bitumens as shown in Table 4-10.



## **Chapter 5**

### **Solubilities of Carbon Dioxide, Hydrogen Sulfide and Sulfur Dioxide In Physical Solvents**

#### **Introduction**

The removal of acidic impurities such as carbon dioxide ( $\text{CO}_2$ ), hydrogen sulfide ( $\text{H}_2\text{S}$ ) and sulfur dioxide ( $\text{SO}_2$ ) from industrial gases is an essential step in industrial processes such as petroleum refining, natural gas purification, hydrogen manufacture, coal gasification and ammonia production. Some processes require the separation of acidic impurities from the major gas stream as acidic gases would cause problems in subsequent processes, such as poisoning of catalysts. Other processes remove the acidic impurities for specification of products and for environmental requirements since  $\text{H}_2\text{S}$  and  $\text{SO}_2$  are among the most harmful gases to human and other life. To remove these impurity gases, many methods have been suggested and used, with emphasis on absorption of impurity gases into a liquid agent, either by physical absorption or absorption into a solution of chemical base.

The liquid agents used as absorbents for absorption of acidic gases can be classified into two groups in terms of the kind of interaction with the gas. The first group consists of chemical solvents (chemical bases) that are characterized by reactions between acidic gases and basic liquid solvents. This chemical absorption approach takes advantage of the relative acidity of the impurities.

Included in this group are aqueous solutions of alkanolamines such as monoethanolamine (MEA), diethanolamine (DEA), and diisopropanolamine (DIPA), potassium carbonate, and some caustic bases. The second group consists of physical solvents, in which acidic impurities are physically absorbed into solvents without any chemical reactions between gas and solvent. The separation of contaminants from the main gas stream achieved by physical absorption is based on a difference in solubility. The commonly used physical solvents are organic polar compounds such as propylene carbonate, Selsol (dimethylether of polyethylene glycol), methyl cyanoacetate, sulfolane (tetrahydrothiophene 1, 1-dioxide), N-formyl-morpholine, N-methyl-pyrrolidone and methanol.

The principal differences between physical and chemical solvents have been summarized by Astarita *et al.*<sup>73</sup> (see Table 5-1). These differences imply that physical solvents tend to be preferred when the partial pressure of acid gas in the feed is high, whereas chemical solvents are preferred when feed acid gas partial pressure is low. Although chemical solvents have some advantages, such as high degree of removal of acid gas, and usefulness in cases of low acid gas partial pressure, they possess considerable disadvantages including cost, high heat of absorption, corrosion of carbon steel, side reactions (base degradation) and possible environmental concerns. Considering the differences between physical and chemical solvents, it appears that physical solvent absorption may increase in importance in the future since physical solvents have the advantages of low enthalpy of absorption heat, low cost,

Table 5-1 Principal differences between physical and chemical solvents<sup>73</sup>

Physical absorption	Chemical absorption
Capacity (solubility) proportional to acid gas partial pressure in feed gas	Capacity not highly sensitive to acid gas partial pressure
Low heat of absorption	High heat of absorption
Desorb by flashing (sometimes)	Need low level steam for desorption
Difficult to remove acid gas completely (need many stages)	Easily reduce acid gas to low level in treated gas

absence of side reactions and suitability for high concentrations of acidic gas. The fact that physical solvents have a low heat of solution and can be recovered by flashing, which lead to low operational cost, will become more important in the future as energy costs continue to rise. Therefore it is most likely that more and more physical absorption units will be built.

The solubilities of acidic gases in physical solvents, along with the enthalpies of solution that are related to the temperature dependence of solubility are fundamental knowledge needed for the design and evaluation of absorption systems. Solubility data are also useful in selection of solvents. Although the solubilities of acidic gases in some solvents such as propylene carbonate have been studied by quite a few investigators, the data for other solvents still scarce. We have used gas-liquid chromatography to measure solubilities of carbon dioxide, hydrogen sulfide and sulfur dioxide in four physical solvents, including propylene carbonate, Selexol, methyl cyanoacetate and N-formyl-morpholine. The solubility data at several temperatures have been used in calculating the enthalpies and entropies of solution.

### **Experimental**

The physical solvents were coated onto the solid support by dissolving each solvent into acetone that was later evaporated. The stationary phase loadings (ratio of liquid to solid support) for each solvent were as follows: propylene carbonate, 14.0%; Selexol, 18.2%; methyl cyanoactate, 13.5% and N-formyl morpholine, 13.2%. Teflon tubing of 3/16" internal diameter and 6 feet

long was used for the columns in place of stainless steel to avoid any possible reaction between acidic gases and the metal.

In this study, neon was used to determine the dead time of the column.  $\text{H}_2\text{S}$  and  $\text{SO}_2$  were injected individually with neon because their retention times were much longer than those of neon and therefore the peaks were well separated. The total injection volumes ( $\text{H}_2\text{S}$  or  $\text{SO}_2$  plus neon) were 1 microliter ( $\mu\text{L}$ ). The retention times for both  $\text{H}_2\text{S}$  and  $\text{SO}_2$  were found to be sample size dependent and so an extrapolation procedure, as described in Chapter 4, was employed to obtain the retention volumes at infinite dilution (Henry's law range). The retention times of carbon dioxide were found to be very close to the retention times of neon and also to be sample size independent. Therefore,  $\text{CO}_2$  and neon were injected separately at least seven times. The average retention times of  $\text{CO}_2$  and neon were then used for calculations.

Methyl cyanoacetate and propylene carbonate were obtained from Aldrich Chemicals and were 99.0% pure. Selexol was supplied as a mixture with 0.87% of water, by Harrisons and Crosfield, Ltd. The water content in Selexol was determined using the Karl Fisher method by the microanalytical laboratory in the Department of Chemistry, University of Alberta. 99.0% N-formyl morpholine was provided by BASF. All solute gases were supplied by Matheson Gas Products Canada. Skeletal formula and physical properties of these physical solvents are listed in Table 5-2. Although Selexol is a mixture of polymers, the average value of  $n$  can be estimated from the average molecular

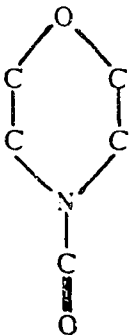
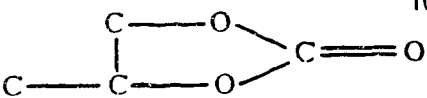
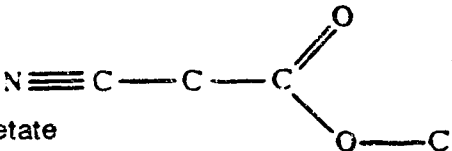
weight. For an average molecular weight of  $266 \text{ g mol}^{-1}$ , the average value of  $n$  is estimated to be 4 for this particular sample.

## Results and Discussion

Retention times of carbon dioxide, hydrogen sulfide and sulfur dioxide in the physical solvents listed in Table 5-2 were measured. The specific retention volumes were calculated using Equation (2-13). Solubilities expressed as Henry's law constants for the acidic gases in the physical solvents were obtained using Equation (2-33) and are presented in Table 5-3. The average enthalpies of solution of the acidic gases in the physical solvents were obtained from the slopes of the graphs of  $\ln V_g^\circ$  against  $1/T$  (or  $\ln K_H$  against  $1/T$ ) and are listed in Table 5-4. The entropies of solution at  $25^\circ\text{C}$  are also included in Table 5-4. Figures 5-1 to 5-3 are graphs of  $\ln K_H$  against  $1/T$  that represent the temperature dependence of the solubilities.

The data on hydrogen sulfide in N-formyl-morpholine and sulfur dioxide in both Selexol and N-formyl-morpholine are not included in the tables and figures. Measurements of these systems were attempted, but the gases did not elute out from columns. For other columns such as propylene carbonate or methyl cyanoacetate, hydrogen sulfide and sulfur dioxide eluted in half a minute to several minutes after the neon peak, depending on the temperature and flow rate, but they did not elute from N-formyl morpholine column after one to two hours under the same experimental conditions (even increasing column

Table 5-2 Properties of physical solvents

solvent	structural	molecular weight (g mol <sup>-1</sup> )	boiling point (°C)	viscosity	density
	formula			(cps) (25°C)	(g cm <sup>-3</sup> ) (25°C)
Selexol	$\text{c-o-c-c-(o-c-o)}_n\text{-o-c}$	266*	276	3.6	1.027
N-formyl Morpholine		115.3	—	—	1.144
Propylene Carbonate		102.8	240	2.4	1.189
Methyl Cyanoacetate		100.1	202	1.8	1.103

\* The average molecular weight of Selexol was measured in the microanalytical laboratory in Department of Chemistry, U. of A. The method used is V.P.O. at 40°C with benzene as solvent.

Table 5-3 Henry's law constants (atm) for acid gases  
in four physical solvents

Solvent	Gas	Temperature (°C)					
		25	30	40	50	60	70
Propylene	CO <sub>2</sub>	84.2	94.0	113	122	152	159
Carbonate	H <sub>2</sub> S	23.1	26.1	31.7	34.8	43.6	49.1
	SO <sub>2</sub>	1.46	1.79	2.44	3.36	4.63	6.18
Methyl	CO <sub>2</sub>	88.1	89.6	111	133	141	—
Cyanoacetate	H <sub>2</sub> S	28.1	28.8	36.0	44.1	48.7	—
	SO <sub>2</sub>	2.37	2.62	3.78	5.25	6.97	—
Solexol	CO <sub>2</sub>	35.2	39.0	46.1	55.5	64.7	—
	H <sub>2</sub> S	4.34	5.00	6.33	7.77	9.94	—
N-Formyl Morpholine	CO <sub>2</sub>	70.5	80.0	91.2	110	131	147



Table 5-4      Average enthalpies and entropies of solution for acid gases in four physical solvents

Solvent	Gas	$-\Delta H_s^\circ$ (kJ mol <sup>-1</sup> )	$-\Delta S^\circ_{298}$ (J mol <sup>-1</sup> K <sup>-1</sup> )
Propylene Carbonate	CO <sub>2</sub>	12.2	40.9
	H <sub>2</sub> S	14.1	47.3
	SO <sub>2</sub>	27.0	90.6
Methyl Cyanoacetate	CO <sub>2</sub>	12.4	41.6
	H <sub>2</sub> S	14.1	47.3
	SO <sub>2</sub>	26.3	88.2
Solexol	CO <sub>2</sub>	14.3	48.0
	H <sub>2</sub> S	19.1	64.1
N-Formyl-Morpholine	CO <sub>2</sub>	13.7	46.0

temperature). The most likely explanation is that some chemical reaction such as complexation between  $\text{H}_2\text{S}$  or  $\text{SO}_2$  and the solvents or impurities took place and so held the gases in the stationary phase. For some of these systems ( $\text{H}_2\text{S}$  in N-formyl morpholine) our partial molar volume measurements (see Chapter 6) show an unusual phenomenon (color change) which also suggested the possibility of a chemical reaction.

Chemical solvents such as alkanolamines have been widely studied, but only a few physical solvents have been investigated.<sup>24,74-82</sup> In these studies, most of the solubility results have been published directly as gas-liquid equilibrium data, such as the weight percent, volume percent or mole fraction of gases dissolved in liquids at specified temperatures and pressures. For the four physical solvents studied here, only Henry's law constants of  $\text{CO}_2$ ,  $\text{H}_2\text{S}$  and  $\text{SO}_2$  in propylene carbonate and  $\text{CO}_2$  in N-formyl morpholine have been published by a few authors.<sup>24,74-77,81,90</sup> The solubilities (expressed as mole fractions) of  $\text{H}_2\text{S}$  and  $\text{CO}_2$  in Sclerox have been measured<sup>82</sup> but values of Henry's law constant are not available. Solubilities of  $\text{H}_2\text{S}$  and  $\text{CO}_2$  in methyl cyanoacetate and  $\text{SO}_2$  in three of these four solvents have not been published. We now compare the available data to our experimental results.

We start our comparison first by comparing available literature values of Henry's law constants for  $\text{CO}_2$ ,  $\text{H}_2\text{S}$ , and  $\text{CO}_2$  in propylene carbonate and  $\text{CO}_2$  in N-formyl morpholine with our experimental data. Table 5-5 lists all available previous Henry's law constants along with our values at the same temperatures.

Some of the data in this table are listed as reported by the original authors while other values were obtained by interpolation from graphs of Henry's law constants against temperatures ( $\ln K_H$  against  $1/T$ ) as given in the literature. It should be noted that the literature data shown in Table 5-5 were obtained by different methods. Values labelled a, b, d, e, f, h and i (Table 5-5) were obtained from a static method using an equilibrium cell, whereas value c and g (Table 5-5) were obtained by gas-liquid chromatography. Generally our results are in good agreement with the literature values, even though the latter were obtained by different authors using various methods.

Solubility data expressed as mole fractions at different pressures for  $\text{CO}_2$  and  $\text{H}_2\text{S}$  in Selexol were obtained by Mather *et al.*<sup>82</sup> These solubility data at lower pressures and dilute concentrations can be used to calculate the Henry's law constants. The calculation of Henry's law constant is based on the basic definition,  $K_H = \lim_{x \rightarrow 0} (f/x)$ . The fugacities of the gases were first calculated using the virial equation. Then the fugacities were plotted against mole fractions. The slope of this plot gives the Henry's law constant. The Henry's law constants estimated from Mather's data for  $\text{H}_2\text{S}$  in Selexol at  $25^\circ\text{C}$  and  $40^\circ\text{C}$  are 4.47 and 5.17 atm, compared to our values of 4.34 and 6.33 atm, respectively. The same procedure gives  $K_H$  for  $\text{CO}_2$  to be 34.3 atm at  $25^\circ\text{C}$  and 41.8 atm at  $40^\circ\text{C}$  as compared to our GLC results of 35.2 and 46.1 atm respectively. We can conclude that the Henry's law constants from our GLC measurements and from Mather's equilibrium cell measurements are in reasonable agreement.

Table 5-5 Comparison of Henry's law constants for CO<sub>2</sub>, H<sub>2</sub>S and SO<sub>2</sub>  
in propylene carbonate (PC) and CO<sub>2</sub> in N-formyl morpholine(NFM)

system	25°C	30°C	40°C	50°C	70°C
CO <sub>2</sub> -PC	84.2 <sup>*</sup> 82.8 <sup>a,b</sup>	94.0 <sup>*</sup> 85 <sup>b'</sup> 85 <sup>c</sup>	113 <sup>*</sup> 112 <sup>c</sup> 116 <sup>d</sup> 113 <sup>e</sup> 105 <sup>b'</sup>	122 <sup>*</sup> 123 <sup>b</sup>	
H <sub>2</sub> S-PC	23.1 <sup>*</sup> 25.3 <sup>a,b</sup> 21.9 <sup>f</sup> 20.9 <sup>g</sup>	26.1 <sup>*</sup> 27 <sup>b'</sup>	31.7 <sup>*</sup> 33 <sup>b'</sup>	34.8 <sup>*</sup> 38.6 <sup>b</sup> 34.5 <sup>f</sup> 33.8 <sup>g</sup>	
CO <sub>2</sub> -NFM	70.5 <sup>*</sup> 68.0 <sup>h</sup>		91.2 <sup>*</sup> 88.0 <sup>h</sup>		147 <sup>*</sup> 136 <sup>h</sup>
SO <sub>2</sub> -PC	1.46 <sup>*</sup> 1.20 <sup>g</sup> 1.51 <sup>i</sup>				

\*: our work

a: reference 75

b: reference 77,      b': interpolated values from the graphs in reference 77

c: reference 24

d: reference 76

e: cited values in reference 76

f: reference 79

g: reference 74

h: reference 81

i: reference 90

The Henry's law constant is related to the maximum acidic gas load possible in a physical solvent,  $\alpha_{\max}$ , and the acidic gas partial pressure in the feed gas,  $P_i$ , by Henry's law:

$$\alpha_{\max} = P_i / K_H \quad (5-1)$$

Equation (5-1) indicates that the smaller the Henry's law constant is, the greater the solubility of the acid gas in the solvent. From Table 5-3 and Figures 5-1 to 5-3 we have seen that  $H_2S$  and  $CO_2$  have the smallest Henry's law constants and consequently, the largest solubilities in Selexol. Therefore, Selexol is the strongest absorbent for  $CO_2$  and  $H_2S$ . We also note that for all solvents at a give temperature, the Henry's law constants for different gases have the trend  $CO_2 > H_2S > SO_2$ . This trend means that under the same conditions and in the same solvent,  $SO_2$  is the most soluble gas. This is potentially very useful information for industrial acidic gas separation. In industry sulfur dioxide is most commonly removed by absorption into a limestone-water slurry in a process known as the throwaway process. This is an economical method since it uses the cheapest chemical absorbents. However, this throwaway process generates a large amount of waste sludge and is not always suitable because of problems with the disposal of the sludge. Therefore, recoverable processes are of interest. Recoverable processes have not been studied as much as the throwaway processes, although some recoverable processes, such as sodium sulfite solution absorption and sodium citrate

absorption have been suggested. Our solubility measurement results indicate that sulfur dioxide is highly soluble in the physical solvents studied in this work. From a thermodynamic point of view, these physical solvents can certainly be used to remove sulfur dioxide.

The enthalpy of solution is an important consideration for the gas removal absorption process. The effects of enthalpy of solution on absorption are two-fold. First, the enthalpy of solution determines the heat generated during the absorption process. Since the absorption takes place at lower temperatures, a high heat of solution would result in more energy being required to keep the temperature down. On the other hand, heat of solution is directly proportional to the temperature dependence of the solubility. A small temperature dependence makes the regeneration of solvent more difficult because the temperature swing required between the absorption and desorption steps is greater for a lower temperature dependence. The heat requirement for a process increases with increasing temperature swing. Thus, a solvent with a strong temperature dependence (large heat of solution) requires less energy to desorb the absorbed acid gases to regenerate the solvent. Table 5-4 shows that different acid gases have different enthalpies of solution.  $\Delta H^\circ$  values for  $\text{SO}_2$  are much larger than those for  $\text{CO}_2$  and  $\text{H}_2\text{S}$  in the same solvent.  $\Delta H^\circ$  values for the same gas in different solvents do not show significant differences.

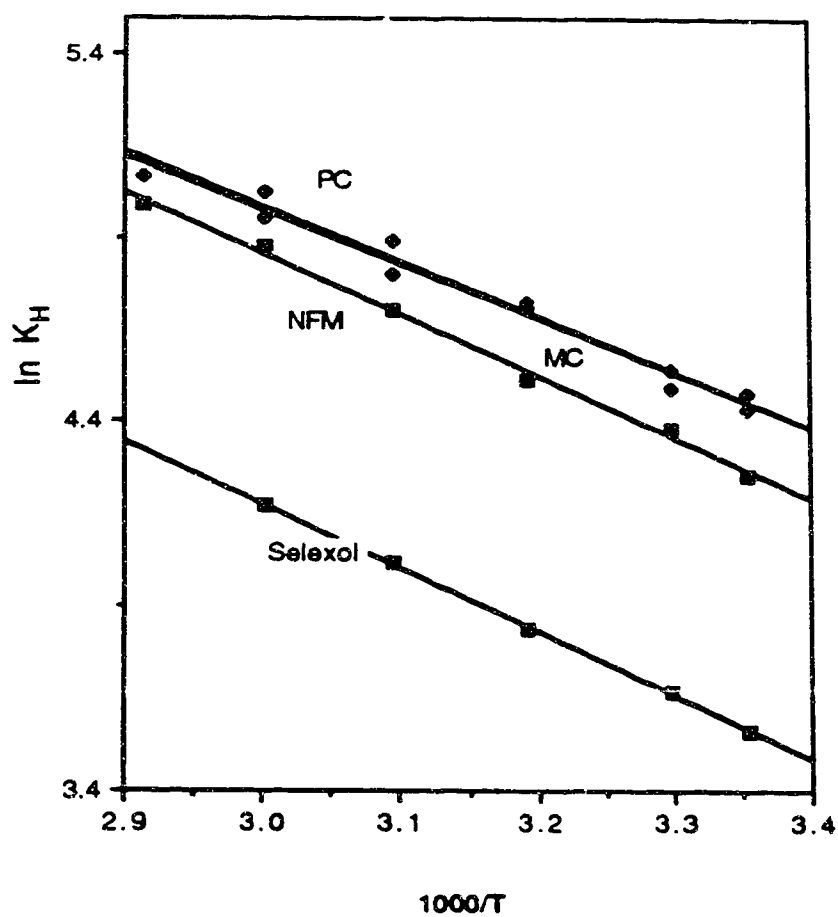


Figure 5-1 Henry's law constants for  $\text{CO}_2$  in physical solvents as a function of temperature.

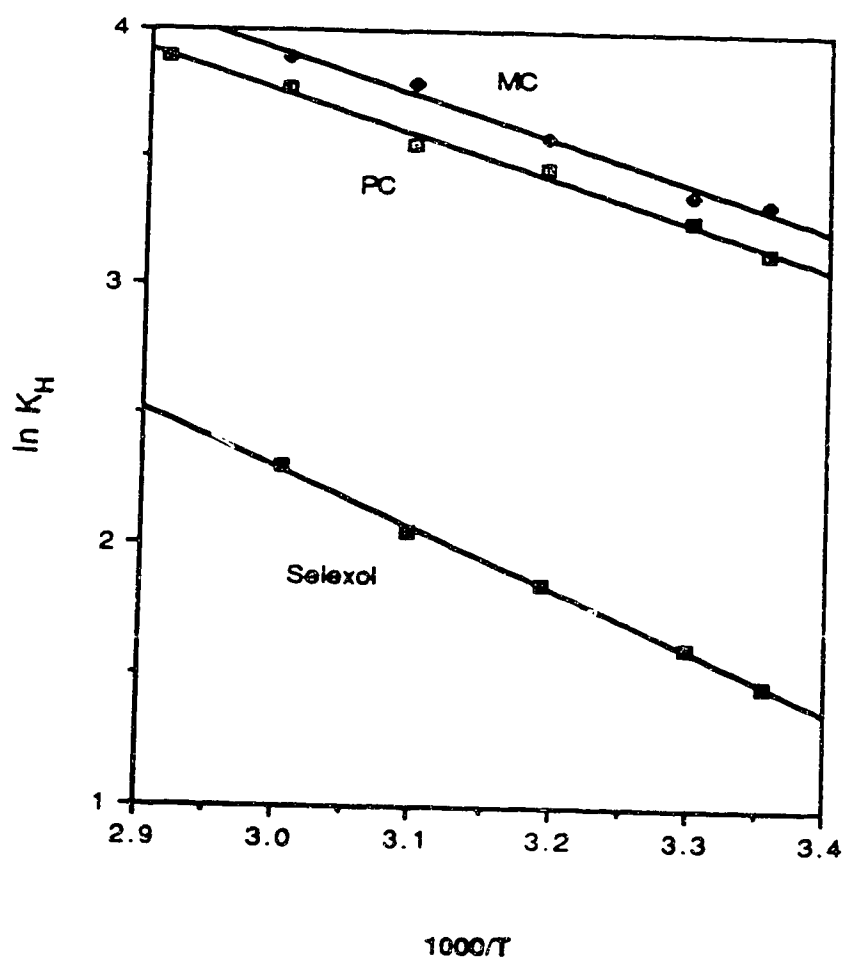


Figure 5-2 Henry's law constants for  $H_2S$  in physical solvents as a function of temperature.



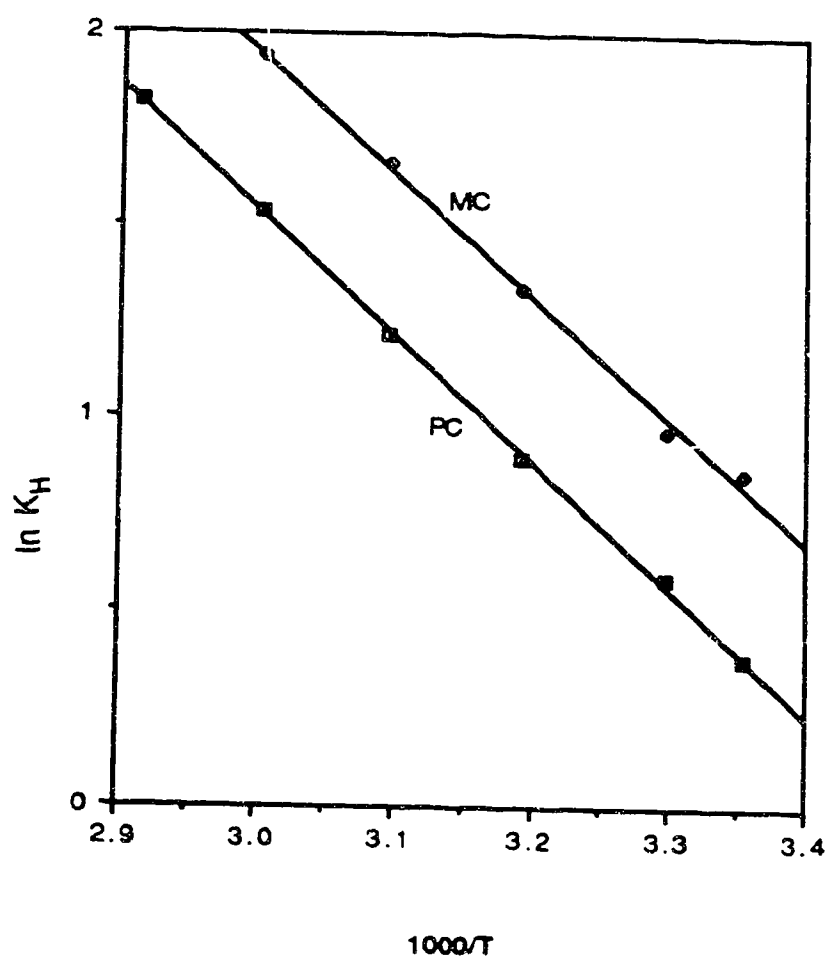


Figure 5-3 Henry's law constants for  $\text{SO}_2$  in physical solvents as a function of temperature.

## Chapter 6

### Partial Molar Volumes of Acid Gases In Physical Solvents

#### Introduction

The partial molar volumes of gases in liquids are important for theoretical considerations and in engineering applications. For example, the volume expansion on mixing significantly contributes to entropy of solution.<sup>70</sup> The theoretical calculation of the partial molar entropy of solution of a dilute solute requires values of solvent internal pressure related term  $(\partial p/\partial T)_V$ , and solute partial molar volume,  $\bar{V}_2$ . The partial molar volume is important in engineering because it is needed to estimate the solubility of a gas in a liquid at higher pressure. The Henry's law constant can be used to calculate the solubility of a gas in a liquid at lower pressures and very dilute solutions (Henry's law region), as was discussed in previous chapters. However, in practical applications, the pressures are usually high and Henry's law cannot be assumed to be valid. Therefore, the pressure dependence of Henry's law constant or an equation which correlates the solubility of a gas with pressure and temperature is needed. The Krichevsky-Kasarnovsky equation<sup>11,83</sup> has been suggested for this calculation:

$$\ln \left( \frac{f_2}{X_2} \right) = \ln K_H + \frac{\bar{V}_2^\infty (P - P_1^s)}{RT} \quad (6-1)$$

In Equation (6-1)  $P_1^s$  represents the saturated vapor pressure of the solvent at

temperature  $T$ ;  $P$  is the pressure of the gas at which the solubility is calculated;  $K_H$  represents the Henry's law constant at the pressure of  $P_1^s$  and  $\bar{V}_2^\infty$  represents the partial molar volume of the gas in the liquid at infinite dilution;  $X_2$  represents the mole fraction of the gas in the liquid and  $f_2$  is the fugacity of the gas at pressure  $P$  and temperature  $T$ .

Equation (6-1) can be used in two ways. First, if the values of  $K_H^{(P_1^s)}$  and  $\bar{V}_2^\infty$  are known, the solubility expressed in mole fraction  $X_2$  at any pressure  $P$  can be predicted. Another way for using Equation (6-1) is to calculate the Henry's law constant and partial molar volume from the values of solubilities,  $X_2$ , at different pressures,  $P$ . According to Equation (6-1), a plot of  $\ln(f_2/X_2)$  against  $(P - P_1^s)$  gives a slope of  $\bar{V}_2^\infty/RT$  and intercept of  $\ln K_H^{(P_1^s)}$ . In both of the applications, the fugacity of the gas at pressure  $P$  should be known prior to the calculations.

The relation between fugacity and total pressure  $P$  has been given by

$$\left(\frac{\partial \ln f}{\partial P}\right)_T = \frac{V}{RT} \quad (6-2)$$

and the ratio of fugacity to pressure is given by

$$\left(\frac{\partial \ln (f/P)}{\partial P}\right)_T = \left(\frac{\partial \ln f}{\partial P}\right)_T - \left(\frac{\partial \ln P}{\partial P}\right)_T = \frac{V}{RT} - \frac{1}{P} \quad (6-3)$$

Integration of equation (6-3) from zero pressure (at which  $f/P=1$  and  $\ln(f/P)=0$ ) to  $P$  gives

$$\ln \left( \frac{f}{P} \right) = \int_0^P \left[ \frac{V}{RT} - \frac{1}{P} \right] dP \quad (6-4)$$

Equations of state (P-V-T equation) can be placed in Equation (6-4) to obtain the values of  $f/P$ . A simple way to use Equation (6-4) is using the virial equation if the virial coefficients are available:

$$PV = RT (1 + B/V + C/V^2 + D/V^3 + \dots) \quad (6-5)$$

or

$$PV = RT (1 + B'P + C'P^2 + D'P^3 + \dots) \quad (6-5')$$

in which  $B$  or  $B'$  is the second virial coefficient, and  $C$  or  $C'$  is the third virial coefficient. The relation between  $B$  and  $B'$  is given by  $B = B'RT$ . Similarly, we have  $C = (RT)^2 (C' + B'^2)$ . Substitution of Equation (6-5') into (6-4) and integration then leads to

$$\ln \frac{f}{P} = B'P + \frac{C'}{2}P^2 + \frac{D'}{3}P^3 + \dots \quad (6-6)$$

A virial equation that contains only the second virial coefficient ( $B$ ) is accurate enough for our practical use. In this case, Equation (6-6) reduces to

$$\ln (f/P) = \frac{BP}{RT} \quad (6-7)$$

or

$$\ln (f/P) = B'P \quad (6-7')$$

in which the second virial coefficient  $B$  or  $B'$  can be obtained from the literature or estimated as described in Chapter 3.

The use of Equation (6-1) for predicting the solubilities of gases in liquids at different pressures requires knowledge of Henry's law constants and the partial

molar volumes of the gases in liquids. We have applied gas-liquid chromatography (Chapter 5) to obtain the Henry's law constants for acidic gases in physical solvents. In this chapter, the results of measurements of partial molar volumes of these acidic gases in the solvents are reported. The solubilities at higher pressures are estimated and compared with experimental values.

Partial molar volumes of gases in liquids have been summarized by Battino and Clever<sup>84</sup>, Clever and Battino<sup>85</sup>, Handa and Benson<sup>86</sup> and Handa *et al.*<sup>87</sup> The measurement of partial molar volume,  $\bar{V}_2$ , can be carried out by one of the three methods: (1) by measuring the density difference between degassed liquid and gas-saturated liquid, (2) by determining the dilation of the liquid due to dissolution of the gases, or (3) by studying the pressure dependence of the gas solubility in liquid. Of these methods most investigators have used the dilatometric method. The first dilatometric measurements of partial molar volumes were described by Horiuti.<sup>88</sup> Since then, Horiuti's dilatometer and many modified versions have been widely used in the determination of partial molar volumes. Although these kinds of apparatus have given accurate results, they are very complicated. A new and simpler dilatometer has been designed and used in this research laboratory.<sup>57</sup> In this chapter we will describe briefly the dilatometer, and then report the use of this dilatometer to make partial molar volume measurements on acidic gases in physical solvents.

## Experimental

### Principles of the Dilatometer

the partial molar volume of a solute in solution is defined by

$$\bar{V}_2 = \left( \frac{\partial V}{\partial n_2} \right)_{n_1, T, P} \quad (6-8)$$

In Equation (6-8),  $V$  represents the total volume of solution and  $n_2$  represents the number of moles of dissolved gas. Knowing the volume of solution as a function of composition, Equation (6-8) can be used to obtain  $\bar{V}_2$  directly by differentiation of the function with respect to  $n_2$ . However, in practice, the partial molar volumes are more conveniently calculated from apparent molar volumes ( $\phi V_2$ ) that are defined by

$$\phi V_2 = \frac{\text{total volume} - \text{volume of pure solvent}}{\text{moles of solute}} = \frac{V - n_1 V_1^*}{n_2} \quad (6-9)$$

in which  $V_1^*$  is the molar volume of the pure solvent and  $n_1$  is the moles of solvent. It is also known that

$$V = n_1 \bar{V}_1 + n_2 \bar{V}_2 \quad (6-10)$$

where  $\bar{V}_1$  represents the partial molar volume of solvent. At infinite dilution,  $\bar{V}_1 = V_1^*$ ; then

$$V = n_1 V_1^* + n_2 \bar{V}_2 \quad (6-11)$$

Substituting Equation (6-11) into Equation (6-9) gives

$$\lim_{n_2 \rightarrow 0} \phi V_2 = \frac{n_1 V_1^* + n_2 \bar{V}_2 - n_1 V_1^*}{n_2} = \bar{V}_2 \quad (6-12)$$

Equation (6-12) indicates that the partial molar volume of a solute is equal to the apparent molar volume of the solute at infinite dilution.

Rearranging Equation (6-9) yields

$$V = n_2 \phi V_2 + n_1 \bar{V}_1^{\circ} \quad (6-13)$$

Differentiation of Equation (6-13) with respect to  $n_2$  then leads to

$$\bar{V}_2 = \phi V_2 + n_2 \left( \frac{\partial \phi V_2}{\partial n_2} \right)_{n_1, T, P} \quad (6-14)$$

When the solution approaches infinite dilution, the second term on the right side of Equation (6-14) approaches zero, and thus the apparent molar volume approaches the partial molar volume, which gives the same result as Equation (6-12). Equation (6-14) can be used to obtain partial molar volumes at finite concentration for which the apparent molar volume is a function of concentration. If the apparent molar volume is expressed as a numerical function of  $n_2$ , differentiation of the function leads to  $(\partial \phi V_2 / \partial n_2)_{n_1}$ , which, combined with Equation (6-14), gives the partial molar volume.

The dilatometer was designed to obtain partial molar volumes based on Equation (6-12) as described by Bottomley *et al.*<sup>57</sup>

## Apparatus

The dilatometer is illustrated in Figure 7-1. It consists of a pyrex glass bulb with volume 68 cm<sup>3</sup>, fitted with a straight capillary tube 100 mm long with a 3 mm internal diameter. A thin copper wire surrounds the capillary tube half way up as a reference mark. The open end of the capillary tube can be closed with a loose

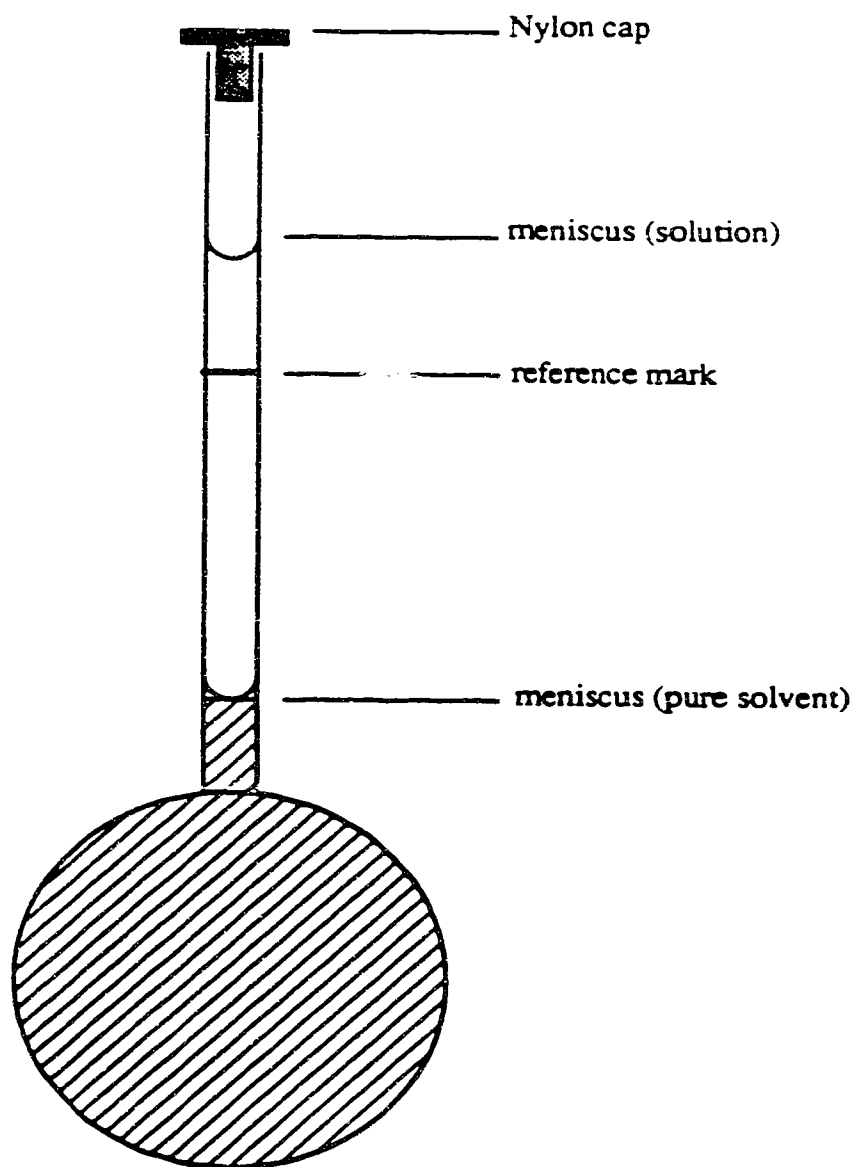


Figure 6-1. Diagram of dilatometer



fitting Nylon cap.

The volume of the capillary tube was calibrated as follows. The dilatometer was loaded with a liquid of known density and then placed in a constant temperature water bath. When temperature equilibrium had been achieved, the distance of the meniscus relative to the reference mark was determined with a cathetometer. The mass of the liquid in the dilatometer was also measured. A small amount (known mass) of the same liquid was then added to the dilatometer and the measurement process repeated. The change in mass, combined with the density, gives the change in volume of liquid that corresponds to the volume of capillary tube. The average cross-sectional area of the capillary tube was obtained by dividing the volume change by the change in meniscus height.

### **Measurement Procedure**

The dilatometer was cleaned, dried and weighed. The solvent was degassed with a vacuum pump for three to five minutes and was then injected into the dilatometer with a 100 cm<sup>3</sup> hypodermic syringe, until the solvent meniscus was about 10 mm up the capillary tube. The dilatometer was then closed with the Nylon stopper and placed in a constant temperature water bath to allow for temperature equilibration. When the temperature of the liquid achieved equilibrium the height of the meniscus relative to the reference mark was measured with a cathetometer. The dilatometer was then removed from the water bath, carefully dried and weighed.

The gas was introduced into the dilatometer under hydrostatic pressure slightly above atmospheric pressure by connecting the top of the capillary tube to a gas cylinder with Tygon tubing. The bulb was placed in ice-water that contracted the solvent to produce a gas space of about 1 cm<sup>3</sup>. With gentle rocking and shaking, the gas was gradually dissolved into the liquid. After some gas had dissolved into the solvent, the dilatometer was disconnected from the Tygon tubing, closed with the stopper and replaced in the water bath. When the temperature reached equilibrium, a new meniscus level and a new weight were measured. The difference between the meniscus level of pure solvent and that of solvent plus dissolved gas, in combination with the average cross-sectional area of the capillary tube, led to the volume change of the solution. The weight difference of the dilatometer before and after dissolution of gas led to the mass of the gas dissolved in the solvent. Division of this volume change by the number of moles of gas led to the apparent molar volume of the gas in the solvent. As shown in Equation (6-5), the apparent molar volume can be regarded as the partial molar volume only when the solution approaches infinite dilution. It was found that when the meniscus of the solvent changed from 20 mm to 40 mm (equivalent to change of volume from 0.16 cm<sup>3</sup> to 0.31 cm<sup>3</sup>) and the gain in mass was from 0.2 to 0.5 gram, the apparent molar volume was nearly independent of the amount of gas dissolved. This indicates that the solution is dilute enough so that  $(\partial \phi V_2 / \partial n_2)_{n_1, T, p}$  is close to zero and the apparent molar volume approaches the partial molar volume. Repeated measurements were carried out and an average value was obtained and reported.

## Results and Discussion

The apparent molar volumes for carbon dioxide ( $\text{CO}_2$ ), hydrogen sulfide ( $\text{H}_2\text{S}$ ) and sulfur dioxide ( $\text{SO}_2$ ) in the physical solvents studied in Chapter 5 have been measured. All measurements were done at  $25^\circ\text{C}$ . Since the solutions are very dilute, the apparent molar volumes have been taken to be equal to the partial molar volumes. The values of partial molar volumes for the acid gases in physical solvents are listed in Table 6-1.

Few data for partial molar volumes of acid gases in physical solvents have been published. Mather *et al.*<sup>81</sup> have measured the solubilities of  $\text{CO}_2$  and  $\text{H}_2\text{S}$  in N-formyl morpholine and correlated their solubility data to obtain the three parameters in the Krichevsky-Ilinskaya equation: the Henry's law constant, partial molar volume and the Margules parameter. Their calculated results for partial molar volumes are  $35.55$  and  $35.07 \text{ cm}^3 \text{ mol}^{-1}$  for  $\text{CO}_2$  and  $\text{H}_2\text{S}$  in N-formyl morpholine, respectively, in good agreement with our values of  $33.5$  and  $37.8 \text{ cm}^3 \text{ mol}^{-1}$ .

As was stated before, the partial molar volumes in combination with Henry's law constants can be used in the Krichevsky-Kasarnovsky equation for predicting the solubilities at higher pressures. Since we have both Henry's law constants and partial molar volumes for acid gases in physical solvents we are able to estimate solubilities at high pressure. First we apply the Krichevsky-Kasarnovsky equation using our values of Henry's law constants and partial molar volumes to estimate the solubilities (mole fractions) of  $\text{CO}_2$  in propylene

carbonate and N-formyl morpholine at pressures for which solubility data in the literature are available for comparison. Using the Krichevsky-Kasarnovsky equation (Equation 6-1) values of  $f_2 / X_2$  were first obtained. Values of  $f_2$  at different pressures were calculated by using Equation (6-7). Then,  $X_2$  values at different pressures were obtained. Some results of these calculations along with the literature data are listed in Table 6-2.

From Table 6-2 it can be seen that for  $\text{CO}_2$  in propylene carbonate and N-formyl morpholine at low to medium pressures the solubilities calculated by the Krichevsky-Kasarnovsky equation using our experimental values of Henry's law constant and partial molar volume are in agreement with the measured solubility values. At higher pressures (high solubilities) the differences between the values of measured and calculated are over the experimental uncertainties.

In the application of Krichevsky-Kasarnovsky equation, there are two assumptions that the systems should obey. One of these is that the activity coefficient of the solute does not change noticeably over the range of  $X_2$  being studied. The other assumption is that the infinitely dilute liquid solution must be essentially incompressible. The second assumption can be approximately met at temperatures far below the critical temperature of the solution. The first assumption is true only for sparingly soluble gases or to moderate pressures under which the solubilities are still small and the solutions dilute. For example, the Krichevsky-Kasarnovsky equation represents the solubilities of hydrogen and nitrogen in water to very high pressure (1000 bar).<sup>83</sup> For systems with

larger solubilities, the activity coefficients and partial molar volumes of solutes in liquids cannot be expected to be unchanged with  $X_2$ . Therefore, the Krichevsky-Kasarnovsky equation will not give correct results. Prausnitz *et al.*<sup>11</sup> have used the solubility data of Wiebe and Gaddy<sup>89</sup> for nitrogen in liquid ammonia to illustrate the limitation of the Krichevsky-Kasarnovsky equation. At 0°C the solubility of nitrogen in ammonia is very small (only 2.2 mol % at 1000 bar) and the Krichevsky-Kasarnovsky equation holds accurately to 1000 bar. At 70°C the solubility is larger (12.9 mol % at 1000 bar), and the Krichevsky-Kasarnovsky equation holds only to 600 bar. In our CO<sub>2</sub>-physical solvent systems the solubilities are reasonably large. The mole fractions of gas in solvent are over 0.1 at about 10 atm. Thus as pressure increases further, the solubility becomes larger and activity coefficients as well as partial molar volumes are no longer constant, at which point the Krichevsky-Kasarnovsky equation no longer applies accurately. Therefore, the solubilities calculated from the Krichevsky-Kasarnovsky equation are expected to deviate from the measured values at higher pressures.

Data for the CO<sub>2</sub>-Sulfolane system were not reported in Table 6-2 because CO<sub>2</sub> has a much higher solubility in Sulfolane than in the two solvents mentioned above and the Krichevsky-Kasarnovsky equation cannot be expected to hold. For the same reason, the Krichevsky-Kasarnovsky equation is not justified for predicting solubilities of H<sub>2</sub>S and SO<sub>2</sub> in these solvents at high pressures.

Table 6-1              Partial molar volumes ( $\text{cm}^3 \text{mol}^{-1}$ ) of acidic gases  
in physical solvents at 25°C

solvent	$\text{CO}_2$	$\text{H}_2\text{S}$	$\text{SO}_2$
Propylene Carbonate	42.2	40.4	43.7
Methyl Cyanoacetate	39.6	40.6	44.1
Selexol	42.2	38.5	39.8
N-Formyl Morpholine	33.5	37.8*	33.1

\* The color of the solvent N-formyl morpholine changed from nearly colorless to light green, to dark green as hydrogen sulfide dissolved.

Table 6-2 Predicted (Krichëvsky-Kasarnovsky equation) solubilities ( $x_2$ , mole fractions) of CO<sub>2</sub> at higher pressures at 25°C

Pressure(atm)	$x_{2,\text{predicted}}$	$x_{2,\text{measured}}$
N-formyl morpholine <sup>a</sup>		
3.74	0.0518	0.0524
11.06	0.146	0.145
29.12	0.341	0.369
58.30	0.564	0.720
propylene carbonate <sup>b</sup>		
2.951	0.0344	0.0359
6.370	0.0725	0.0770
11.20	0.1235	0.1341
16.11	0.1720	0.1878

a:  $x_{2,\text{measured}}$  are from reference 81

b:  $x_{2,\text{measured}}$  are from reference 79

## **Chapter 7**

### **Calibrating and Testing the C-80 Heat-Flow Calorimeter**

Of several types of calorimeters, the Tian-Calvet heat-flow calorimeter has shown more and more advantages and applications. The C-80 calorimeter manufactured by SETARAM of Lyon, France, is a typical Tian-Calvet type heat flow calorimeter. This calorimeter has been designed for high pressure (up to 100 bar) and medium temperature (ambient to 300°C) measurements and for applications in many scientific research fields.

The C-80 calorimeter is based on Tian-Calvet heat flow principles that have been described in detail elsewhere.<sup>91-92</sup> In this chapter, we first briefly summarize the basic Tian-Calvet theories of heat flow calorimetry. Then we describe the construction and calibration of the calorimeter. Finally, we summarize testing the calorimeter by measuring the heat capacities of synthetic sapphire ( $\alpha\text{-Al}_2\text{O}_3$ ) over a wide temperature range.

#### **Principles of Heat - Flow Calorimetry**

Similar to many other types of calorimeters, the heat-flow calorimeter is composed of an inner vessel, in which the thermal phenomenon under study is created, and a surrounding medium (thermostat). However, in heat-flow calorimetry a thermal fluxmeter surrounds the calorimetric vessel to detect the



heat flow. The fluxmeter consists of thermopiles, which are connected in series so that they thermally connect the vessel to the thermostat. When a thermal phenomenon is produced in the calorimetric vessel, the thermal power flows through the thermopiles to the thermostat. There are three situations to consider:

(1). Constant and continuous power at constant temperature

When a constant thermal power,  $W$ , is produced in the vessel, energy is transferred to the surrounding medium through the thermopiles (Figure 7-1). Each thermopile delivers an elementary thermal power,  $W_i$ , which is represented by

$$W_i = C_i (\theta_i - \theta_e) \quad (7-1)$$

in which  $C_i$  is the thermal conductivity of thermocouple,  $\theta_i$  is the temperature of the vessel and  $\theta_e$  is the temperature of the thermostat. In heat flow calorimetry the difference between  $\theta_i$  and  $\theta_e$  is very small. This elementary power exchange then produces an elementary emf,  $e_i$

$$e_i = \varepsilon_i (\theta_i - \theta_e) \quad (7-2)$$

where  $\varepsilon_i$  is thermoelectric power of the thermocouple. Combination of Equations (7-1) and (7-2) gives

$$e_i = \frac{\varepsilon_i}{C_i} W_i \quad (7-3)$$

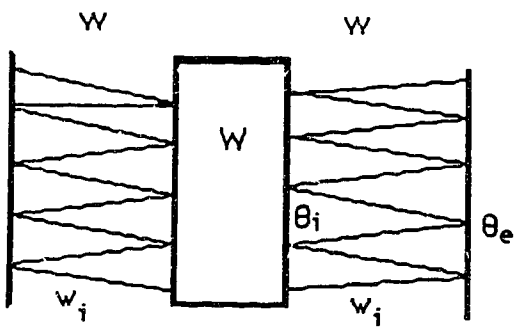


Figure 7-1: Illustration of the principle of a heat-flux meter

Since all thermocouples are connected in series, the total power transferred ( $W$ ) and the total emf produced ( $E$ ) are

$$W = \sum_{i=1}^n W_i = nC_i (\theta_i - \theta_e) = a(\theta_i - \theta_e) \quad (7-4)$$

$$E = \sum_{i=1}^n e_i = n\varepsilon_i (\theta_i - \theta_e) = b(\theta_i - \theta_e) \quad (7-5)$$

Because all couples are identical,  $\varepsilon_i$  and  $C_i$  for all couples are the same.

Therefore,

$$E = \frac{\varepsilon}{C} \sum_{i=1}^n W_i = \frac{\varepsilon}{C} W = KW \quad (7-6)$$

$$\text{or} \quad W = kE \quad (7-7)$$

in which  $K$  and  $k$  are constants. Equations (7-6) and (7-7) indicate that the total emf generated by the thermopiles is proportional to the heat flux (thermal power exchanged).

## (2). Variable heat flux at constant temperature.

In practice, measurements are usually carried out with variable thermal power produced in the calorimetric vessels. Let us assume the thermal power produced in the vessel at time  $t$  to be  $W$  and the temperature difference between the cell and the thermostat to be  $\theta$ . Part of the power transfers to the thermostat through the flux meter and part of it still remains in the cell at time  $t$ . The power exchanged through thermocouples is expressed by Equation (7-4). The remaining part of  $W$  increases the temperature of cell. If we assume the temperature increase,  $d\theta$ , through the cell during the time interval  $dt$  to be

uniform, then the remaining power is equal to  $M (d\theta/dt)$  in which  $M$  is the heat capacity of the cell. Therefore, the total thermal power at time  $t$  is represented as

$$W = w + M d\theta / dt \quad (7-8)$$

Combination of equations (7-4) and (7-8) yields Equation (7-9)

$$W = a\theta + M d\theta / dt \quad (7-9)$$

This equation is a fundamental equation of heat-flow calorimetry and is called the Tian equation.

The combination of equations (7-5) and (7-9) leads to

$$W = \frac{a}{b} \left( E + \frac{M}{a} \frac{dE}{dt} \right) = A \left( E + \tau \frac{dE}{dt} \right) \quad (7-10)$$

in which constants  $A$  and  $\tau$  are constants of calorimetry. " $A$ " represents the static calibration constant of the calorimeter; it depends only on the heat fluxmeter.  $\tau$  represents the dynamic calibration constant and is called the calorimeter time constant since it has the dimension of time.  $\tau$  depends upon both the fluxmeter and the heat capacity of the cell.

The amount of heat generated by a thermal process during a time period from  $t$  to  $t'$  can be obtained from the electrical signal by integration of Equation (7-10):

$$Q_t^{t'} = A \int_t^{t'} E dt + A\tau \int_t^{t'} dE \quad (7-11)$$

If the integration time limits  $t$  and  $t'$  are chosen such that the whole thermal process is included, then the second term on right side of equation (7-11)

becomes zero, so that

$$Q_{\text{process}} = A \int_{\text{process}} E dt \quad (7-12)$$

in which  $Q_{\text{process}}$  represents the total heat developed by the thermal process under study.

The term  $\int E dt$  is equal to the area under the curve of the recorded electrical signal over the time interval  $(t' - t)$ . The calibration constant,  $A$ , is obtained from the integration of the electrical signal produced from a calibration experiment.

(3). Variable temperature of thermostat.

If the temperature of the calorimetric block,  $\theta_0$ , changes due to the residual instability of the regulator, or as a result of temperature programming, the temperature of the vessel follows the change and move towards  $\theta_0$ . As a result of this temperature variation, thermal power is transmitted through the fluxmeter, which produces a disturbing electrical signal. To reduce this disturbing signal, the calorimeter is fitted with a second vessel with identical features which is surrounded by a second fluxmeter connected in opposition to the first fluxmeter. Therefore, disturbing signals due to temperature variation are essentially cancelled.

### Apparatus

A block diagram of the C-80 heat-flow calorimeter is shown in Figure 7-2. Figure 7-3 offers a more detailed description of the C-80 calorimeter block, cells, and heat fluxmeters.

The calorimeter shell is cylindrical and has a massive aluminum block in its center, which is used as a calorimetric thermostat. Two identical cylindrical cavities, symmetrically located from the center line, house the two calorimetric cells (C1 and C2). The cells, identical in design, are machined to fit snugly into the cavities in the aluminum block. One cell acts as a sample/measurement cell and the other as a reference cell.

The cells used in heat capacity measurement are stainless-steel cylinders with threaded top caps. Each cell can be securely closed and sealed with an aluminum "o" ring so that it is able to withstand moderately high pressures. The volumes of the cells were determined using a standard densimetric approach in which doubly distilled water at 25 °C was used as the calibration liquid. Volumes were calculated to be 6.0591 cm<sup>3</sup> and 6.1434 cm<sup>3</sup> for the measurement and reference cells respectively.

When placed in the calorimetric block, each cell is surrounded by a thermopile (fluxmeter). The two fluxmeters are designed identically and are connected in opposition to give a differential thermopile output. This arrangement cancels interfering signal disturbances caused by the presence of residual temperature instability or temperature programming. The fluxmeters thermally connect the two cells to the calorimetric block. Hence, any thermal

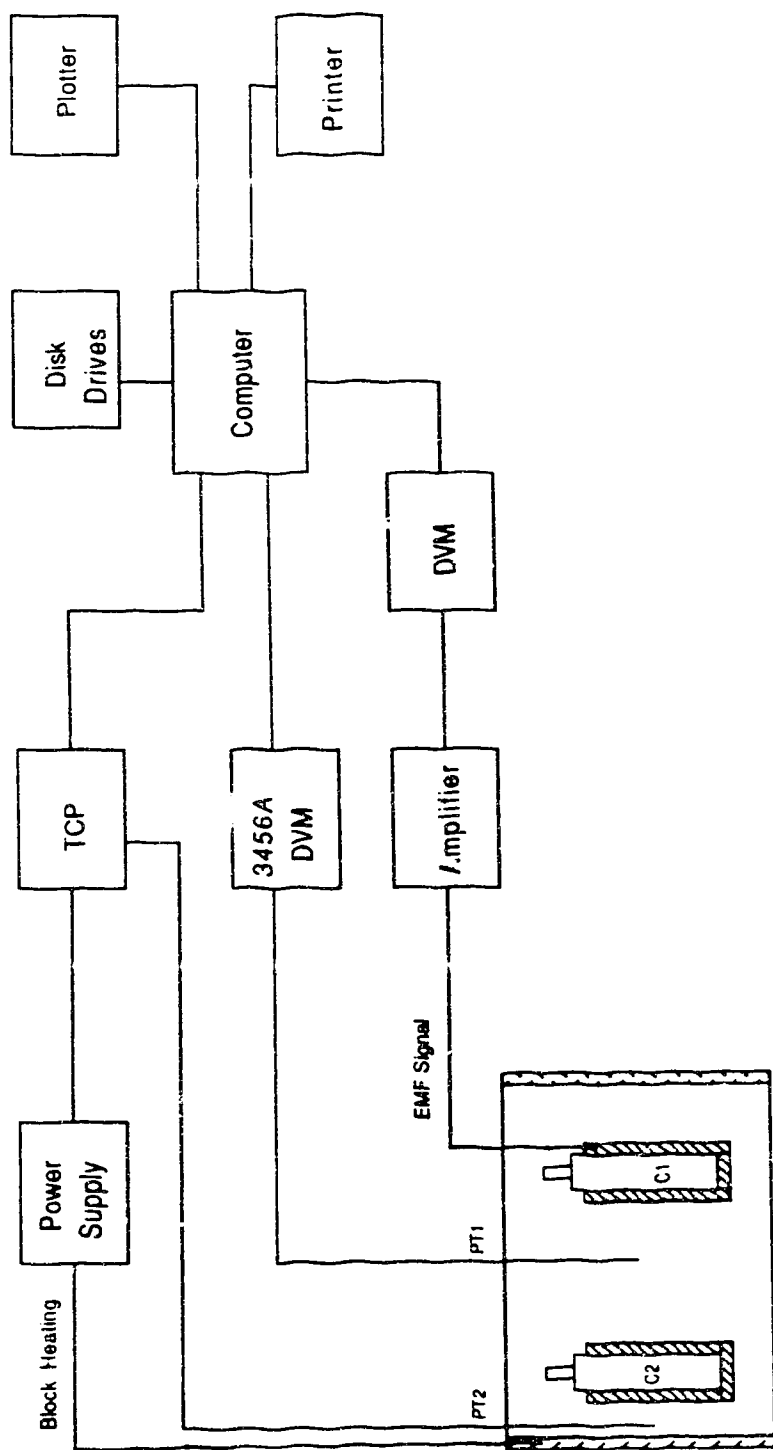


**Figure 7-2. Block diagram of C-80 heat flow calorimeter and accessories.**

**C1 and C2: calorimetric cells; PT1 and PT2: platinum temperature measuring and controlling probes; DVM: digital voltmeter; TCP: temperature controller and programmer**

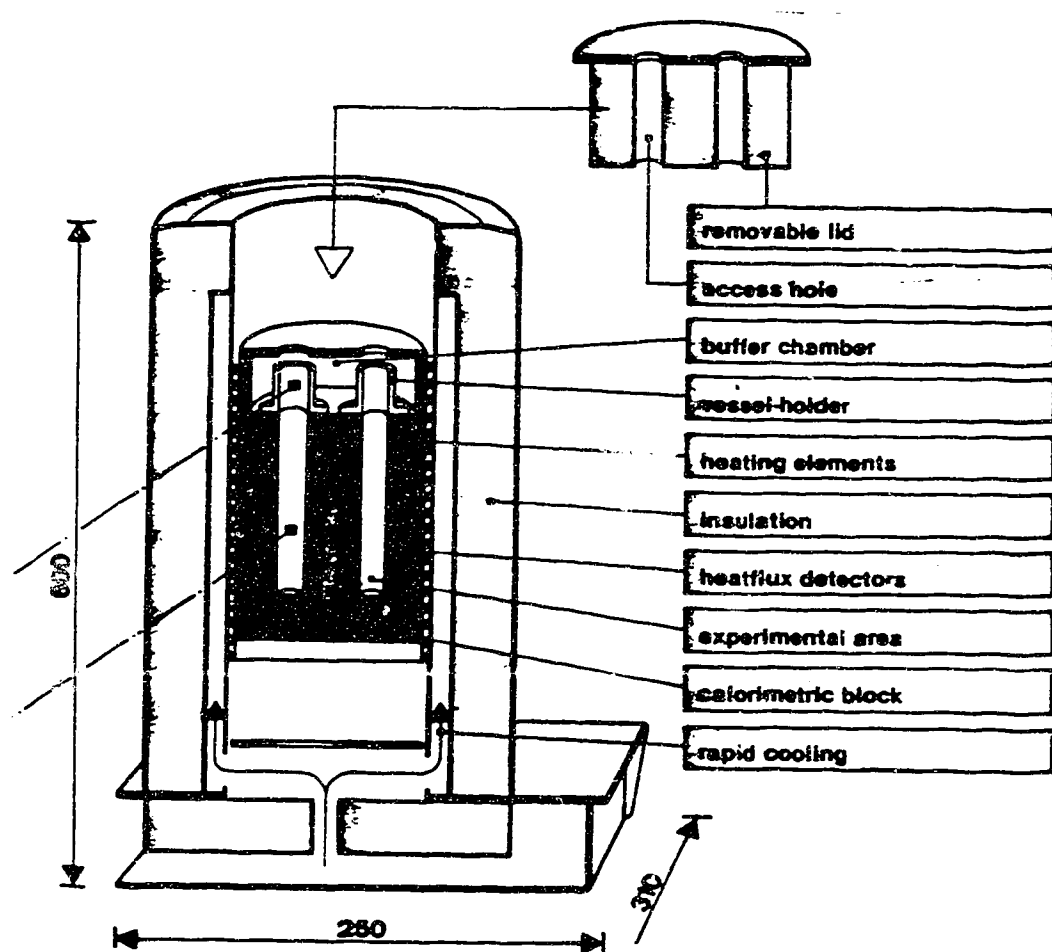


Figure 7-3. A cross-sectional diagram of the C-80 calorimeter



exchange between the cells and the calorimetric block leads the fluxmeter to output a proportional signal, which is channelled to a digital voltmeter.

Two platinum resistance probes are located within the calorimeter. They are labelled PT1 and PT2 in Figure 7-1.

Probe PT2 (we call it the controlling probe) is used to control the temperature of the calorimetric block. It has a resistance of approximately  $200\ \Omega$  at  $0\ ^\circ\text{C}$  and is connected via a four wire arrangement to a temperature control unit. A heater wrapped around the outside of the aluminum block, also connected to the temperature control unit, maintains the set experimental temperature of the calorimeter in the range  $30$  to  $300\ ^\circ\text{C}$ .

Sensor PT1 (we call it the measuring probe) is used to obtain the temperature of the cells within the calorimeter. It is located on the center line of the apparatus between the measurement and the reference cell. It has a resistance of approximately  $100\ \Omega$  at  $0\ ^\circ\text{C}$  and was initially connected using a four wire arrangement to a temperature safety unit (SETARAM TS1). This unit converts the measured voltage and current across probe PT1 into a resistance and thence to a temperature. If the temperature of the calorimeter were to exceed the set safety temperature, then power to the calorimeter heater would be cut off automatically. From the safety unit the temperature signal is channelled to a digital display unit supplied by SETARAM. Unfortunately the temperature can only be read to one decimal place with this unit, which is not accurate enough for our purposes. Therefore, probe PT1 was reconnected, using a four wire arrangement, to a Hewlett-Packard HP-3456A six figure

The software necessary to control the operation of our calorimetric system was written in-house, using Hewlett Packard BASIC. Our programs have been designed to enable users unfamiliar with the complexities of the C-80 calorimeter to obtain calorimetric data in a routine fashion.

The computer is connected to a 3½" dual disc drive unit (HP-9121), which permits the storage of collected calorimetric data. Hard copies of results are obtained from an HP-82906A printer, supported by an HP-7470A two pen plotter.

### **Calibration of the Platinum Resistance Probe PT1**

The relationship between resistance and temperature for device PT1 was not supplied by SETARAM; hence it was necessary to calibrate the device using a standard resistance probe. A Rosemount 162N standard platinum resistance probe, calibrated for the temperature range -189°C to 500°C on the International Practical Temperature Scale of 1968 by the Physical Division of the National Research Council of Canada, was utilized in this procedure.

The standard probe was secured in the center of one of the cavities and connected via a four wire arrangement to the HP-3456A nanovoltmeter. A computer program was written for the HP-86 computer to ramp the temperature of the calorimeter from 30°C to 100°C in 10°C intervals and from 100°C to 300°C in 25°C intervals. This program ensured that each new temperature was held constant for six hours. It then separately averaged the resistance readings

taken from both the standard resistance probe and PT1 in the seventh hour, before ramping to the next temperature.

The values of temperature were calculated from the resistance of the standard platinum probe, using the equation supplied with the Rosemount probe by National Research Council of Canada. Table 7-1 lists the resistances of probe PT1 and the corresponding temperatures. A graph that correlates the temperature and resistance of the measuring probe PT1 is given in Figure 7-4. The polynomial equation used to fit the data is

$$t = A + BR + CR^2 + DR^3 \quad (7-13)$$

in which  $t$  is temperature ( $^{\circ}\text{C}$ ),  $R$  is the resistance of probe PT1 ( $\Omega$ ) and  $A$ ,  $B$ ,  $C$ , and  $D$  are constants. The values of these constants obtained from the fit are given in Table 7-2. The maximum deviation between the temperature calculated by Equation (7-13) and that listed in Table 7-1 is less than  $0.005^{\circ}\text{C}$ , which is the same as the quoted temperature stability of the temperature control system.

Table 7-1 Calorimetric block temperature calibration (PT1)

t (set) (°C)	R (PT1) (Ω)	t (calibration) (°C)
35	113.575	34.932
50	119.235	49.545
60	123.045	59.408
70	126.834	69.256
80	130.629	79.149
90	134.408	89.029
100	138.176	98.906
125	147.512	123.518
150	156.833	148.279
175	166.036	172.902
200	175.198	197.609
225	184.260	222.233
250	193.284	246.233
275	202.219	271.598
295	209.301	291.281

Table 7-2 Constants for Equation (7-13)

Constants	Value	Unit
A	-245.908	°C
B	2.37962	°C $\Omega^{-1}$
C	$7.32375 \times 10^{-4}$	°C $\Omega^{-2}$
D	$7.68533 \times 10^{-7}$	°C $\Omega^{-3}$

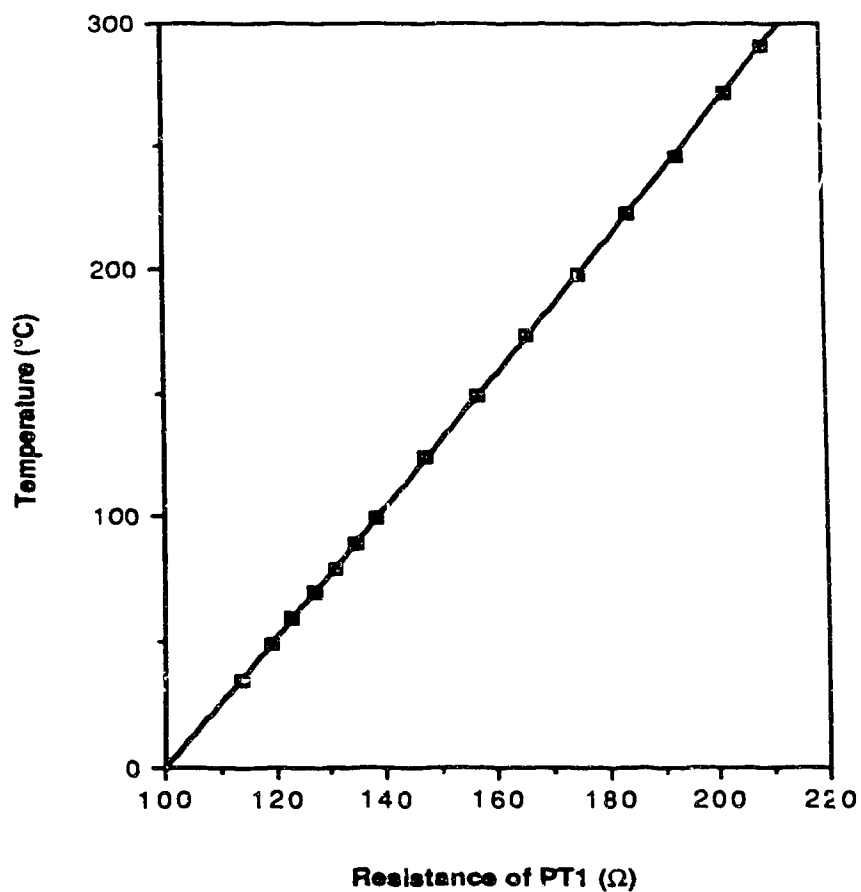


Figure 7-4. A graph showing the calibration of calorimetric block temperature: the points were measured with a standard platinum probe and the solid line was the result calculated from Equation (7-13)

### Sensitivity Calibration

The differential thermopile output (emf signal) from the fluxmeter can be converted into a calorimetric signal, CS (in mW), using the equation

$$CS \text{ (mW)} = S \times D \times 0.1 \times L^{-1} \quad (7-14)$$

in which S is the amplified fluxmeter signal reading on the digital voltmeter (DVM); D is the amplification range setting on the amplifier (unit A10); L is the sensitivity in units of  $\mu\text{V/mW}$  and 0.1 is a unit conversion factor.

Equation (7-14) indicates that the sensitivity values at different temperatures are prerequisites to obtaining useful calorimetric signals. The sensitivity L is actually a calibration constant which converts the electrical signal to thermal power. Calibration can be achieved by utilizing a standard reaction that is similar to the one under investigation and carried out in the same experimental conditions. In practice, however, it is rare to obtain suitable standard reactions. Therefore, calibration is most commonly performed electrically. SETARAM provides two Joule effect calibration cells and a calibration unit (including constant power supply and time counter) for this purpose. This arrangement was used to obtain a sensitivity calibration curve for our calorimeter.

The two calibration cells are identical in design. Each cell comprises two hollow concentric stainless steel cylinders between which a  $1000\Omega$  resistance is embedded. During the calibration, one cell is connected to the calibration unit using a Joule Effect Cable. (The choice of cell is arbitrary. However, we have customarily chosen cavity C1 as the experimental chamber. Therefore, the

calibration cell placed in cavity C1 is connected to the power supply). The underlying principle of the Joule effect calibration procedure is to supply a constant power to the calibration resistance heater for a known period of time. In our calibrations the calorimeter was allowed to reach thermal equilibrium at the temperature of interest for approximately six hours before starting a calibration experiment. On obtaining a suitable baseline, the Joule Effect Calibration Procedure was initiated by pressing the "impulsion start" button on the EJ2 unit. A constant power, manually set on the unit, was then automatically supplied to the resistance heater of the calibration cell. Power settings available are 0.1, 1, 10 and 100 mW. In our calibrations, we used a power setting of 10 mW. The power supply setting of 10 mW was examined by measuring the voltage and current and found to be 9.996 mW. After initiation of the experiment, the differential fluxmeter signal increased and eventually leveled off with time. After a pre-programmed time interval, power to the calibration cell was terminated and the fluxmeter signal returned to the baseline. The signal and time data were downloaded to a floppy-disk and plotted by the computer. A typical signal for the calibration procedure is shown as Figure 7-5.

The sensitivity (or calibration constant) of the calorimeter at the temperature of interest can be calculated from the results of the calibration experiment in either of two ways :

(1) Find the difference in fluxmeter signal between the baseline (before power was supplied to the calibration cell) and the equilibrium level (level of signal after power was supplied to the calibration cell). Division of this quantity (in  $\mu\text{V}$ )



by the power (mW) supplied to the calibration cell gives the sensitivity (L). A summary of this procedure is offered by Equation (7-15)

$$L (\mu\text{v} / \text{mW}) = [(S2 - S1) \times 0.1 \times D] / p \quad (7-15)$$

in which p is the power supplied to the cell (9.996 mW), S2 and S1 are defined in Figure 7-5, and the other symbols have been defined earlier.

(2) Since all of the heat produced by the electrical power is eventually transferred through the fluxmeter to the calorimetric block, the sensitivity can be calculated by an alternative integration method. In this method, the area under the calibration curve is found by integration. Division of this value ( $\mu\text{v.s}$ ) by the total energy (mJ) supplied to the calibration cell leads to the sensitivity. The sensitivity calculated using this method once again has units of  $\mu\text{v}/\text{mw}$ . This approach is summarized by the equation

$$L = \int_{t_1}^{t_2} \frac{S \times 0.1 \times D}{p \Delta t} dt \quad (7-16)$$

in which  $t_1$  and  $t_2$  are the recorded times for run initiation and termination respectively and  $\Delta t$  is time duration for which power is supplied.

The second method of calculation was used in our computer program. Calibration experiments were conducted at  $10^\circ\text{C}$  intervals in the range  $30^\circ\text{C}$  to  $100^\circ\text{C}$  and at  $25^\circ\text{C}$  intervals in the range  $100^\circ\text{C}$  to  $300^\circ\text{C}$ . The sensitivities of our calorimeter at different temperatures are reported in Table 7-3. The

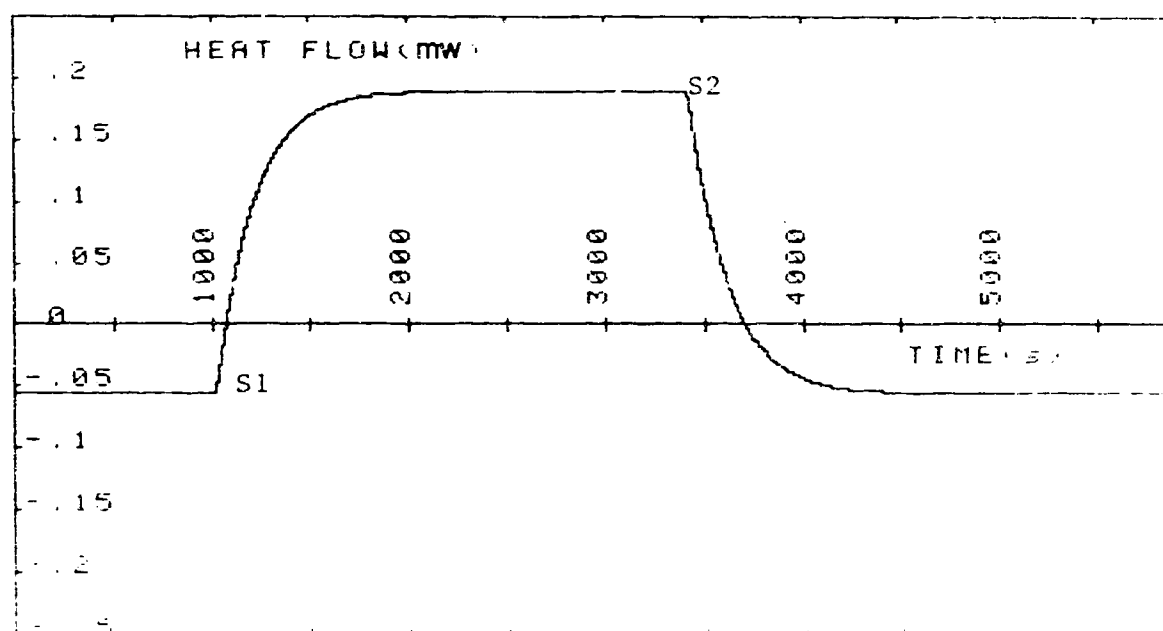


Figure 7-5. Joule effect calibration signal for the C-80 calorimeter

sensitivities reported are the average values of at least two separate isothermal determinations. The precisions of the sensitivities are better than  $\pm 0.1\%$  over the temperature range studied. A plot of the calculated sensitivities of our calorimetric system as a function of temperature is included as Figure 7-6. This calibration curve can be seen to differ only very slightly from the general calibration curve supplied by SETARAM.

Equation (7-17) was fitted to our sensitivity/temperature data using the method of least squares:

$$L = a_0 + a_1t + a_2t^2 + a_3t^3 + a_4t^4 \quad (7-17)$$

where  $t$  is the temperature ( $^{\circ}\text{C}$ ) and  $a_0$  to  $a_4$  are constants. Estimates for these constants are contained in Table 7-4. The standard deviation of fit was calculated to be  $0.005 \mu\text{V/mW}$ .

Table 7-3                      Sensitivities of C-80 calorimeter

T (°C)	L ( $\mu\text{V}/\text{mW}$ )	L (SETARAM)
29.939	30.780	30.807
39.769	30.669	30.689
44.687	30.592	30.621
49.606	30.531	30.548
59.448	30.360	30.386
69.296	30.179	30.204
79.149	29.970	30.003
89.007	29.752	29.783
98.869	29.501	29.547
123.537	28.835	28.888
148.261	28.093	28.144
172.889	27.278	27.338
197.620	26.414	26.477
222.250	25.518	25.585
247.051	24.590	24.668
271.614	23.650	23.754
291.322	22.892	23.027

Table 7-4 Sensitivity calibration equation constants

Constant	Estimate
$a_0$	30.974
$a_1$	$-1.9190 \times 10^{-3}$
$a_2$	$-1.5865 \times 10^{-4}$
$a_3$	$3.0525 \times 10^{-7}$
$a_4$	$-2.2294 \times 10^{-10}$

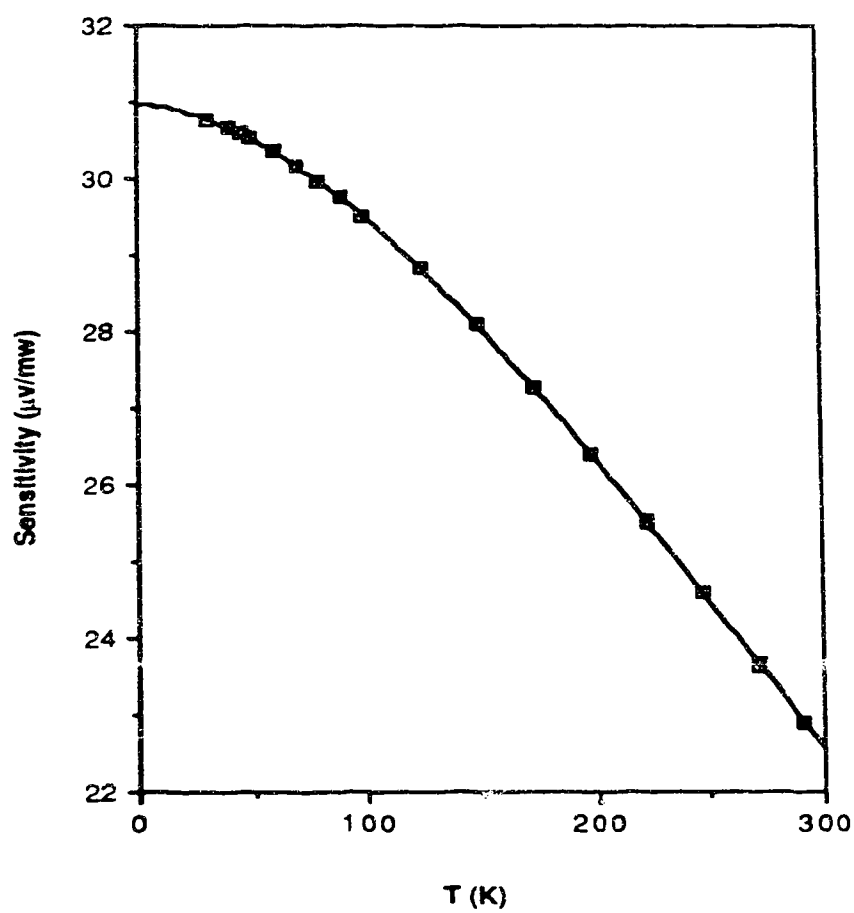


Figure 7-6. Sensitivity curve for the C-80 calorimeter: solid line is calculated from Equation (7-17), individual points are experimental data

### Heat Capacity Measurement

The C-80 microcalorimeter is capable of measuring heat capacities in the temperature range from ambient to 300°C. In addition, the instrument can be modified to measure heat capacities as a function of pressure up to 100 atmospheres. The experiments described in this section were conducted using closed cells; hence the only pressures applied to the systems investigated were atmospheric pressure and the saturated vapor pressures of the samples under study.

For heat capacity measurements the sample under investigation was placed in the measurement cell, which in turn was placed in the measurement chamber (C1) of the calorimeter. The cell placed in the reference chamber of the calorimeter remained empty. Both cells were allowed to come to thermal equilibrium over a period of 4-6 hours at the temperature of interest. The temperature was then automatically ramped, at a precisely known rate, to a temperature approximately 2°C higher than the initial set temperature. During this time the calorimetric signal increases as a function of time. On attainment of the higher set temperature the calorimeter automatically reverted to isothermal mode, causing the calorimetric signal to return to the baseline. Prior to a measurement run it was necessary to conduct a reference run. The same two cells, both empty, were used in this procedure. The reference experiment was designed to duplicate the experimental conditions used in the measurement run. The purpose of a reference run was to correct for the very slight asymmetry

found between the reference cell and the measurement cell and also between fluxmeters.

The calorimetric signal of the sample under study can be obtained from these data by subtracting the reference signal from the measurement signal. The heat capacity of the sample under study can be calculated from the resulting signal by utilizing the following procedures.

By definition the heat capacity at constant pressure,  $C_p$ , is defined by Equation (7-18).

$$C_p = (\partial H / \partial T)_p \quad (7-18)$$

Integration of Equation (7-18) gives

$$C_p = Q / \Delta T \quad (7-19)$$

in which  $\Delta T$  represents the temperature difference between initial temperature  $T_1$  and final temperature  $T_2$ .  $Q$  is the total heat absorbed by the sample during the temperature ramping procedure, which is obtained by the integration of calorimetric signal using

$$Q = \int_{t_1}^{t_2} (CS_m - CS_r) dt \quad (7-20)$$

Here  $t_1$  is the time of run initiation and  $t_2$  is the time of run termination.  $CS_m$  and  $CS_r$  are the calorimetric signals obtained from the measurement and the reference runs respectively. Therefore, the specific heat capacity of the sample is calculated by



$$C_p (\text{J g}^{-1} \text{K}^{-1}) = \frac{\int_{t_1}^{t_2} (CS_m - CS_r) dt}{(T_2 - T_1) W} \quad (7-21)$$

in which  $W$  is the mass of the sample in the calorimetric cell.

We have developed a computer program to apply the above method. The program was written to initiate and terminate the temperature ramping procedure and to collect and then store the calorimetric signal and temperature data. At the end of a run the program allows for numerical integration of the signal peak over the appropriate time interval to yield a value of the specific heat capacity of the sample under study using Equation 7-21.

The heat capacity calculated using this method is an average heat capacity over the temperature range  $T_1$  to  $T_2$ .

### **Testing on Heat Capacities of Synthetic Sapphire ( $\alpha\text{-Al}_2\text{O}_3$ )**

Synthetic sapphire ( $\alpha\text{-Al}_2\text{O}_3$ ) has been recommended and used by many investigators as a standard reference material for the calibration and testing of calorimetric systems.<sup>93-97</sup> The enthalpies and heat capacities of sapphire over a large temperature range have been studied.<sup>96-99</sup>

The procedure for heat capacity measurement has been summarized earlier. In the computer program used for heat capacity measurement, we used our calibrated temperatures and our measured sensitivities. The heat capacity measurements were conducted over the temperature range 320 K to 450 K at

intervals of 10 K and in the range 470 K to 550 K at intervals of 20 K. About 2 grams of sapphire was used in each run, using temperature ramp rate of 2 K h<sup>-1</sup>.

Sapphire was provided by Johnson Matthey. The purity of this  $\alpha$ -Al<sub>2</sub>O<sub>3</sub> was 99.998%. The resulting heat capacities of sapphire are presented in Table 7-5. Ditmars *et al.*<sup>97</sup> have published smoothed heat capacity values from 10 K to 2250 K at intervals of 10 K. They also presented a summarizing equation for the heat capacity values. We have used this equation to calculate the heat capacities at the same temperatures as our experimental temperatures. The values are also shown in Table 7-5.

In 1953, Ginnings and Furukawa<sup>98</sup> reported heat capacity values of five recommended heat capacity standards, one of which was  $\alpha$ -aluminum oxide. They reported the values of heat capacity of  $\alpha$ -Al<sub>2</sub>O<sub>3</sub> from 14 to 1173 K, measured by precision adiabatic calorimetry. Mraw and Naas<sup>96</sup> measured heat capacities of  $\alpha$ -Al<sub>2</sub>O<sub>3</sub> from 100 to 800 K using a differential scanning calorimeter (DSC). They reported their data for 10 K intervals. More recently, Inaba<sup>99</sup> used an adiabatic calorimeter to measure the heat capacities of sapphire in the temperature range 70 to 700 K. To compare our data with these literature data, we plotted the heat capacities against temperatures for our values and literature values in the same graphs, as shown in Figures 7-7a to 7-7d.

A fourth-degree polynomial equation has been fitted to our heat capacity data for  $\alpha$ -Al<sub>2</sub>O<sub>3</sub> using the method of least-squares. The resulting equation is

Table 7-5

Heat capacities of synthetic sapphire ( $\alpha$ -Al<sub>2</sub>O<sub>3</sub>)

T (K)	C <sub>p</sub> (J K <sup>-1</sup> mol <sup>-1</sup> ) (this work)	C <sub>p</sub> (J K <sup>-1</sup> mol <sup>-1</sup> ) <sup>a</sup> (literature data)
318.73	82.60	83.25
330.54	85.49	85.50
340.41	87.34	87.22
	87.18	
	87.43	
	87.72	
350.29	88.47	88.89
360.14	89.79	90.47
370.02	91.00	91.97
390.74	95.13	94.89
400.66	95.70	96.17
410.45	97.15	97.38
420.33	98.07	98.55
430.26	99.49	99.65
440.09	101.58	100.70
449.95	101.91	101.70
470.57	103.25	103.66
490.42	104.87	105.36
510.16	105.81	106.91
529.93	108.90	108.34
550.71	109.43	109.72

a: calculated from the smoothing equation in reference 97

represented by

$$C_p / \text{J K}^{-1} \text{mol}^{-1} = 74.084 - 0.45498T + 2.8927 \times 10^{-3}T^2 - 5.3959 \times 10^{-6}T^3 \\ + 3.3712 \times 10^{-9}T^4 \quad (7-22)$$

To assess the accuracy of the calorimeter, deviations from equation (7-22) of our data and the literature data have been plotted in Figure 7-8. Table 7-5 and Figures 7-7 to 7-8 have shown that the heat capacities of sapphire measured with our C-80 calorimeter are in good agreement with those measured with an adiabatic calorimeter. However, from Figures 7-7-a and 7-8 it is seen that the differences between our results and Mraw and Naas' results at some temperatures are as high as 2.5%. The disagreement is due mostly to the inaccuracy of the DSC calorimeter. Previous experience has shown that the heat capacity measurement results obtained from adiabatic calorimeters should be regarded as the "best" results. Therefore the accuracy of our calorimeter is determined by the comparison of our results to those from adiabatic calorimeter, which leads to the conclusion that the accuracy of our data is almost 1% in the temperature range from ambient to 550 K. To test the precision of the calorimeter, we repeated the heat capacity measurement at 340.4K four times. Each run was done separately over a period of several days. The results shown in Table 7-5 indicate that the standard deviation for heat capacities at this temperature is less than 0.5 %.

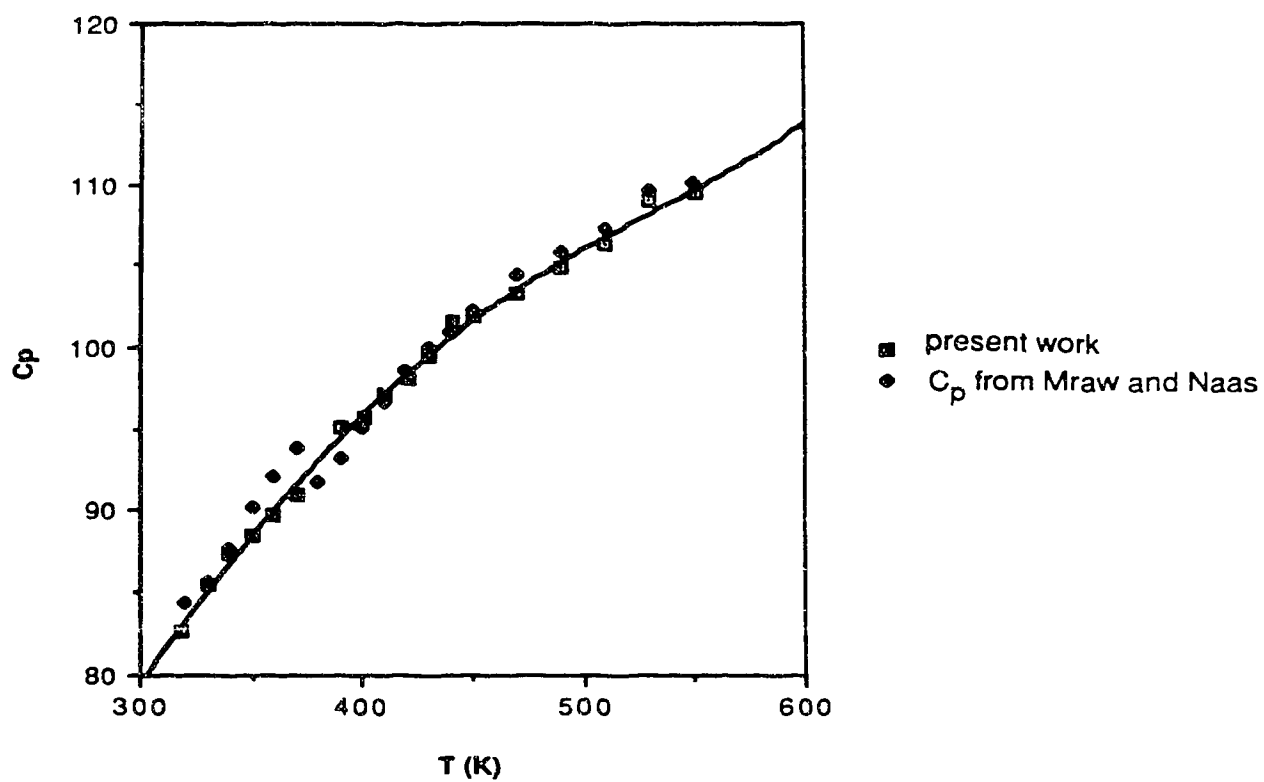


Figure 7-7-a. Heat capacities of  $\alpha$ - $\text{Al}_2\text{O}_3$  in the temperature range 300 K to 550 K, measured with the C-80 calorimeter in comparison with the data of Mraw and Naas

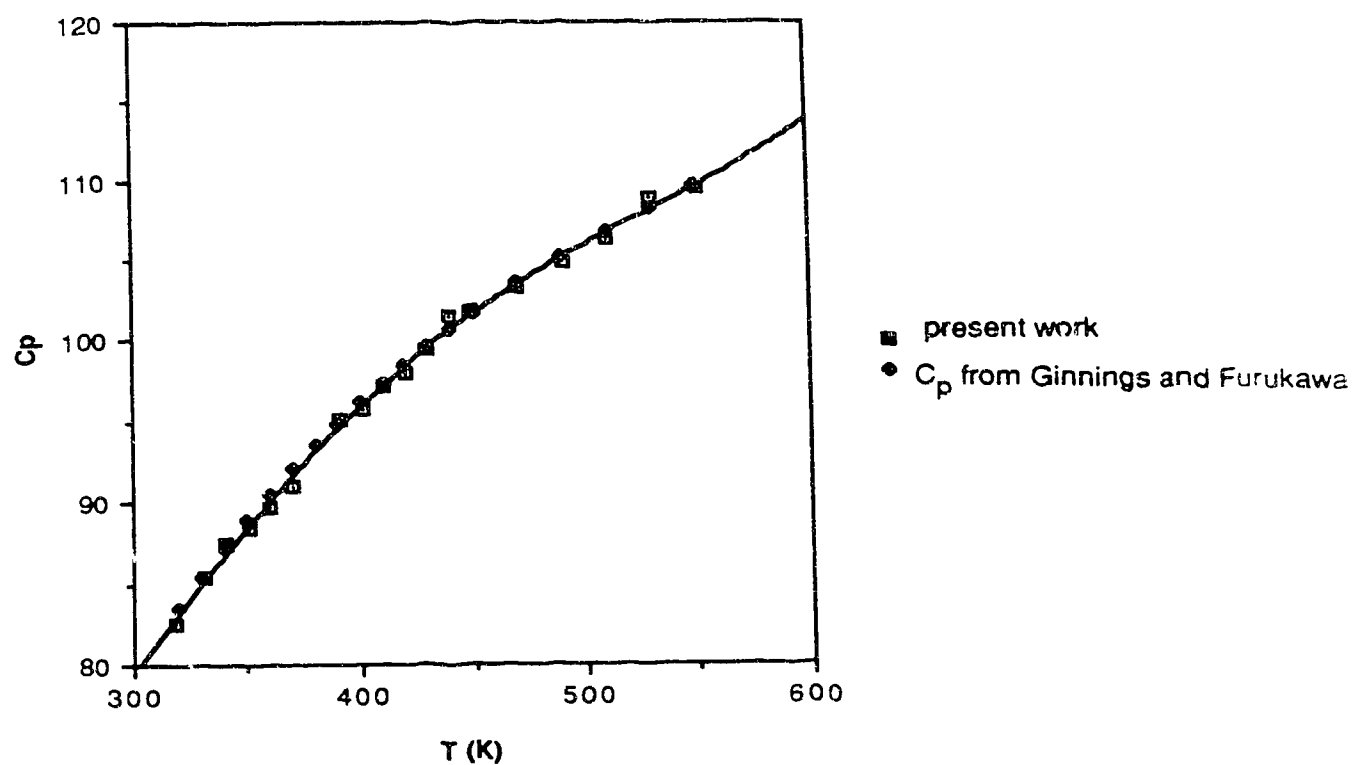


Figure 7-7-b. Heat capacities of  $\alpha$ - $\text{Al}_2\text{O}_3$  in the temperature range 300 K to 550 K, measured with the C-80 calorimeter in comparison with the data of Ginnings and Furukawa

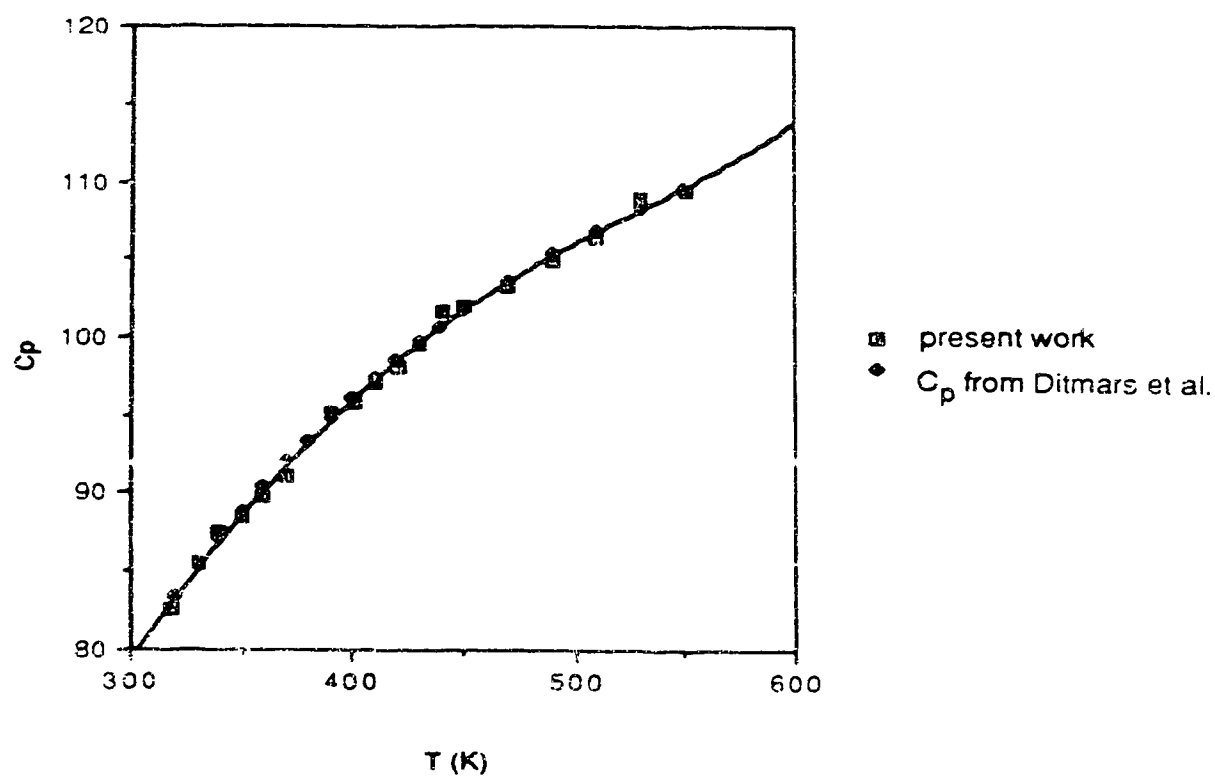


Figure 7-7-c Heat capacities of  $\alpha$ - $\text{Al}_2\text{O}_3$  in the temperature range 300 K to 550 K measured with the C-80 calorimeter in comparison with the data of Ditmars.

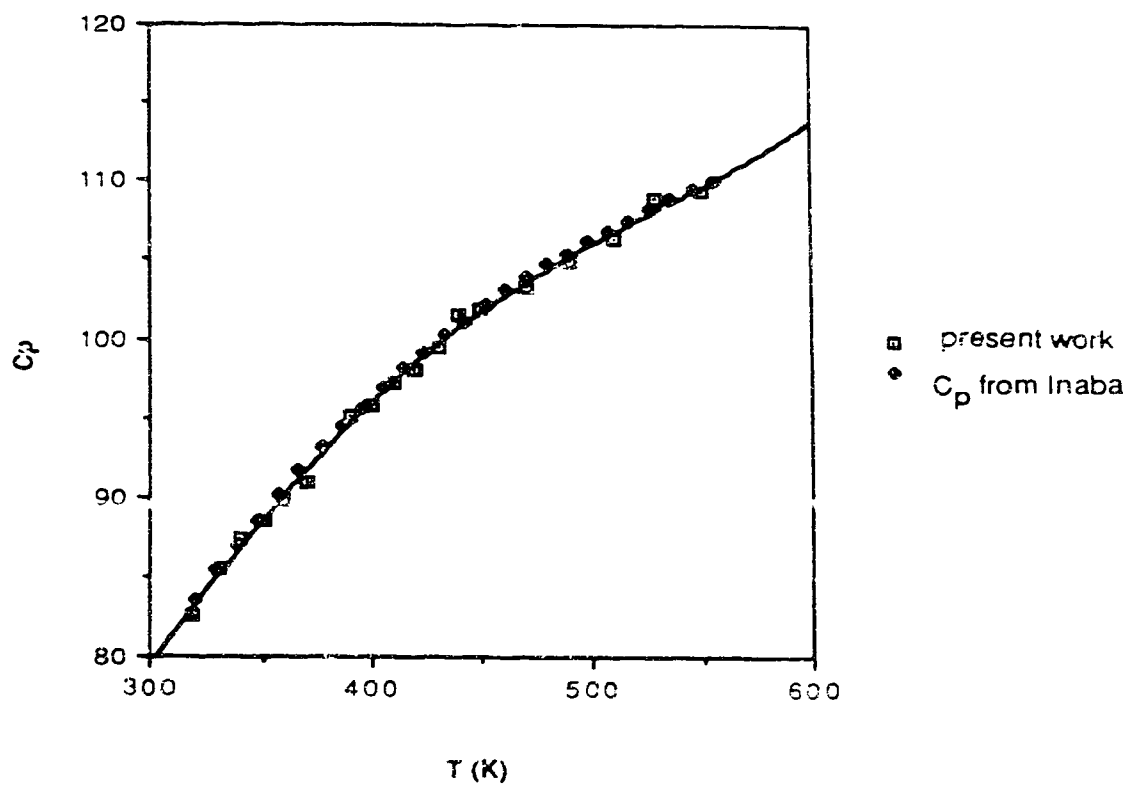


Figure 7-7-d. Heat capacities of  $\alpha$ - $\text{Al}_2\text{O}_3$  in the temperature range 300 K to 550 K, measured with the C-80 calorimeter in comparison with the data of Inaba



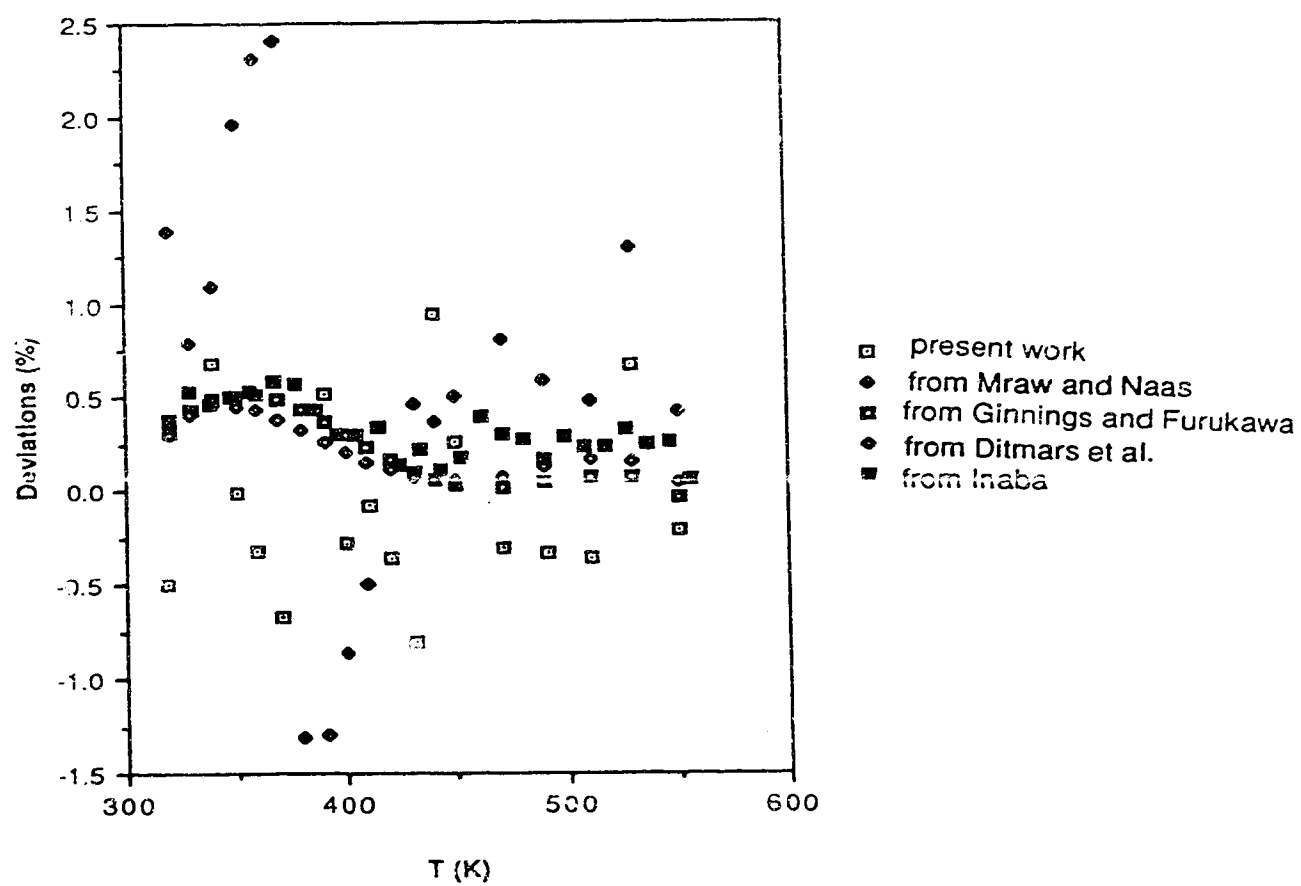


Figure 7-8. Deviations of heat capacity data for  $\alpha\text{-Al}_2\text{O}_3$  from the fitted results of Equation 7-22

## Chapter 8

### Heat Capacities of Saturated Water and Deuterium Oxide

#### Introduction

Measurements of heat capacities of water and deuterium oxide were made for two reasons. First, we recognized the need for accurate heat capacity data for water and deuterium oxide, especially at temperatures above 100°C. The other purpose is to test the accuracy of the C-80 calorimeter for heat capacity measurements of liquids at temperatures above the normal boiling points.

The importance of the heat capacity of water is straightforward. As a chemical, water is the most important solvent. As a heat-transfer medium, water plays principal role in many units for heating and cooling industrial processes. Water and steam can also be used as a power producing medium to drive turbines in the electric power industry. In addition, water has been recommended by the National Bureau of Standards (now, the National Institute of Standards and Technology) as one of the standard materials for calibration or testing calorimeters.

The study of the properties of heavy water ( $D_2O$ ) is of great interest in the study of isotopic effects on the properties of water. Heavy water has been widely applied in nuclear reactors as a moderator; hence an accurate knowledge of the thermodynamic properties of heavy water is necessary for designing heavy water nuclear reactors.

### Heat Capacities of Saturated Two Phase System

In general, heat capacities depend on the conditions of measurement. The two kinds of heat capacity that are most common are the heat capacity at constant pressure,  $C_p$ , and the heat capacity at constant volume,  $C_v$ . However, the heat capacities of liquid we have measured with C-80 calorimeter are for closed cell systems so that we have obtained neither  $C_p$  nor  $C_v$ . In a closed cell system both the volume of the liquid and the pressure over the liquid (vapor pressure) are functions of temperature. Hence the heat capacities we measured are the heat capacities of a two-phase system (i.e., the liquid plus its saturated vapor) that we identify by the symbol  $C_{II}$  in which the subscript "II" indicates equilibrium two phase system. This heat capacity includes the heat capacity of liquid, heat capacity of vapor, and a contribution from the heat of vaporization.  $C_{II}$  is not the same as the heat capacity of the saturated liquid at the saturation pressure, which we will denote by  $C_{SL}$ . It is this latter heat capacity that is needed for several purposes. Therefore, we have made the appropriate thermodynamic derivation to obtain an equation that allows us to calculate the heat capacity of saturated liquid  $C_{SL}$  from the measured two-phase heat capacity  $C_{II}$ ; This derivation is presented in Appendix A.

The water ( $H_2O$ ) used was double distilled and degassed. The sample of deuterium oxide was provided by Aldrich Chemical Company, Inc. with the minimum purity of deuterium of 99.996 atom %. The saturation heat capacities,

$C_{II}$ , of water and deuterium oxide were measured with C-80 calorimeter over the temperature range 40 to 275°C, using the procedure described earlier.

About 4.5 grams of liquid sample was placed in the experimental cell, initially at room temperature. The liquid sample occupied 80 to 90% of the volume of the cell, which left enough space for liquid expansion at higher temperatures. The cell was sealed by an aluminum "O" ring and tightened to prevent leaking of vapor and to withstand high pressure (at 275°C the vapor pressure of water is close to 60 atm.). Using the same procedure as for the  $\alpha$ -Al<sub>2</sub>O<sub>3</sub> system, we obtained the heat capacities of the two phase system  $C_{II}$  for water and deuterium oxide, which are presented in Table 8-1 and Figure 8-1.

Ginnings and Furukawa<sup>98</sup> have published their very accurate values of saturation heat capacities of water in the temperature range of 0 to 100°C. We included their data in Figure 8-1 to compare with our data. Again the accuracy of our data is seen to be within 1% of the best available earlier results.

Eucken and Eigen<sup>101</sup> studied the specific heat of D<sub>2</sub>O between 20 and 130°C, using an adiabatic calorimeter. We also include their data in Figure 8-1. Our heat capacities of D<sub>2</sub>O are in good agreement (better than 0.5%) with Eucken and Eigen's data. Both sets of data show the same trend with temperatures. At lower temperatures the heat capacity of D<sub>2</sub>O decreases with increasing temperature and reaches a minimum near 100°C.

### Heat Capacities of Saturated Liquid

As mentioned earlier, the heat capacity of a liquid directly measured with a closed cell is the heat capacity for both the liquid and its saturated vapor, and also includes a contribution from enthalpy of vaporization. At temperatures lower than the normal boiling point of the liquid under study, since the vapor pressure of the system is relatively small,  $C_{SL}$  is very nearly equal to  $C_{II}$ . But as the temperature of the system increases to temperatures beyond the normal boiling point of the sample, the heat capacity of saturated vapor and the heat of vaporization make contributions to the total measured heat capacity of the system so that  $C_{SL} > C_{II}$ . The heat capacity of the saturated liquid,  $C_{SL}$ , can be calculated from the measured quantity  $C_{II}$  as outline below.

Osborne and van Dusen<sup>102</sup> were the first to give a full thermodynamic analysis of the heat capacity of a two phase system. Later, Hoge<sup>103</sup> offered a more concise derivation of the relationship between measured  $C_{II}$  and desired  $C_{SL}$ . More recently, Steele *et al.*<sup>104</sup> have done similar work dealing with  $C_{II}$  and  $C_{SL}$ . We have adopted the basic ideas of Hoge and derived an equation that relates  $C_{SL}$  to  $C_{II}$  as shown by Equation (8-1):

$$C_{SL} = C_{II} + \left(\frac{dP}{dT}\right) \left[ T \left(\frac{dV_L}{dT}\right) - \frac{T}{M} \left(\frac{dV}{dT}\right) \right] + \left(\frac{d^2P}{dT^2}\right) \left[ V_L T - \frac{VT}{M} \right] \quad (8-1)$$

The detailed derivation is presented in the attached Appendix A. In Equation (8-1)  $P$  represents the saturated vapor pressure of the liquid at temperature  $T$ ,  $V_L$  represents the specific volume of the saturated liquid,  $V$  is the volume of the

Table 8-1 Saturation two phase heat capacities ( $\text{J K}^{-1} \text{mol}^{-1}$ ) of  $\text{H}_2\text{O}$  and  $\text{D}_2\text{O}$ 

T ( $^{\circ}\text{C}$ )	$C_{\text{II}}-\text{H}_2\text{O}$	$C_{\text{II}}-\text{D}_2\text{O}$
39.65	74.42	83.66
49.54	74.73	
49.89		83.27
59.37	75.04	83.50
70.27	75.15	83.05
80.16	74.83	82.87
90.04	75.37	82.41
99.91	75.60	82.46
125.51	76.94	83.37
150.18	78.08	84.41
174.88	79.47	85.83
200.60	81.43	87.73
225.24	83.95	88.47
249.90	85.27	89.82
274.60	91.45	95.98

Molecular Weight for  $\text{H}_2\text{O}$ : 18.0153; for  $\text{D}_2\text{O}$ : 20.026  $\text{g mol}^{-1}$

Mass of water or Deuterium oxide: 4 - 4.5 grams

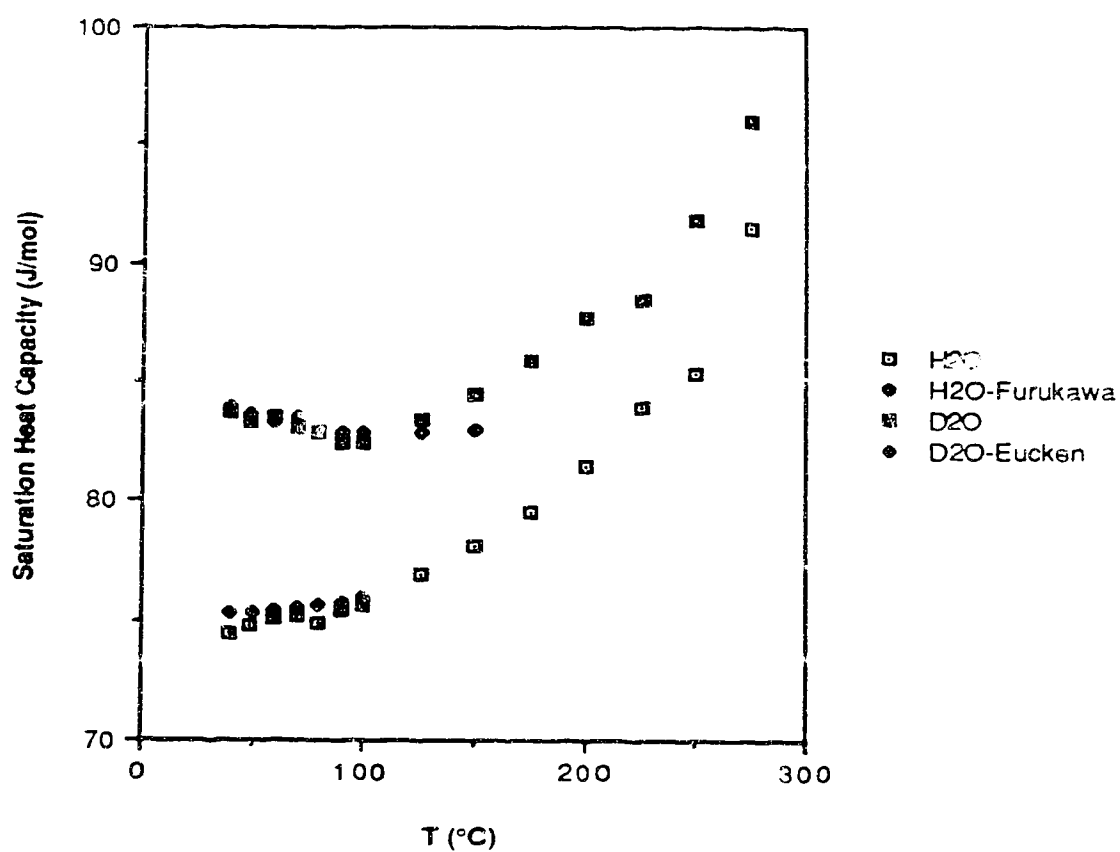


Figure 8-1. Saturation two phase heat capacities for water and deuterium oxide as a function of temperature.

experimental cell and  $M$  is the total mass of the liquid plus vapor.

For water and deuterium oxide, the saturated vapor pressures and specific volumes of the saturated liquid over wide temperature ranges<sup>105-107</sup> are available, which make it possible for us to apply Equation (8-1) to calculate the heat capacities of saturated liquid.

We have fitted polynomial equations to the saturated vapor pressure and specific volumes. These equations have been differentiated to give the quantities  $dp/dT$ ,  $d^2p/dT^2$  and  $dV_L/dT$  that are required in Equation (8-1). Another quantity appearing in Equation (8-1), the expansibility of the calorimetric cell,  $dV/dT$ , was obtained by using Equation (8-2) as derived in Appendix A:

$$\frac{dV}{dT} = 3V_0 \varepsilon [1 + \varepsilon (T - T_0)]^2 \quad (8-2)$$

In this equation  $V_0$  is the volume of the experimental cell at room temperature  $T_0$  and  $\varepsilon$  is the linear expansion coefficient of the material of the calorimetric cell. When these quantities were calculated, the heat capacities of saturated liquid for water and deuterium oxide at different temperatures were obtained from the measured saturation heat capacities using Equation (8-1). These values are presented in Table 8-2.

Comparison of the values of  $C_{II}$  and  $C_{SL}$  in Tables 8-1 and 8-2 shows that the difference between  $C_{II}$  and  $C_{SL}$  increases with increasing temperature. For example, at 40°C the difference between  $C_{II}$  and  $C_{SL}$  is less than 0.1%, while at 200°C, the difference is 1%.



### Heat Capacities of Liquid at Constant Saturation Pressures

The constant pressure heat capacity  $C_p$  under saturated vapor pressure  $P_s$  can also be calculated from the heat capacity of saturated liquid,  $C_{SL}$ . The relation between  $C_p$  and  $C_{SL}$  is

$$C_{SL} = C_p - T \left( \frac{\partial V_L}{\partial T} \right)_P \frac{dP_s}{dT} \quad (8-3)$$

The detailed derivation of Equation (8-3) is given in Appendix B. We have used Equation (8-3) for calculating the values of  $C_p$  at different temperatures that are presented in Table 8-2. Again, the difference between  $C_{SL}$  and  $C_p$  increases with increasing of temperature. At temperatures below normal boiling point the differences between  $C_p$  and  $C_{SL}$  are negligibly small. The comparison of our calculated  $C_p$  data with the literature data from the "NBS/NRC Steam Tables" is also given in Table 8-2. This comparison shows that the differences between our calculated  $C_p$  data and the literature data are less than 1.5 %.

$C_p$  under any other constant pressures can be obtained by using the thermodynamic equation

$$\left( \frac{\partial C_p}{\partial P} \right)_T = -T \left( \frac{\partial^2 V_L}{\partial T^2} \right)_P \quad (8-4)$$

Table 8-2 Saturated liquid heat capacities and heat capacities of liquid at constant saturation pressures ( $\text{J K}^{-1} \text{mol}^{-1}$ ) for water and deuterium oxide

$T$ ( $^{\circ}\text{C}$ )	$C_{\text{SL}}\text{-H}_2\text{O}$	$C_{\text{p}}\text{-H}_2\text{O}$	$C_{\text{p}}\text{-H}_2\text{O}^*$	$C_{\text{SL}}\text{-D}_2\text{O}$	$C_{\text{p}}\text{-D}_2\text{O}$
39.65	74.35	74.35	75.348	83.59	83.59
49.54	74.65	74.65	75.334	83.18	83.18
59.37	74.96	74.96	75.352	83.38	83.38
70.27	75.01	75.0 <sup>*</sup>	75.431	82.88	82.89
80.16	74.71	74.72	75.562	82.65	82.66
90.04	75.15	75.16	75.744	82.12	82.13
99.91	75.31	75.33	75.969	82.09	82.11
125.51	76.44	76.49	76.723	82.75	82.80
150.18	77.30	77.41	77.689	83.49	83.60
174.88	78.50	78.72	83.584	84.59	84.81
200.60	80.34	80.78	80.924	86.24	86.69
225.24	82.84	83.65	83.586	87.51	88.38
249.88	84.62	86.11	87.472	90.76	92.40
274.60	91.95	94.59	93.396	96.30	99.32

\*: The literature data were supplied to us by Dr. R. N. Goldberg from the equation in the "NBS/NRC Steam Tables".

## Chapter 9

### Calorimetric Investigations on Thermodynamics of

### Calcium Nitrate Tetrahydrate $\text{Ca}(\text{NO}_3)_2 \cdot 4\text{H}_2\text{O}$

#### Introduction

Investigation of molten salt hydrates has two fundamental considerations. In the first place, molten salt hydrates can function as a link between dilute aqueous electrolyte solutions and fused salts. Because the molten salt hydrates are very concentrated aqueous solutions, studies of the molten salt hydrates will certainly provide useful information to theorists for understanding electrolyte solution chemistry. Dilute solutions have been extensively studied and theories have been successfully established. Concentrated solutions are now stimulating more and more investigators' interests, and are becoming a new branch of solution chemistry. Since molten salt hydrates are perhaps the most concentrated electrolyte solutions obtainable by ordinary laboratory techniques, they are attracting primary attention.

The second reason for studying molten hydrate salts is due to potentially important applications. Hydrated salts have been used as a substance for the storage of solar energy, making use of the solid-liquid phase transition. Needed information about hydrated salts to be used for energy storage includes melting or crystallizing temperature, specific heats of solid and liquid, enthalpy of melting or solution, thermal conductivity, viscosity of the liquid, and volume change upon melting.

In the present work, the thermodynamic properties of one of the most commonly used hydrate salts, calcium nitrate tetrahydrate,  $\text{Ca}(\text{NO}_3)_2 \cdot 4\text{H}_2\text{O}$ , are investigated. The selection of calcium nitrate tetrahydrate as our substance to be investigated is based on its useful low melting temperature and its ready availability. In this chapter, we report experimental results for heat capacities of crystalline (before melting) and liquid (after melting) calcium nitrate tetrahydrate, partial molar heat capacities of  $\text{Ca}(\text{NO}_3)_2$  and water in concentrated aqueous calcium nitrate solution, melting temperature, and melting enthalpy.

### Heat Capacities

Analytical reagent calcium nitrate tetrahydrate  $\text{Ca}(\text{NO}_3)_2 \cdot 4\text{H}_2\text{O}$  was obtained from Fisher Scientific Company, and was used in the experiments without further purification. The solid  $\text{Ca}(\text{NO}_3)_2 \cdot 4\text{H}_2\text{O}$  (crystal) was ground to 40-140 mesh prior to filling the calorimetric cell. The samples (either original or ground) were stored in very carefully sealed bottles to avoid any possible change of water content.

The water content of the hydrate was determined by vacuum dehydration at  $150^\circ\text{C}$  to constant weight, which led to the ratio of moles of  $\text{H}_2\text{O}$  to moles of  $\text{Ca}(\text{NO}_3)_2$  equal to 4.02.

Heat capacity measurements were performed using the same procedure as discussed in Chapter 7. Heat capacities of crystalline  $\text{Ca}(\text{NO}_3)_2 \cdot 4\text{H}_2\text{O}$  were measured over the temperature range  $32\text{--}41^\circ\text{C}$  (the melting point of

$\text{Ca}(\text{NO}_3)_2 \cdot 4\text{H}_2\text{O}$  is about  $42.7^\circ\text{C}^{108}$ ). The heat capacities for liquid  $\text{Ca}(\text{NO}_3)_2 \cdot 4\text{H}_2\text{O}$  were measured over the temperature range between  $45$  to  $80^\circ\text{C}$  and for supercooled liquid  $\text{Ca}(\text{NO}_3)_2 \cdot 4\text{H}_2\text{O}$  were measured from  $33$  to  $42^\circ\text{C}$ . The values of molar heat capacities for crystalline and liquid  $\text{Ca}(\text{NO}_3)_2 \cdot 4\text{H}_2\text{O}$  are presented in Table 9-1. The heat capacities are plotted against temperatures as shown in Figure 9-1. Figure 9-1 shows that the heat capacity of the crystal increases slightly with increasing temperature. However, the heat capacity of the liquid in the temperature range from the melting point to  $80^\circ\text{C}$  is almost independent of temperature. In preliminary experiments we noted the occurrence of supercooling and therefore made some heat capacity measurements on the supercooled liquid molten hydrate, with results also presented in Table 9-1 and Figure 9-1. The heat capacities of the supercooled liquid appear to be the same as the heat capacities of the stable liquid at higher temperatures. The standard deviation of the  $C_p$  for molten hydrate is within the uncertainty of the experiments (the uncertainty for heat capacity measurement is 1% as determined in Chapters 7 and 8). Therefore, we take the average value of  $C_p$  as the value of  $C_p$  for liquid  $\text{Ca}(\text{NO}_3)_2 \cdot 4\text{H}_2\text{O}$  over the temperature range studied.

The supercooling of molten  $\text{Ca}(\text{NO}_3)_2 \cdot 4\text{H}_2\text{O}$  was noted by Moynihan<sup>108</sup> 20 years ago. When he performed the experiments on conductivity, viscosity and density of molten calcium nitrate tetrahydrate, he noted the ready formation of supercooled liquid below its equilibrium freezing temperature. He has shown

that the properties of the liquid change in a regular and continuous fashion as it passes into the metastable supercooled region.

Angell and Tucker<sup>109</sup> have used a DSC calorimeter to measure the heat capacity of  $\text{Ca}(\text{NO}_3)_2 \cdot 4\text{H}_2\text{O}$ . They measured heat capacities of the crystal at temperatures lower than 300 K. Their results show that the heat capacity of the crystal increases slightly with temperature, which agrees with our experimental results at higher temperatures. Their results on the heat capacity of liquid  $\text{Ca}(\text{NO}_3)_2 \cdot 4\text{H}_2\text{O}$  show a very slight increase with temperature:  $C_p = 126.0 \text{ cal K}^{-1} \text{ mol}^{-1}$  at 300 K and  $126.4 \text{ cal K}^{-1} \text{ mol}^{-1}$  at 380 K; an increase of only 0.3% over a temperature range of 80 K. However, they reported that the uncertainty of their DSC calorimeter for  $C_p$  measurement was  $\pm 4\%$ , which is greater than the 0.3% change with increasing temperature. Therefore, the change of  $C_p$  with temperature was within the limit of experimental uncertainty, which also agrees with our results (the standard deviation of our  $C_p$  is 0.7% as shown in Table 9-1, which is also less than the experimental uncertainty of 1%). Their heat capacity data on liquid  $\text{Ca}(\text{NO}_3)_2 \cdot 4\text{H}_2\text{O}$  are about 4% higher than our values. Considering the uncertainties of the two calorimeters (4% and 1%, respectively), the values of  $C_p$  are in reasonable agreement.

To develop a suitable model for interpreting the behavior of molten hydrate salts, investigators have studied the similarities of fused anhydrous salt and molten salt hydrates. Angell<sup>110</sup> has correlated the electrical conductance of hydrate melts with that in water-free molten salt systems. He has also found that

the hydrate melts show the ability to dissolve large amounts of other salts of a fairly similar nature, which is similar to most fused anhydrous salts. Braunstein *et al.*<sup>111-115</sup> have studied the association equilibria in hydrate melts and in molten anhydrous salts, through which they have developed a model<sup>115</sup> to describe the hydration and association equilibria in hydrated salts.<sup>111</sup>

To investigate the similarity of thermodynamic properties of anhydrous molten salts and molten hydrates, we compare our heat capacity graph (Figure 9-1) with a graph of the heat capacities of crystalline and liquid  $\text{ZnCl}_2$  as a function of temperature,<sup>116</sup> which is shown in Figure 9-2 and is discussed in more detail later. Figures 9-1 and 9-2 indicate that the variation of heat capacities of crystal and liquid with temperature for  $\text{Ca}(\text{NO}_3)_2 \cdot 4\text{H}_2\text{O}$  and  $\text{ZnCl}_2$  is similar. The heat capacity of liquid  $\text{ZnCl}_2$  is nearly temperature independent over a wide temperature range, while the  $C_p$  of the crystalline  $\text{ZnCl}_2$  shows a slight increase with increasing temperature. The supercooled liquid of  $\text{ZnCl}_2$  has also nearly the same heat capacity as the stable liquid salt. For both  $\text{Ca}(\text{NO}_3)_2 \cdot 4\text{H}_2\text{O}$  and  $\text{ZnCl}_2$ , the heat capacity of the liquid phase is larger than that of the crystalline phase. We also note that in both graphs there is a heat capacity discontinuity (sudden jump) at the temperature of the phase change (melting). In the graph for  $\text{ZnCl}_2$ , the heat capacity of the supercooled liquid shows another discontinuity at a temperature labelled  $T_0$ . This low transition temperature is corresponding to another phase change (glass forming), which is discussed later.

Table 9-1 Heat capacities of crystalline and liquid  $\text{Ca}(\text{NO}_3)_2 \cdot 4\text{H}_2\text{O}$ 

Crystal		Liquid	
T (°C)	$C_p$ (J K <sup>-1</sup> mol <sup>-1</sup> )	T (°C)	$C_p$ (J K <sup>-1</sup> mol <sup>-1</sup> )
33.70	337	78.20	503
34.74	340	68.26	502
36.68	343	58.42	499
38.70	351	49.54	498
39.61	344	45.58	496
40.65	349	*41.64	504
		*40.65	504
		*38.67	503
		*34.71	508
		*33.68	505
		Ave.	502±3.6

Formula weight of  $\text{Ca}(\text{NO}_3)_2 \cdot 4\text{H}_2\text{O}$ : 236.15 g mol<sup>-1</sup>

\*: supercooled liquid



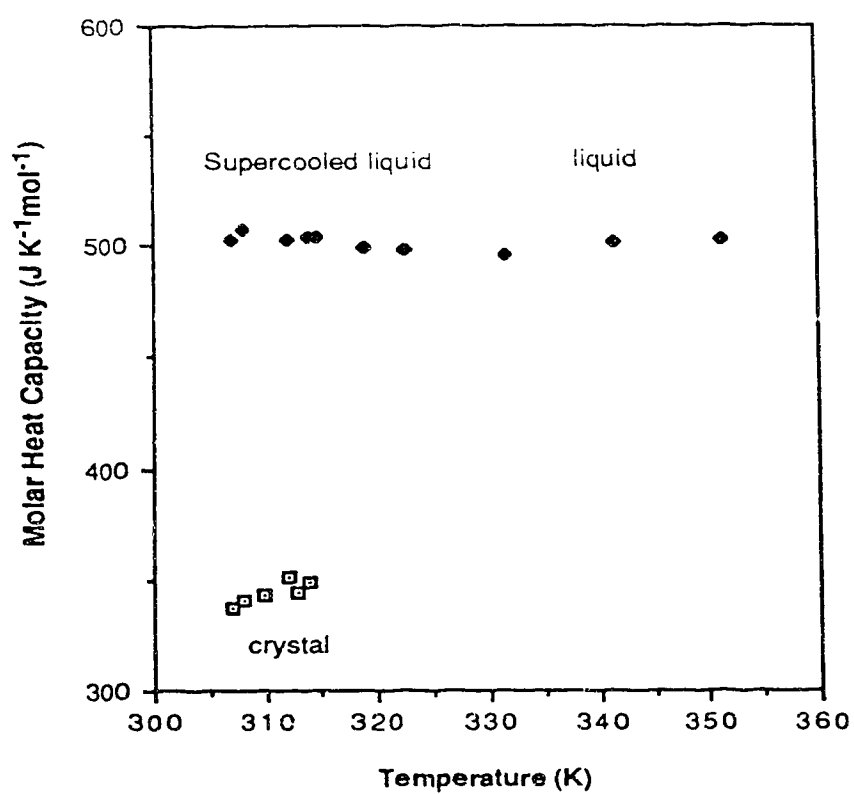


Figure 9-1 Heat capacities of crystalline and liquid  $\text{Ca}(\text{NO}_3)_2 \cdot 4\text{H}_2\text{O}$  as a function of temperature

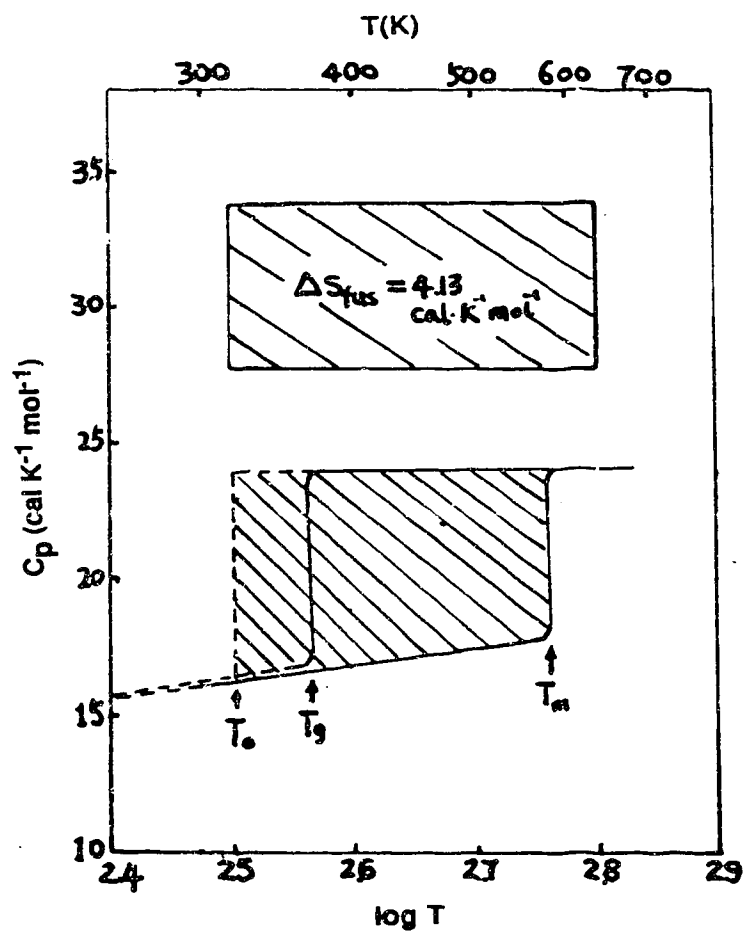


Figure 9-2 Heat capacities of crystalline and liquid  $\text{ZnCl}_2$  as a function of temperature (obtained from the data in references 131 and 116)

## **Composition Dependence of Heat Capacity: Partial Molar Heat**

### **Capacities of $\text{Ca}(\text{NO}_3)_2$ in Concentrated Aqueous Solution**

The behavior of water in molten salt has received more and more attention in recent years. For example, Claes and Glibert<sup>117</sup> have investigated concentration dependence of molar volumes, conductivities and viscosities of molten salts and concentrated salt solutions. Combes<sup>118</sup> studied the solubilities of water in molten salts and discussed the consequences of the presence of water in high temperature molten salts. Lovering and Oblath<sup>119</sup> have presented a paper dealing with the effects of water on electrode processes and electrochemistry of water in molten salts. Recently, Emons and his coworkers have published a series of paper on the subject of molten salt hydrates.<sup>120-121</sup> They have reported the concentration dependence of enthalpy of evaporation of water and partial molar enthalpy of dilution for the system  $\text{MgCl}_2 + \text{H}_2\text{O}$ . They also obtained values of water activities for mixtures of  $\text{KCl} + \text{MgCl}_2 + \text{H}_2\text{O}$ .

To study the thermodynamics of very concentrated aqueous electrolyte solutions, we have measured the heat capacities of aqueous  $\text{Ca}(\text{NO}_3)_2$  solutions over the composition range from 3 mole  $\text{kg}^{-1}$  to 13.88 mole  $\text{kg}^{-1}$  at three different temperatures and calculated partial molar heat capacities for  $\text{Ca}(\text{NO}_3)_2$  and water.

The solutions were obtained by adding known amounts of distilled water to known amounts of calcium nitrate tetrahydrate. To calculate the molality of the

solute salt  $\text{Ca}(\text{NO}_3)_2$ , the crystalline water in the hydrate was regarded as a part of solvent water. The total mass of water was obtained by adding the mass of diluent water to the mass of crystalline water. The solution obtained can be represented by



Therefore the molality of the solution was  $[1000 / (n+4)18.02 \text{ mol kg}^{-1}]$ .

The quantity obtained most directly from calorimetric measurement is the specific heat capacity ( $\text{J K}^{-1} \text{ g}^{-1}$ ). The specific heat capacities of the  $\text{Ca}(\text{NO}_3)_2$  solutions at different molalities and temperatures are presented in Table 9-2. The results indicate that the specific heat capacities of solutions are a function of the molality. But the specific heat capacities are almost independent of temperature in the temperature range under study. Therefore further measurements at lower molalities were performed at only one temperature (331.6 K).

The partial molar heat capacity of  $\text{Ca}(\text{NO}_3)_2$  is defined by

$$\bar{C}_{p,2} = \left( \frac{\partial C_{p,\text{sol}}}{\partial n_2} \right)_{n_1, T, p} \quad (9-1)$$

Equation (9-1) shows that to obtain the partial molar heat capacity  $C_{p,2}$  the heat capacity of solution  $C_{p,\text{sol}}$  should be expressed as the heat capacity at constant amount of solvent,  $n_1$ . We now choose to express  $C_{p,\text{sol}}$  as that for 1000 gram of water (i.e.,  $n_1 = 55.5 \text{ mol}$ ) with  $m$  mole solute ( $\text{mol kg}^{-1}$ ). Then Equation (9-1) becomes

Table 9-2      Specific heat capacities of  $\text{Ca}(\text{NO}_3)_2$  solution at different concentrations ( $\text{mol kg}^{-1}$ ) and temperatures (K)

Molality ( $\text{mol kg}^{-1}$ )	$C_p$ ( $\text{J K}^{-1} \text{g}^{-1}$ )		
	T = 322.7 K	T = 331.6 K	T = 341.4 K
13.88	2.11	2.10	2.13
12.77	2.16	2.15	2.17
11.89	2.20	2.20	2.19
10.93	2.23	2.23	2.23
10.87	-	2.25	2.24
9.428	-	2.34	-
8.447	-	2.41	-
5.685	-	2.70	-
4.828	-	2.81	-
2.983	-	3.14	-

$$\bar{C}_{p_2} = \left( \frac{\partial C_{p_{\text{sol}}}}{\partial m} \right)_{T,p} \quad (9-2)$$

$C_{p_{\text{sol}}}$  can be calculated from the specific heat capacity of the solution  $C_p$  at the given molality by

$$C_{p_{\text{sol}}} = C_p (1000 + m M_2) \quad (9-3)$$

in which  $m$  is the molality of the solute  $\text{Ca}(\text{NO}_3)_2$ , and  $M_2$  is the molar weight of  $\text{Ca}(\text{NO}_3)_2$ . The values for heat capacity of solution  $C_{p_{\text{sol}}}$  have been calculated from Equation (9-3) and are presented in Table (9-3). To obtain  $(\partial C_{p_{\text{sol}}}/\partial m)_T$  we have fitted a polynomial equation to the experimental data of  $C_{p_{\text{sol}}}$  and  $m$  at 331.6 K and obtained

$$C_{p_{\text{sol}}} (\text{J K}^{-1}) = 4117.8 + 186.70m + 0.6856m^2 + 0.0179m^3 \quad (9-4)$$

The partial molar heat capacity of  $\text{Ca}(\text{NO}_3)_2$  is obtained by differentiation of Equation (9-4) with respect to  $m$ , leading to

$$\bar{C}_{p_2} (\text{J K}^{-1} \text{mol}^{-1}) = 186.70 + 1.3712 m + 0.0537 m^2 \quad (9-5)$$

The relation between the heat capacity of a solution  $C_{p_{\text{sol}}}$  and the partial molar heat capacities of the components ( $C_{p_{\text{H}_2\text{O}}}$  and  $C_{p_2}$ ) is

$$C_{p_{\text{sol}}} = n_{\text{H}_2\text{O}} \bar{C}_{p_{\text{H}_2\text{O}}} + n_2 \bar{C}_{p_2} \quad (9-6)$$

This equation leads to

$$C_{p_{\text{sol}}} = 55.5 \bar{C}_{p_{\text{H}_2\text{O}}} + m \bar{C}_{p_2} \quad (9-6')$$

Table 9-3      Heat capacities for solutions with a constant amount of solvent  
 (1000 grams  $\text{H}_2\text{O}$ ) and  $m$  moles  $\text{Ca}(\text{NO}_3)_2$

$m$	$C_{p\text{sol}} (\text{kJ K}^{-1})$		
(mol $\text{kg}^{-1}$ )	$T = 322.7 \text{ K}$	$T = 331.6 \text{ K}$	$T = 341.4 \text{ K}$
13.88	6.91	6.88	6.96
12.77	6.67	6.65	6.72
11.89	6.48	6.48	6.47
10.93	6.22	6.24	6.22
10.87	-	6.26	6.24
9.428	-	5.95	-
8.447	-	5.75	-
5.685	-	5.22	-
4.828	-	5.03	-
2.983	-	4.68	-

from which we can calculate the partial molar heat capacity of the solvent water in the concentrated solution. Rearranging Equation (9-6') gives

$$\bar{C}_{p_{H_2O}} = (C_{p_{sol}} - m \bar{C}_{p_2}) / 55.5 \quad (9-7)$$

Substitution of Equation (9-4) and (9-5) into Equation (9-7) leads to

$$\bar{C}_{p_{H_2O}} = 74.19 - 1.235 \times 10^{-3} m^2 - 6.450 \times 10^{-4} m^3 \quad (9-8)$$

Figures 9-3 and 9-4 show the graphs of heat capacities of solution, and partial molar heat capacities for  $\text{Ca}(\text{NO}_3)_2$  and  $\text{H}_2\text{O}$  as functions of molality.

Many investigators of electrolyte solutions use apparent molar heat capacity to express the heat capacity of the solution. Apparent molar heat capacity  $\phi C_p$  is defined as

$$\phi C_p = (C_{p_{sol}} - n_{H_2O} C_{p_{H_2O}}^{\circ}) / n_2 \quad (9-9)$$

in which  $C_{p_{H_2O}}^{\circ}$  is the molar heat capacity of pure water. Apparent molar heat

capacity  $\phi C_p$  can be calculated from specific heat of solution by

$$\phi C_p = [C_p(1000 + m M_2) - 1000 C_{p_{H_2O}}^{\circ}] / m \quad (9-10)$$

in which  $C_{p_{H_2O}}^{\circ}$  is the specific heat capacity of pure water, and  $C_p$  is the specific heat capacity of the solution. Rearrangement of Equation (9-9) gives

$$C_{p_{sol}} = n_2 \phi C_p + n_{H_2O} C_{p_{H_2O}}^{\circ} \quad (9-11)$$

or



$$C_{p_{sol}} = m \phi C_p + 55.5 C_{p_{H_2O}}^o \quad (9-11')$$

Partial molar heat capacity can also be calculated from apparent molar heat capacity  $\phi C_p$  by

$$\bar{C}_{p_2} = m \left( \frac{\partial \phi C_p}{\partial m} \right)_{n, T, P} + \phi C_p \quad (9-12)$$

Therefore, if we express  $\phi C_p$  as a function of  $m$ , the values of  $C_{p_2}$  can be obtained by differentiation of  $\phi C_p$  with respect to  $m$  in combination with Equation (9-12). The values of  $C_{p_2}$  calculated using Equation (9-12) and (9-5) show very small differences, which are explained by the uncertainties of the fitting of equations to  $C_{p_{sol}}$  values and  $\phi C_p$  values. However, if the equations for  $C_{p_{sol}}$  and  $\phi C_p$  were exactly fitted to the experimental data,  $C_{p_2}$  obtained from these two equations would be the same. This can be understood by the fact that the substitution of Equations (9-4) and (9-10) to (9-12) leads to the same expression of  $C_{p_2}$  as Equation (9-5).

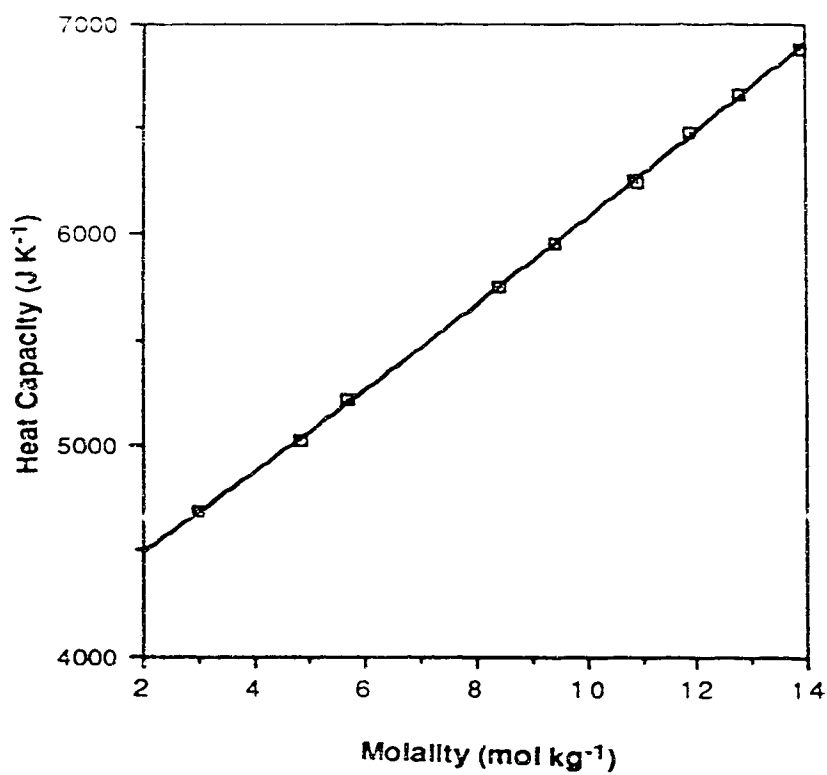


Figure 9-3 Heat capacities of concentrated  $\text{Ca}(\text{NO}_3)_2$  solutions as a function of molality at 331.6 K

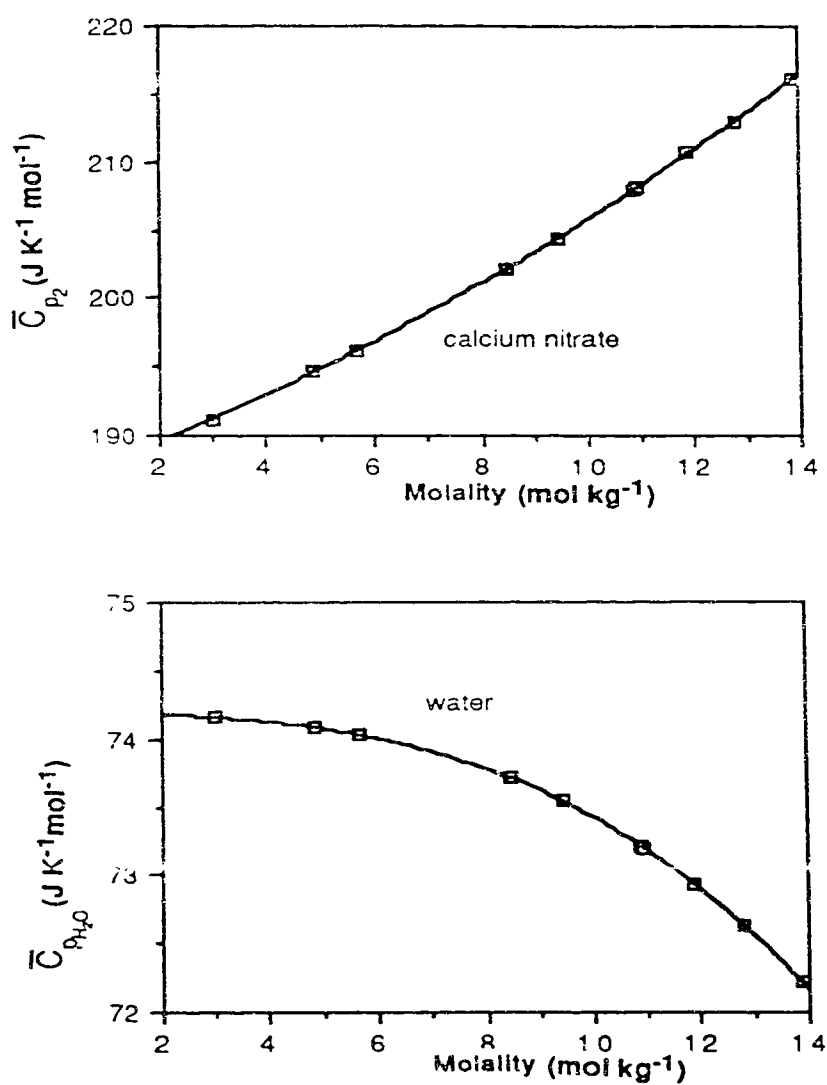


Figure 9-4 Partial molar heat capacities for  $\text{Ca}(\text{NO}_3)_2$  and  $\text{H}_2\text{O}$  in concentrated aqueous solution at 331.6 K

### Melting Temperature, Enthalpy, and Entropy

The melting temperature and melting enthalpy of calcium nitrate tetrahydrate have been determined previously. The uses of these data in connection with solar energy storage have been discussed by Guion *et al.*<sup>122</sup> They have compiled the melting temperatures and melting enthalpies for several hydrates<sup>122</sup> from scientific journals and contract reports. The literature data on  $\text{Ca}(\text{NO}_3)_2 \cdot 4\text{H}_2\text{O}$  summarized by Guion *et al.*<sup>122</sup> show that the reported melting points are distributed over the temperature range 39 to 47°C and the enthalpies of melting over the range 33.3 to 50 cal g<sup>-1</sup>. We have used our C-80 calorimeter for determining the melting temperature and enthalpy to resolve the uncertainties in the literature data.

The experimental procedure for determination of melting point and enthalpy is basically the same as the procedure for heat capacity measurement. About 0.6-0.8 gram of crystal sample (60-140 mesh) was placed in the sample cell. The calorimeter temperature was initially controlled at a temperature slightly below the melting point of the hydrate. The calorimeter temperature was then increased to a few degrees above the melting point. Specifically, the temperature ranges for our measurements were 38.65-48.53°C, 41.66-49.73°C and 41.66-51.55°C. To avoid any local over-heating of the sample, the temperature ramping was controlled at the slow rate of 3 °C per hour.

Figure 9-5 shows a typical thermopile output during the melting of  $\text{Ca}(\text{NO}_3)_2 \cdot 4\text{H}_2\text{O}$ . It is found that a small baseline shift through the melting process is observable in Figure 9-5. The shift of baseline is due to the difference

between the heat capacities of crystal hydrate and molten hydrate (liquid), which we have measured separately. It is observed that the baseline after melting is slightly higher than that before melting. This indicates that the heat capacity of liquid (molten) hydrate is larger than that of crystalline hydrate, which is in accord with the results of our direct heat capacity measurements.

The melting point was determined from the intercept of the initial baseline and the front peak as shown in Figure 9-5. The uncertainty of the melting point is estimated to be  $\pm 0.2^\circ\text{C}$ .

The enthalpy of melting was calculated from the melting signal curve as

$$\Delta H_m = \Delta H_{\text{total}} - C_{p_L} (T_2 - T_m) - C_{p_c} (T_m - T_1) \quad (9-13)$$

in which  $\Delta H_{\text{total}}$  is the total enthalpy change obtained by integration of the area under the curve from initial temperature to final temperature;  $C_{p_L}$  and  $C_{p_c}$  are heat capacities of liquid and crystal form  $\text{Ca}(\text{NO}_3)_2 \cdot 4\text{H}_2\text{O}$ , respectively;  $T_m$  is the melting temperature, and  $T_1$  and  $T_2$  are initial temperature and final temperature, respectively.

Once the value of  $\Delta H_m$  was obtained, the entropy of melting  $\Delta S_m$  was then calculated by

$$\Delta S_m = \Delta H_m / T_m \quad (9-14)$$

in which the melting temperature  $T_m$  is expressed in K.

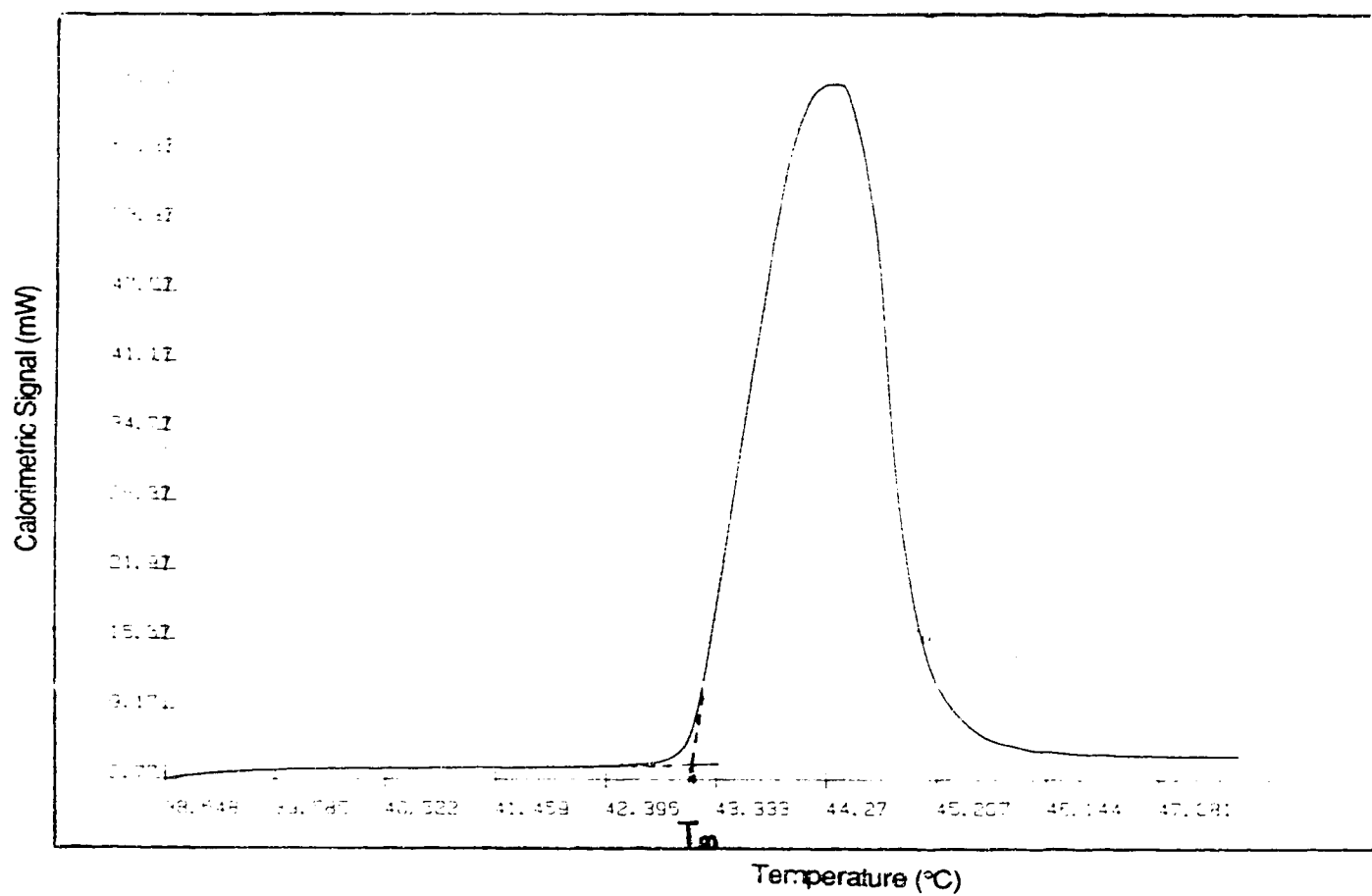


Figure 9-5 A typical heat flux meter signal for melting of  $\text{Ca}(\text{NO}_3)_2 \cdot 4\text{H}_2\text{O}$ . The dashed lines show the method for obtaining the melting temperature.

Five independent measurements on melting of calcium nitrate tetrahydrate have been done and the values of  $T_m$ ,  $\Delta H_m$  and  $\Delta S_m$  are reported in Table 9-3.

We obtained an average melting temperature  $316.05 \pm 0.15$  K, which compares well with values of 316.15 K,<sup>123,124</sup> 315.75 K,<sup>125,126</sup> 315.85 K,<sup>127,128</sup> and  $315.95 \pm 0.2$  K (measured with a capillary melting point apparatus in the Department of Chemistry, University of Alberta). The average value of  $\Delta H_m$  we obtained is  $34.1 \pm 0.8$  kJ mol<sup>-1</sup>, which also agrees with 33.6 kJ mol<sup>-1</sup> from reference 129 and 33.5 kJ mol<sup>-1</sup>.<sup>126,130</sup>

Furbo and Svendsen<sup>123</sup> have correlated the experimental values of  $\Delta H_m$  and  $\Delta S_m$  with the number of water molecules,  $n$ , in hydrated compounds of type  $MX \cdot nH_2O$ . They proposed the following linear correlations:

$$\Delta H_m \text{ (kcal mol}^{-1}\text{)} = 1.62n + 0.41 \quad (9-15)$$

$$\Delta S_m \text{ (cal K}^{-1} \text{ mol}^{-1}\text{)} = 5.48n - 1.16 \quad (9-16)$$

Their empirical correlations led to  $\Delta H_m$  and  $\Delta S_m$  for  $Ca(NO_3)_2 \cdot 4H_2O$  to be 6.89 kcal mol<sup>-1</sup> (28.8 kJ mol<sup>-1</sup>) and 20.76 cal K<sup>-1</sup> mol<sup>-1</sup> (86.8 J K<sup>-1</sup> mol<sup>-1</sup>) that are 15 to 20 percent difference from our measured results.

Guion *et al.*<sup>122</sup> selected literature values for 60 hydrates to correlate  $\Delta H_m$  and  $\Delta S_m$  with moles of water,  $n$ , in hydrates. They proposed two similar linear correlations:

Table 9-3 Experimental determinations of  $t_m$ ,  $\Delta H_m$  and  $\Delta S_m$ 

Run	Temperature Range (K)	$T_m$ (K)	$\Delta H_m$ (kJ mol <sup>-1</sup> )	$\Delta S_m$ (J K <sup>-1</sup> mol <sup>-1</sup> )
1	311.80-321.34	316.0	34.17	108
2	311.80-321.34	315.9	33.94	107
3	314.81-322.88	316.0	32.79	104
4	314.80-324.70	316.2	34.77	110
5	311.80-321.68	316.1	34.65	110
Average		$316 \pm 0.15$	$34.1 \pm 0.8$	$108 \pm 2$



$$\Delta H_m (\text{kcal mol}^{-1}) = 1.692 n + 1.314 \quad (9-17)$$

$$\Delta S_m (\text{cal K}^{-1} \text{mol}^{-1}) = 4.89 n + 6.35 \quad (9-18)$$

These correlations give  $\Delta H_m$  and  $\Delta S_m$  for  $\text{Ca}(\text{NO}_3)_2 \cdot 4\text{H}_2\text{O}$  equal to 8.082 kcal  $\text{mol}^{-1}$  (33.8 kJ  $\text{mol}^{-1}$ ) and 25.91 cal  $\text{K}^{-1} \text{mol}^{-1}$  (108.4 J  $\text{K}^{-1} \text{mol}^{-1}$ ) that are in excellent agreement with our experimental values of 34.1 kJ  $\text{mol}^{-1}$  and 108 J  $\text{K}^{-1} \text{mol}^{-1}$ , respectively.

A hydrate compound can be represented by the formula  $\text{MX} \cdot n\text{H}_2\text{O}$  in which M represents metallic ion, X represents the anion. Thus the melting process can be represented by



in which the subscripts S and L represent solid (crystal) and liquid form hydrate. Guion *et al.*<sup>122</sup> and Telkes<sup>125</sup> have proposed a very simple model for predicting the theoretical value of melting entropy  $\Delta S_m$ :

$$(\Delta S_m)_{th} = \Delta S_m(\text{MX}) + n \Delta S_m(\text{H}_2\text{O}) \quad (9-20)$$

Here  $(\Delta S_m)_{th}$  is a theoretical prediction of  $\Delta S_m$  for the process represented by Equation (9-19),  $\Delta S_m(\text{MX})$  is the melting entropy of one mole of MX compound, and  $\Delta S_m(\text{H}_2\text{O})$  is melting entropy of one mole of water.

We now use Equation (9-20) to predict the  $(\Delta S_m)_{th}$  for  $\text{Ca}(\text{NO}_3)_2 \cdot 4\text{H}_2\text{O}$ .  $\Delta S_m(\text{H}_2\text{O})$  is equal to 22.03 J  $\text{K}^{-1} \text{mol}^{-1}$  from the literature<sup>93</sup> and  $\Delta S_m(\text{Ca}(\text{NO}_3)_2)$  is 25.60 J  $\text{K}^{-1} \text{mol}^{-1}$ .<sup>126</sup> Using Equation (9-20) we obtained the predicted value of  $\Delta S_m$  to be 113.7 J  $\text{K}^{-1} \text{mol}^{-1}$ , which differs by 5% from our experimental value.

### Prediction of the Glass Phase Transition Temperature

As mentioned earlier, the supercooled liquid  $\text{Ca}(\text{NO}_3)_2 \cdot 4\text{H}_2\text{O}$  has been observed in the neat capacity measurement. When the temperature was decreased to ambient temperature the molten  $\text{Ca}(\text{NO}_3)_2 \cdot 4\text{H}_2\text{O}$  was still in the liquid state. The heat capacity of the supercooled liquid was found to be independent of temperature. Because our calorimetric temperature could not be reduced lower than room temperature, we were unable to measure the heat capacity of supercooled liquid  $\text{Ca}(\text{NO}_3)_2 \cdot 4\text{H}_2\text{O}$  at the temperatures that are lower than room temperatures. Generally, if the temperature is further reduced, it eventually reaches a temperature at which the supercooled liquid undergoes a phase transition and forms a solid (either crystal or glass). The phase transition is characterized by a more or less sudden decrease in some intensive thermodynamic properties such as the specific heat capacity or the expansion coefficient.

We have mentioned the heat capacity graph of  $\text{ZnCl}_2$  (Figure 9-2) earlier. Now we use this figure to discuss the phase transition phenomenon in more detail.

Heat capacities of solid and molten  $\text{ZnCl}_2$  were initially measured by Cubicciotti and Eding.<sup>131</sup> They obtained a constant heat capacity of  $24.1 \text{ cal K}^{-1} \text{ mol}^{-1}$  for the liquid state and a temperature dependent heat capacity for the solid (crystal) that can be represented by a linear function of temperature,  $C_p(\text{cal K}^{-1}$

$\text{mol}^{-1}) = 14.5 + 5.5 \times 10^{-3} T$ . Angell and Moynihan<sup>116</sup> have analysed the heat capacity data and constructed a graph of heat capacities against temperature similar to Figure 9-2.

In Figure 9-2, the temperature was expressed using a logarithmic scale so that the area under the curve between any two values of  $\ln T$  represents the entropy difference of the phase between the two temperatures.  $T_m$  in Figure 9-2 represents the temperature of melting.  $T_g$  represents a temperature at which the transition from supercooled liquid to glassy state is experimentally observed, called the glass transition temperature.  $T_0$  is regarded as the true thermodynamic glass transition temperature. According to Gibbs and DiMarzio<sup>132</sup>  $T_0$  is slightly lower than the experimental glass transition temperature  $T_g$ , but can not be reached in a finite time scale experiment due to kinetic considerations.

The parameter  $T_0$  may be interpreted theoretically as the temperature at which molecular or ionic migration stops because the free volume<sup>133</sup> or configurational entropy<sup>134</sup> of the melt vanishes. If the melt is carefully and slowly cooled, we can pass the  $T_m$  and obtain the supercooled liquid. When the temperature is further reduced, the viscosity of the liquid increase rapidly and as it approaches  $T_0$ , the viscosity increases to about  $10^{11}$ - $10^{15}$  poise<sup>116,135</sup> and the melt appears to be a solid in many ways. Because the liquid phase has a higher heat capacity than the solid phase, when the temperatures of both phases are reduced over the same interval, the liquid phase loses more entropy than does

the solid phase. The difference between the entropy loss of two phases is represented by the quadrilateral graphical area bounded above the crystalline phase curve and below the supercooled liquid curve and between two vertical lines of  $\ln T_m$  and  $\ln T$  in question. When the temperature is reduced to  $T_g$ , it is found that the quadrilateral area between  $\ln T_m$  and  $\ln T_g$  is somewhat smaller than the  $\Delta S_{\text{mer}}$  at the normal melting temperature,  $T_m$ . For example, in the  $\text{ZnCl}_2$  system, Angell *et al.*<sup>116</sup> has shown the entropy loss between  $T_m$  and  $T_g$  to be about three quarters of the entropy of melting. If we continue to extrapolate the supercooled liquid curve below  $T_g$ , eventually, we will reach a temperature at which the corresponding area will exceed  $\Delta S_m$ . It implies that the liquid has lost excess entropy so that an amorphous glassy phase is formed with a total entropy less than that of the crystalline solid at the same temperature. This is impossible from thermodynamic considerations. Therefore, Gibbs and DiMarzio<sup>132</sup> proposed that there must be a lower temperature limit  $T_0$  to the liquid curve extrapolation, so that from  $T_m$  to  $T_0$  the liquid would not lose more entropy than  $\Delta S_m$ . Since this  $T_0$  exists by thermodynamic necessity, it must correspond to a true thermodynamic transition. For the  $\text{ZnCl}_2$  system,  $T_g$  has been found to be 376 K and  $T_0$  has been calculated to be 336 K.

Although  $T_0$  is a theoretical concept and never been attained experimentally, it can be calculated in several ways from thermodynamic or transport property considerations. When Angell<sup>109-110</sup> investigated the

conductance of ionic liquids (molten salt or molten hydrates), he noted the non-Arrhenius temperature dependence of the conductance at low temperature. That is, a plot of  $\ln \lambda$  vs.  $1/T$  shows non-linearity, which indicates the inadequacy of the Arrhenius equation

$$\lambda = B \exp(-E / RT) \quad (9-21)$$

to represent the transport properties in the low temperature region. He then applied the free volume theory of liquid transport proposed by Cohen and Turnbull<sup>133</sup> and developed a three parameter equation

$$\lambda = A T^{-1/2} \exp[-K_A / (T - T_o)] \quad (9-22)$$

where  $\lambda$  is the equivalent conductance,  $A$ ,  $K_A$  and  $T_o$  are constants. The parameter  $T_o$  in Equation (9-22) is the theoretical glass transition temperature. Hence  $T_o$  can be obtained by fitting Equation (9-22) to experimentally determined equivalent conductance data. Equations of type (9-22) are also applicable to other transport properties such as viscosities and diffusion coefficients.<sup>116</sup> Therefore, there are several useful ways to calculate  $T_o$ .

$T_o$  can also be obtained directly from thermodynamic data. As mentioned above, when the temperature of liquid reaches  $T_o$ , the liquid loses all entropy of melting  $\Delta S_m$  and the quadrilateral graphical area bounded from  $\ln T_o$  to  $\ln T_m$  (see Figure 9-2) equals to  $\Delta S_m$ . Therefore  $T_o$  can be found from  $\Delta S_m$ ,  $C_{p,liq}$  and  $C_{p,crystal}$  data by

$$\Delta S_m = \int_{T_o}^{T_m} \frac{\Delta C_p}{T} dT \quad (9-23)$$

in which  $\Delta C_p$  is the difference between heat capacity of liquid and crystal,  $\Delta C_p = C_{p\text{liq}} - C_{p\text{crystal}}$ . Glass forming of supercooled liquid  $\text{Ca}(\text{NO}_3)_2 \cdot 4\text{H}_2\text{O}$  has been reported and discussed by Angell and Moynihan.<sup>108-110,116,136-139</sup> Transport properties such as equivalent conductance and viscosity of liquid  $\text{Ca}(\text{NO}_3)_2 \cdot 4\text{H}_2\text{O}$  and mixtures of  $\text{Ca}(\text{NO}_3)_2 \cdot 4\text{H}_2\text{O}$  with other salts have been extensively studied by these authors. The value of  $T_g$  for  $\text{Ca}(\text{NO}_3)_2 \cdot 4\text{H}_2\text{O}$  has been determined in different ways to be 212 K,<sup>137</sup> 217 K,<sup>109</sup> and 220 K.<sup>140</sup>  $T_o$  has been calculated to be 201 K<sup>139</sup> from conductance measurements, 205 K<sup>139</sup> from viscosity measurements and 200 K<sup>109</sup> from thermodynamic measurements.

We have measured the temperature and entropy of melting and heat capacities of both liquid and crystalline  $\text{Ca}(\text{NO}_3)_2 \cdot 4\text{H}_2\text{O}$ , which enable us to use Equation (9-23) to calculate  $T_o$  from the thermodynamic data to compare with  $T_o$  obtained from transport property measurements.  $C_p$  for liquid  $\text{Ca}(\text{NO}_3)_2 \cdot 4\text{H}_2\text{O}$  has been found to be almost temperature independent. Thus an average value from 10 measurements, 502 J K<sup>-1</sup> mol<sup>-1</sup>, is used as the heat capacity of the liquid. A two term equation has been fitted to heat capacities of the crystal:

$$C_{p\text{crys}} (\text{J K}^{-1} \text{mol}^{-1}) = -147.95 + 1.5848 T(\text{K}) \quad (9-24)$$

To a first approximation, we assume that Equation (9-24) can be extrapolated

over the whole temperature range from  $T_o$  to  $T_m$ . Then we place  $C_p$  values into Equation (9-23) and obtain

$$\Delta S_{in} = 649.95 \ln (T_m/T_o) - 1.5848 (T_m - T_o) \quad (9-25)$$

The value of  $T_o$  is calculated to be  $203 \pm 2$  K by solving Equation (9-25). The results indicate that the theoretical glass transition temperature  $T_o$  obtained by thermodynamic methods in the present work is in excellent agreement with those obtained by analysis of transport data.

## Chapter 10

### Heats of Solution of Sodium Chloride and Potassium Nitrate in Molten Calcium Nitrate Tetrahydrate

#### Introduction

Previous investigators have observed very great differences in properties of dilute solutions and very concentrated solutions of electrolytes. In dilute solution there is an excess of water so ions are completely hydrated. However, in very concentrated solutions the ratio of water to salt is much smaller and there is not enough water for ions to form complete hydration sheaths, which makes some such solutions similar to molten salts. When a salt dissolves in water the major interactions are between ions and water. But when a salt dissolves into very concentrated electrolyte solution we must take into account the competition among ion-ion, water-water, and ion-water interactions.

In Chapter 9, we discussed the thermodynamic properties of calcium nitrate tetrahydrate without considering any interactions between  $\text{Ca}(\text{NO}_3)_2$  and other chemicals. In this chapter, we investigate such interactions by in terms of the heats of solution ( $\Delta H_s$ ) of sodium chloride ( $\text{NaCl}$ ) and potassium nitrate ( $\text{KNO}_3$ ) in molten  $\text{Ca}(\text{NO}_3)_2 \cdot 4\text{H}_2\text{O}$  and comparison of these measured  $\Delta H_s$  values with heats of solution of these salts in water.



## Experimental

### Reversal Mixing Cells

In addition to heat capacity measurement the C-80 calorimeter can be used for measurement of heats of mixing, heats of reaction and heats of solution for a solid or liquid in a solvent by using specially designed reversal mixing cells with related accessory parts. The reversal mixing cell, illustrated in Figure 10-1, consists of two concentric stainless steel cylinders. One (we call it the outer cell) has the same dimensions as the regular heat capacity measurement cell. Inside of the outer cell is a smaller (both diameter and height) cylinder (we call it the inner cell). The insides of both ends of the outer cell are threaded. The inner cell is located vertically in one end of the outer cell. It is connected to the outer cell with an "o" ring and a threaded cap. The other end is attached with a second "o" ring and sealed with a threaded top cap. One reagent to be studied is placed in the inner cell and the second one is placed in the outer cell. In normal position, the reagents are isolated from each other. The calorimeter is attached to a motor device. When the rotation switch is in the "on" position the whole calorimeter rotates periodically, which allows the two reagents to mix together.

There are two versions for arrangement of mixing reagents based on reagent properties and measurement requirements, as shown in Figure 10-2.

1. If the vapors of two reagents are required to be completely isolated before mixing (for example mixing two volatile liquids) version A in Figure 10-2 should be used. In this arrangement, the inner cell is completely covered by mercury

and the second reagent is placed on the top of the sealing mercury. This arrangement ensures a complete separation of vapor phases of two reagents.

2. When the vapor pressures of both reagents are very small or vapor phases of the two reagents do not need to be separated, a simpler arrangement (version B) can be used as shown in Figure 10-2. One reagent is placed in the inner cell and the top of the inner cell is opened. The second reagent is placed in the outer cell but the upper level must be lower than the top of the inner cell (actually, the second reagent is in the gap between the wall of inner cell and outer cell). The space above the inner cell is for vapor space. The vapors from different reagents are in equilibrium with two reagents. There are three different sizes of inner cells to be chosen for different situations.

Similar to heat capacity measurements, two identically designed reversal mixing cells are to be used for the measurement of heat of mixing. One is used for mixing of samples and the other is used as a reference cell. The components in the reference cell should be as similar as possible to the components in the sample cell to obtain a good baseline, but the components in the inner and outer compartments of the reference cell must be the same. Commonly, if the sample cell involves mixing of two liquids, a pure solvent or a solution with the same composition as in the sample cell after mixing can be placed in the inner and outer containers in the reference cell. If the sample cell involves a dissolution of a solid into a liquid any pair of the following components can be chosen for the reference cell: pure solvent + pure solvent, or solution + solution (the same composition as in sample cell), or pure solvent + inert solid (e.g., glass beads).

Mixing two components in the sample cell produces a heat change (either exothermic or endothermic) that is detected by the heat flux meter and leads to a signal peak. The signal data are collected by a computer. Again, the software for the computer was developed in house. The program was written to collect calorimetric signal data and integrate the peak to obtain the area under the peak at the end of a run. The data are stored on a 3 1/2" micro-floppy disk. The heat of solution (or reaction, mixing) is calculated from the calorimetric signal by

$$\Delta H_s = \frac{\int_{t_1}^{t_2} CS \, dt}{n} \quad (10-1)$$

in which CS is the calorimetric signal,  $t_1$  is the time starting a run,  $t_2$  is the time required to achieve the final base line, and  $n$  is the number of moles of solute.

## Procedure

In this work we measured the heats of solution of sodium chloride and potassium nitrate in molten calcium nitrate tetrahydrate. To test the calorimeter and program for heat of mixing measurement, a few heats of solution of sodium chloride in water have also been measured at 40°C to compare with the literature data.

Because the vapor pressures of water are not high at the working temperatures, it is not necessary to use arrangement A to completely isolate two reagents. Instead, we used version B for our measurements. In this arrangement, a known amount of solid sample was placed in the outer cell and

a known amount of liquid was placed in the inner cell.

Pure calcium nitrate tetrahydrate was placed in both inner and outer compartments of the reference cell. The mixing cell was tightly closed with the top and lower caps. The cell was then placed in the calorimeter. To get a stable signal for a baseline, the cells were kept in the calorimeter at the set temperature for 4-6 hours before starting the run. When the calorimetric signal became constant, the run was initiated. The computer first collected the signal for several minutes before the calorimeter was rotated. The average of these signal data was used as the initial base line. Then the motor was turned on manually and the calorimeter body started to rotate. After the calorimeter was rotated the signal changed rapidly until it reached the maximum (or minimum), then slowly returned to the baseline. The calorimeter was rotated for several minutes, which is enough for achieving a complete dissolution and forming a homogeneous solution. The total run time was 30 to 40 minutes.

## **Material**

The calcium nitrate tetrahydrate ( $\text{Ca}(\text{NO}_3)_2 \cdot 4\text{H}_2\text{O}$ ) used was the same as that used in the heat capacity measurements described in Chapter 9. To avoid water content change, solid calcium nitrate tetrahydrate powder was added in the cell and closed with the cap. The liquid was obtained after this closed cell was placed in calorimeter at a temperature higher than the melting point.

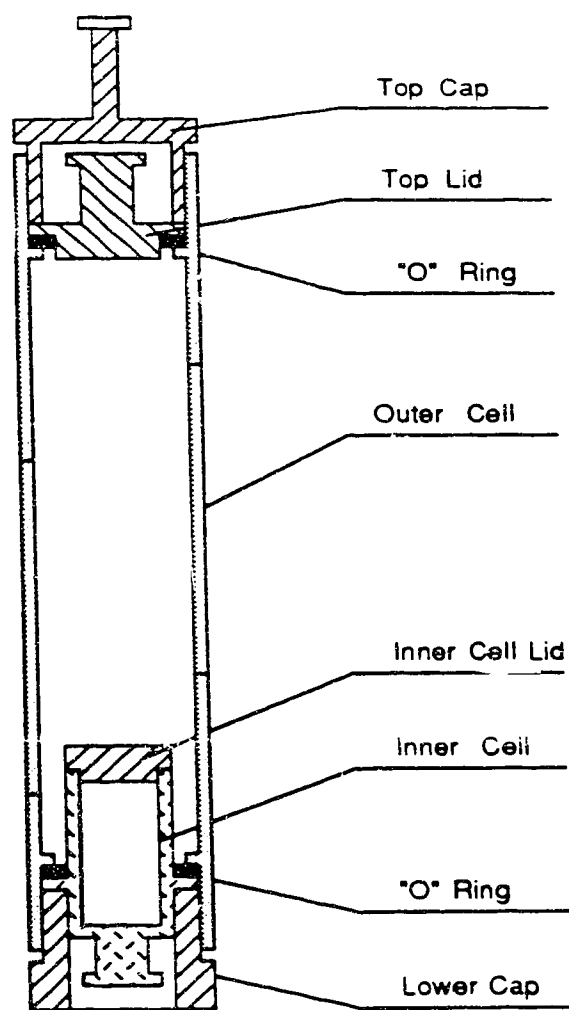


Figure 10-1 Illustration of reversal mixing cell

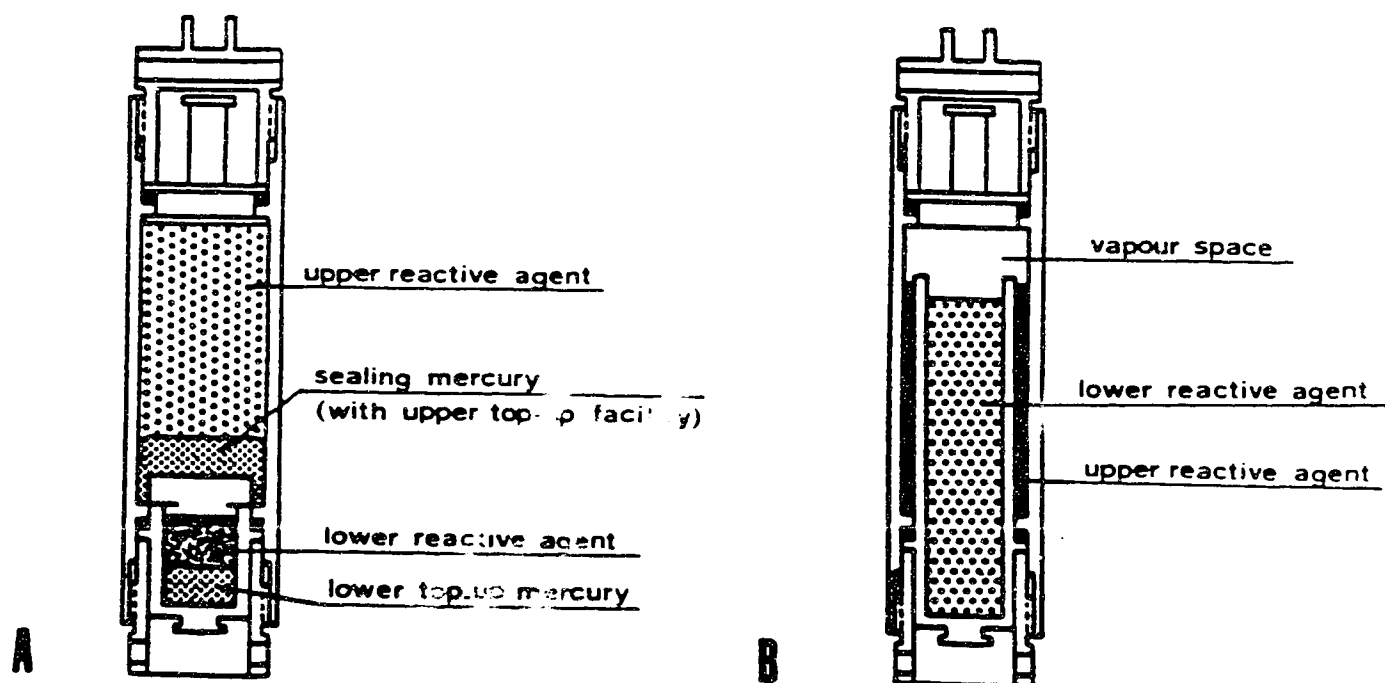


Figure 10-2 Illustration of two different arrangements for mixing components in reversal mixing cell

The NaCl used in the measurements was BDH analytical reagent. The manufacture's specification indicated that the greatest impurity is less than 0.01%, which implied that further purification was unnecessary.  $\text{KNO}_3$  used was also BDH analytical reagent. The greatest impurity was 0.02% according to the specification; therefore,  $\text{KNO}_3$  was used without further purification. NaCl and  $\text{KNO}_3$  samples were dried in a muffle furnace at  $400^\circ\text{C}$  for 4 hours. They were cooled and stored in a vacuum desiccator.

### Results and Discussion

To assess the reliability of the calorimeter and the program for heat of solution measurement we have performed several measurements on heat of solution of sodium chloride in water, which has been studied by many investigators. Up to the present, most measurements on the heat of solution of NaCl in  $\text{H}_2\text{O}$  were done at  $25^\circ\text{C}$ . Only a few investigators have extended the measurements to higher temperatures. Criss and Cobble<sup>141</sup> have measured heats of solution of NaCl in water at very dilute concentration from 0 to  $100^\circ\text{C}$ . The highest concentration they used was only 0.02 mole  $\text{kg}^{-1}$ . For our calorimeter, because of the small volume of mixing cell, if we did the experiment at that low concentration, the amount of NaCl used would be very small, which would lead to a very small heat exchange and a very big uncertainty. More recently, Sanjaja and Cesari<sup>142</sup> reported enthalpies of solution of NaCl in  $\text{H}_2\text{O}$  at 30, 35 and  $40^\circ\text{C}$ . The concentration range they covered was from 0.005 to

0.12 mol kg<sup>-1</sup>. Their higher concentration range is appropriate for our mixing cell. Therefore we compared their results with our data.

Four measurements on heat of solution of NaCl in H<sub>2</sub>O at 40°C have been done. The results are presented in Table 10-1. To compare our results with literature data, we plot  $\Delta H_s$  against molality along with the literature data in Figure 10-4, which indicates that our experimental values agree with the literature data.

Clarke and Glew<sup>143</sup> have used all available literature data on heat of solution of NaCl in water and proposed a computer regression model. Using their regression model they have calculated the integral heats of solution of NaCl in water at different temperatures and in the concentration range from infinite dilute to saturation. We have interpolated their data to obtain the heats of solution at the same temperature and the same concentrations as in our experiments. The differences between our experimental data and the data interpolated from Clarke and Glew's table are less than 3%.

Tables 10-2 and 10-3 present the results of measurements of heats of solution of NaCl and KNO<sub>3</sub> in molten Ca(NO<sub>3</sub>)<sub>2</sub>·4H<sub>2</sub>O at different molalities (moles of solute per kg of molten Ca(NO<sub>3</sub>)<sub>2</sub>·4H<sub>2</sub>O) and different temperatures. Heats of solution at infinite dilute,  $\Delta H_s^\infty$ , were obtained by linear extrapolation from the plots of  $\Delta H_s$  versus molality, m. The values of  $\Delta H_s^\infty$  are also presented in Tables 10-2 and 10-3.

The literature data on heats of solution at infinite dilution indicate that  $\Delta H_s^\infty$



Table 10-1                      Heats of solution of NaCl in water at 40°C

Run	$W_{\text{NaCl}}$	$W_{\text{H}_2\text{O}}$	$m$	$E$	$\Delta H_{\text{sol}}$
	(g)	(g)	(mol kg <sup>-1</sup> )	(J)	(kJ mol <sup>-1</sup> )
1	0.01310	2.5853	0.0867	0.526	2.599
2	0.01317	2.5784	0.0909	0.5985	2.655
3	0.01341	2.8409	0.0808	0.6072	2.646
4	0.01660	2.7064	0.1050	0.7219	2.541

$W_{\text{NaCl}}$ : mass of solute, NaCl

$W_{\text{H}_2\text{O}}$ : mass of solvent, water

$E$  : energy absorbed during the dissolution of NaCl

Table 10-2                      Heats of solution of NaCl in molten  $\text{Ca}(\text{NO}_3)_2 \cdot 4\text{H}_2\text{O}$

m (mol kg <sup>-1</sup> )	$\Delta H_s$ (kJ mol <sup>-1</sup> )	m (mol kg <sup>-1</sup> )	$\Delta H_s$ (kJ mol <sup>-1</sup> )
T = 327.57 K		T = 337.42 K	
0.0963	7.119	0.0997	8.319
0.0983	7.488	0.2180	8.945
0.1352	7.925	0.2286	8.767
0.1503	7.675	0.2332	9.043
0.2020	8.025		
0.2126	8.195		
0.2207	8.101		
$\Delta H_s^\infty = 6.75 \text{ kJ mol}^{-1}$		$\Delta H_s^\infty = 7.85 \text{ kJ mol}^{-1}$	
T = 348.29 K		T = 358.17 K	
0.1079	9.467	0.0915	10.18
0.1466	9.668	0.1427	10.66
0.1503	9.749	0.1761	10.47
0.1533	9.627	0.2121	10.71
$\Delta H_s^\infty = 8.85 \text{ kJ mol}^{-1}$		$\Delta H_s^\infty = 9.92 \text{ kJ mol}^{-1}$	
T = 368.01 K			
0.1180	11.36		
0.1264	11.40		
0.1552	11.41		
0.1707	11.47		
0.2061	11.54		
$\Delta H_s^\infty = 11.13 \text{ kJ mol}^{-1}$			

$\Delta H_s^\infty$ : heat of solution at infinite dilution

Table 10-3      Heats of solution of  $\text{KNO}_3$  in  $\text{Ca}(\text{NO}_3)_2 \cdot 4\text{H}_2\text{O}$ 

$m$ (mol $\text{kg}^{-1}$ )	$\Delta H$ (kJ $\text{mol}^{-1}$ )	$m$ (mol $\text{kg}^{-1}$ )	$\Delta H$ (kJ $\text{mol}^{-1}$ )
T = 317.72 K		T = 327.62 K	
0.0611	7.037	0.0550	7.934
0.0614	7.033	0.0640	7.867
0.0847	6.992	0.0648	7.802
0.0869	6.953	0.0843	7.723
0.1280	6.947	0.1020	7.625
$\Delta H_s^\infty = 7.11 \text{ kJ mol}^{-1}$		$\Delta H_s^\infty = 8.30 \text{ kJ mol}^{-1}$	
T = 337.43 K		T = 348.31 K	
0.0442	8.989	0.0412	10.14
0.0550	8.794	0.0515	9.917
0.0661	8.545	0.0743	9.414
0.0809	8.372	0.0810	9.262
0.0843	8.264		
$\Delta H_s^\infty = 9.74 \text{ kJ mol}^{-1}$		$\Delta H_s^\infty = 11.06 \text{ kJ mol}^{-1}$	
T = 358.20 K			
0.0550	10.99		
0.0629	10.58		
0.0670	10.58		
0.0797	10.19		
0.1110	9.617		
$\Delta H_s^\infty = 11.93 \text{ kJ mol}^{-1}$			

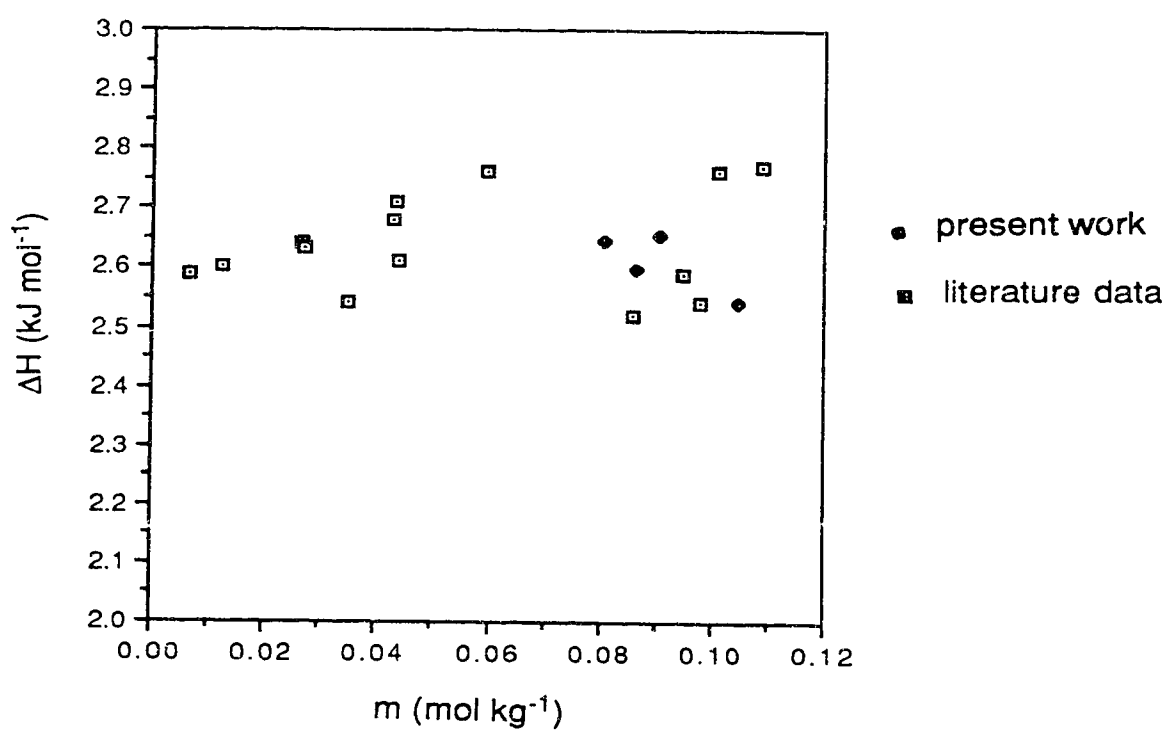


Figure 10-4 Heats of solution of NaCl in  $\text{H}_2\text{O}$  as a function of molality

for NaCl<sup>141-143</sup> and KNO<sub>3</sub><sup>144</sup> are significantly different. For example, at 40 °C  $\Delta H_s^\infty$  for NaCl in H<sub>2</sub>O is 2.015 kJ mol<sup>-1</sup> and  $\Delta H_s^\infty$  for KNO<sub>3</sub> in H<sub>2</sub>O is 33.4 kJ mol<sup>-1</sup>. As the temperature increases  $\Delta H_s^\infty$  for KNO<sub>3</sub> slowly decreases, while  $\Delta H_s^\infty$  for NaCl decreases more rapidly. When the temperature reaches 60°C,  $\Delta H_s^\infty$  for NaCl changes sign, and the dissolution changes from an endothermic to an exothermic.<sup>141-143</sup>

The heats of solution of NaCl and KNO<sub>3</sub> in molten Ca(NO<sub>3</sub>)<sub>2</sub>·4H<sub>2</sub>O, however, are completely different from those in water. The values of the heat of solution for NaCl and KNO<sub>3</sub> in molten Ca(NO<sub>3</sub>)<sub>2</sub>·4H<sub>2</sub>O are similar to each other as can be seen in Table 10-2 and 10-3.

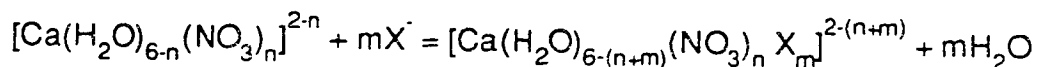
From the determination of association equilibria of cadmium and bromide in concentrated aqueous electrolyte solutions and molten anhydrous salts, Braunstein and his coworkers<sup>111-114</sup> have realized that when the water content was reduced below 4-8 mole of water per mole of salt the solution chemistry of aqueous electrolytes shows marked changes.

Braunstein *et al.*<sup>113</sup> calculated the enthalpies of evaporation of water from aqueous electrolyte solutions of Ca(NO<sub>3</sub>)<sub>2</sub> at different water contents, using the vapor pressures of water for these systems measured by Ewing.<sup>145</sup> They found that the enthalpies of evaporation increased sharply at water concentrations lower than 6-8 mol water per mol salt. Recently, Emons<sup>120</sup> measured the enthalpy of evaporation of water in the system MgCl<sub>2</sub>-H<sub>2</sub>O and found a steep

increase of the evaporation enthalpy starting at the molar ratio of water to  $\text{MgCl}_2$  about seven.

Braunstein *et al.*<sup>113-114</sup> have suggested that the behavior of highly concentrated solutions or molten hydrates approaches that of molten salts. From the studies of transport properties of molten hydrates Angell<sup>108,110</sup> has proposed that aqueous solutions of polyvalent ions might be regarded as molten salts of weak field cations,  $\text{M}(\text{H}_2\text{O})_n^{m+}$ , because the water content is insufficient to form more than a first co-ordination sheath for the cation. Our heats of solution also provide some evidence for this conclusion. We consider molten  $\text{Ca}(\text{NO}_3)_2 \cdot 4\text{H}_2\text{O}$  to behave like a molten salt which consists of  $\text{Ca}(\text{H}_2\text{O})_4^{+2}$  and  $\text{NO}_3^-$  ions.

The solution process may be described by an ion exchange (competition) reaction. When  $\text{NaCl}$  or  $\text{KNO}_3$  was added to molten  $\text{Ca}(\text{NO}_3)_2 \cdot 4\text{H}_2\text{O}$ , the anion interacted with the complex  $\text{Ca}(\text{H}_2\text{O})_4^{+2}$  resulting in an ion exchange between water and anions. This reaction can be formulated as follows:



in which  $\text{X}^-$  represents either  $\text{Cl}^-$  or  $\text{NO}_3^-$ .

The above mentioned water-anion exchange reaction in very concentrated electrolyte solution has been supported by Emons.<sup>120</sup> He used a Raman spectroscopy to obtain the spectra of the  $\text{MgCl}_2 \cdot \text{XH}_2\text{O}$  and  $\text{KCl} \cdot \text{MgCl}_2 \cdot \text{XH}_2\text{O}$  systems. For  $\text{MgCl}_2 \cdot 6\text{H}_2\text{O}$ , he noted a band at  $355 \text{ cm}^{-1}$ , which he attributed to

the  $\text{Mg}(\text{H}_2\text{O})_6^{+2}$  complex. However, when he added 30 to 40 mol % KCl to the hydrates, the  $\text{Mg}(\text{H}_2\text{O})_6^{+2}$  band at  $355\text{ cm}^{-1}$  nearly vanished, which indicated the occurrence of water-chloride ion exchange reactions.

Angell<sup>110</sup> has found that molten  $\text{Ca}(\text{NO}_3)_2 \cdot 4\text{H}_2\text{O}$  can dissolve large amounts of  $\text{KNO}_3$ . The solubility of  $\text{KNO}_3$  in molten  $\text{Ca}(\text{NO}_3)_2 \cdot 4\text{H}_2\text{O}$  is much greater than in  $\text{H}_2\text{O}$ . For example, at  $100^\circ\text{C}$  the saturation solubility of  $\text{KNO}_3$  is about 30 mol% in water but 68 mol% in  $\text{Ca}(\text{NO}_3)_2 \cdot 4\text{H}_2\text{O}$ .<sup>110</sup> This is not surprising after considering the heats of solution. Because the dissolution of a salt in a solvent must be accompanied by a decrease in the Gibbs energy, a lower endothermic enthalpy leads to more decrease of Gibbs energy than higher endothermic enthalpy<sup>11</sup> do and thus leads to a larger solubility. The endothermic enthalpy of solution for  $\text{KNO}_3$  in water is much larger than in  $\text{Ca}(\text{NO}_3)_2 \cdot 4\text{H}_2\text{O}$ . For example, at  $60^\circ\text{C}$   $\Delta H_s^\infty$  in  $\text{H}_2\text{O}$ <sup>144</sup> is  $31.5\text{ kJ mol}^{-1}$  compared to  $9.14\text{ kJ mol}^{-1}$  in  $\text{Ca}(\text{NO}_3)_2 \cdot 4\text{H}_2\text{O}$  (interpolated from experimental data). Therefore,  $\text{KNO}_3$  is more soluble in  $\text{Ca}(\text{NO}_3)_2 \cdot 4\text{H}_2\text{O}$  than in  $\text{H}_2\text{O}$ .

The heats of solution of  $\text{NaCl}$  and  $\text{KNO}_3$  in  $\text{Ca}(\text{NO}_3)_2 \cdot 4\text{H}_2\text{O}$  at infinite dilution at different temperatures are plotted against temperature as shown in Figure 10-5. Silvester and Pitzer<sup>146</sup> proposed that the enthalpy of solution at infinite dilution was a 3rd order polynomial function of temperature. Because we have only five data points, 2nd order polynomial equation is enough for expression of the heat of solution as a function of temperature. Therefore we

fitted 2nd order polynomial equations to the experimental data by the least squares method. The equations obtained are:

for NaCl

$$\Delta H_s^\infty = 5.6131 - 0.0879T + 2.795 \times 10^{-4} T^2 \text{ (kJ mol}^{-1}\text{)} \quad (10-2)$$

and for KNO<sub>3</sub>

$$\Delta H_s^\infty = -103.68 + 0.5493T - 6.321 \times 10^{-4} T^2 \text{ (kJ mol}^{-1}\text{)} \quad (10-3)$$

The temperature coefficient of heat of solution at infinite dilution relates to the heat capacity change for the dissolution process, which can be expressed as

$$\frac{d\Delta H_s^\infty}{dT} = \Delta C_p^\circ \quad (10-4)$$

$$\Delta C_p^\circ = \bar{C}_{p_2}^\infty - C_{p_2}^\circ \quad (10-5)$$

in which  $\bar{C}_{p_2}^\infty$  is the infinite dilution partial molar heat capacity of solute in the solvent  $\text{Ca}(\text{NO}_3)_2 \cdot 4\text{H}_2\text{O}$  and  $C_{p_2}^\circ$  is the heat capacity of pure solid solute.  $\Delta C_p^\circ$  can be obtained by differentiation of Equations (10-2) and (10-3) with respect to T.  $C_{p_2}^\circ$  for solid NaCl and KNO<sub>3</sub> are well-known. Here we use the values for  $C_{p_2}$  reported by Kelley.<sup>147</sup> Therefore we can obtain the partial molar heat capacity of NaCl and KNO<sub>3</sub> in molten  $\text{Ca}(\text{NO}_3)_2 \cdot 4\text{H}_2\text{O}$  using Equation (10-5). Since the  $C_{p_2}^\circ$  was reported as equations by Kelley and  $\Delta C_p^\circ$  obtained from differentiation of two enthalpies of solution (see Equations (10-2) and (10-3)) it is appropriate to obtain  $\bar{C}_{p_2}^\infty$  in terms of an equation. The equations for  $\Delta H_s^\infty$ ,  $\Delta C_p^\circ$



and  $\bar{C}_{p2}^{\infty}$  are summarized in Table 10-4. The partial molar heat capacities of NaCl and KNO<sub>3</sub> in molten Ca(NO<sub>3</sub>)<sub>2</sub>·4H<sub>2</sub>O at any temperature can be calculated from the equations in Table 10-4.

Partial molar heat capacities at other higher concentration are obtained by

$$\bar{C}_{p2} = \bar{C}_{p2}^{\infty} + A_c m_2^{\frac{1}{2}} \quad (10-6)$$

in which  $A_c$  is the slope of Debye-Hückel limiting law.

The values of  $\bar{C}_{p2}^{\infty}$  for NaCl in Ca(NO<sub>3</sub>)<sub>2</sub>·4H<sub>2</sub>O and in H<sub>2</sub>O<sup>141</sup> are considerably different. For example, at 60°C,  $\bar{C}_{p2}^{\infty}$  in Ca(NO<sub>3</sub>)<sub>2</sub>·4H<sub>2</sub>O is equal to 150 J K<sup>-1</sup> mol<sup>-1</sup>, compared to -65 J K<sup>-1</sup> mol<sup>-1</sup> in water.<sup>141</sup>

Table 10-4      Equations for calculating  $\Delta H_s^\infty$ ,  $\Delta C_p^\circ$  and  $\overline{C}_{p2}^\infty$  for  
NaCl and KNO<sub>3</sub> in molten Ca(NO<sub>3</sub>)<sub>2</sub>·4H<sub>2</sub>O

Parameter	Equation
KNO <sub>3</sub>	
$\Delta H_s^\infty$ (J mol <sup>-1</sup> )	$-1.0368 \times 10^5 + 549.3T - 0.6321T^2$
$\Delta C_p^\circ$ (J K <sup>-1</sup> mol <sup>-1</sup> )	$549.3 - 1.264T$
$\overline{C}_{p2}^\infty$ (J K <sup>-1</sup> mol <sup>-1</sup> )	$610.2 - 1.145T$
NaCl	
$\Delta H_s^\infty$ (J mol <sup>-1</sup> )	$5.6131 \times 10^3 - 87.9T + 0.2795T^2$
$\Delta C_p^\circ$ (J K <sup>-1</sup> mol <sup>-1</sup> )	$-87.9 + 0.559T$
$\overline{C}_{p2}^\infty$ (J K <sup>-1</sup> mol <sup>-1</sup> )	$-41.96 + 0.575T$

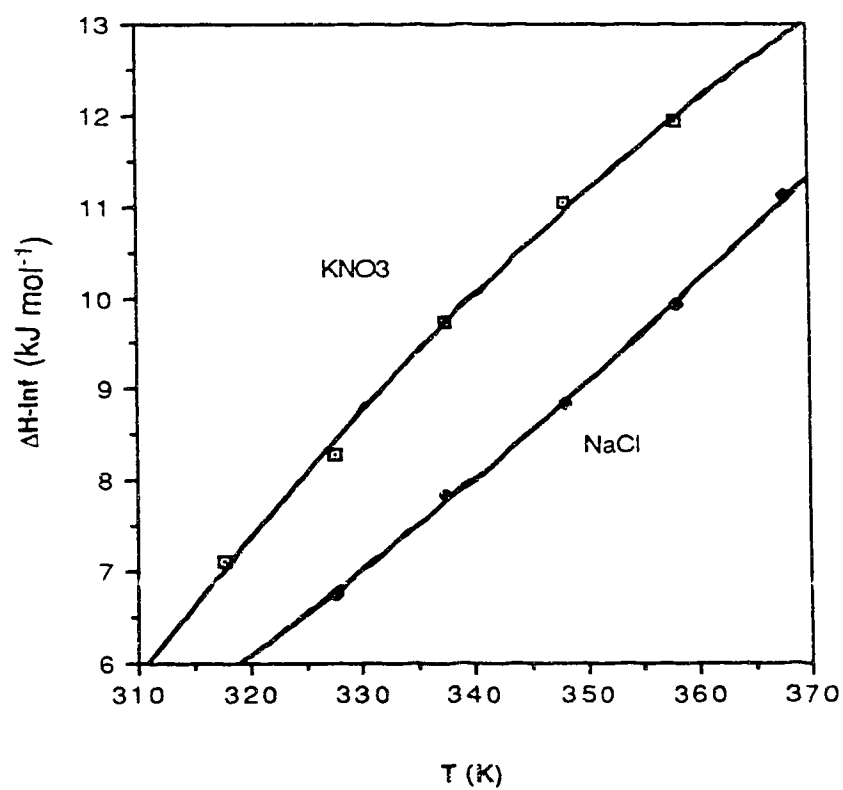


Figure 10-5 Heats of solution at infinite dilution for  $\text{NaCl}$  and  $\text{KNO}_3$  in molten  $\text{Ca}(\text{NO}_3)_2 \cdot 4\text{H}_2\text{O}$  as a function of temperature

## Chapter 11

### Philosophy and Some Conclusions

Thermodynamic measurements are generally of two different kinds, as follows.

One kind of thermodynamic measurement involves experimental work leading toward such equilibrium properties as reversible electrochemical cell potentials, equilibrium constants for chemical reactions, solubilities of gases in liquids (as reported in this thesis), solubilities of solids in liquids, etc. All of these equilibrium results lead to Gibbs energies ( $\Delta G$ ). After such equilibrium results have been obtained at several temperatures or pressures, it is possible to do thermodynamic calculations, all of which involve some mathematical or graphical differentiation, to obtain what are sometimes called "derivative" properties, such as  $\Delta H$ ,  $\Delta C_p$ ,  $\Delta S$ , and  $\Delta V$ . Some calculations of this sort have been described in this thesis.

Another kind of thermodynamic measurement involves experimental work leading to evaluation (without differentiation as mentioned above) of the "derivative" properties. For example, calorimetric measurements (as described in this thesis) can lead to values of  $\Delta H$  (a first derivative of  $\Delta G$  with respect to temperature ) and  $\Delta C_p$  (a second derivative of  $\Delta G$  with respect to temperature); measurements of both kinds are described in this thesis. Measurements of densities or measurements of volumes of known masses of substance can lead

to "partial molar volumes" that are first derivatives of  $\Delta G$  with respect to pressure, as also described in this thesis.

Since all of the quantities that appear in the equations of classical chemical thermodynamics are (at least in principle) measureable, why bother with the equations? Why not just measure directly whatever we want to know?

One answer to the questions above is that some quantities are much easier to measure than are other quantities. It is therefore sometimes desirable to measure the "easy" quantities and then to calculate the "difficult" quantities that we want to know.

Another answer to the questions above is that we can measure some quantities much more accurately than we can measure other quantities. It is sometimes possible to measure quantities "a" and "b" quite accurately and then calculate quantity "c" more accurately than we can measure quantity "c".

Still another answer (and probably the most important answer) to the questions above concerns efficiency, as follows. We do not have and are never likely to have the resources (scientists, time, equipment, lab space, etc.) that are required to measure all of the thermodynamic quantities that are needed for many different purposes in both pure and applied science. But it is possible that we can measure some properties (carefully selected) that will permit us to calculate many other properties. Consider the following example that is pertinent to the research described in this thesis.

There is considerable practical need for information about the solubilities of several gases in several liquids over considerable ranges of temperature and

pressure. All of these solubilities might be measured, but this huge amount of labor is not necessary if we make certain selected measurements and then calculate the other quantities that someone wants to know. Chapters 4 and 5 in this thesis are devoted to accounts of experimental investigations (low pressure) leading to solubilities (expressed as Henry's law constants) of several gases in several liquids. Thermodynamic calculations (all involving mathematical differentiation) permitted evaluation of  $\Delta H^\circ$ ,  $\Delta S^\circ$ , and  $\Delta G^\circ$ , and thence also permit convenient extrapolation to higher and lower temperatures.

The measurements described in Chapters 4 and 5 might have been extended to many different high pressures for each gas in each liquid at each temperature, but there is no need to make all of these measurements. Instead, it was much more efficient to make measurements leading to partial molar volumes of gases dissolved in liquids (as described in Chapter 6) so that these high pressure solubilities can be calculated by way of the Krichevsky-Kasarnovsky equation.

It frequently happens that a particular experimental technique is not applicable to all systems of interest. For example, research described here has shown that the GLC method is not good for obtaining information about such light gases as methane in bitumens. It is therefore potentially very useful to be able to use data for other systems to predict the quantities that we have been unable to measure. An example of this kind of prediction is presented in Chapter 4.

As a cumulative result of the kinds of investigations reported earlier in this

thesis and mentioned in this chapter, we now have reliable and useful data for many (gas + liquid) systems. It has also been shown that the useful and convenient GLC method is not good for certain kinds of investigations, but we have compensated for this limitation by showing that it is possible to make reliable predictions of some of the "missing" data.

As stated earlier in this thesis and as emphasized in this chapter, solubilities of gases and partial molar volumes of gases are directly related to each other. It therefore follows that Chapter 2-6 of this thesis are related to each other in various ways.

Earlier in this chapter the connection between equilibrium properties and "derivative" properties that can be measured calorimetrically has been mentioned. It is because of this connection that the second part of this thesis (Chapters 7-10) has been devoted to an account of calorimetric investigations. Although the specific chemical systems that have been the subject of the present calorimetric investigations are not related to the (gas + liquid) systems described in Chapters 2-6, there is a background connection in terms of the "first kind" and "second kind" of measurements discussed earlier in this chapter.

Because some of the kinds of calorimetry described in this thesis are uncommon and also because the calorimeter used had not yet been thoroughly tested, quite a lot of the present calorimetric research was devoted to working out experimental methods and to determining the limits of accuracy and reliability of these methods and our calorimeter. In addition to this kind of testing and evaluation that is an absolute requirement as a background for good quality

investigations to be carried out in the future, some truly new results have been obtained (see especially Chapters 9 and 10).

Although it is unlikely that the results for water reported in Chapter 8 are sufficiently accurate to make a significant contribution to our present knowledge of this important substance, the methodology described here is applicable to many other systems for which we have nothing comparable to the "steam tables" for water. It is likely that an important extension of the research described here will focus on investigations of the sort described in Chapter 8, but applied to liquids other than water.

Some of the discussion throughout this thesis, including this final chapter, has focussed on the useful applications of chemical thermodynamics. I very much hope that the data (measured and calculated) and the experimental methodologies that have come from this research will be useful in the non-academic world. But it is also important to recognize that there are other components to the kinds of research reported here. For example, the research that I have done was designed to provide me with a breadth and depth of scientific experience. Finally, there is the non-measured matter of beauty and pleasure in science. As just one of many illustrations, I mention the considerable pleasure that came to me while working on the beautiful (to me) equations in Appendix A and in Appendix B.



## References

1. Littlewood, A. B., "Gas Chromatography-Principles, Techniques, and Applications", 2nd ed., Academic Press (1970).
2. Conder, J. and Young, C. L., "Physicochemical Measurements by Gas Chromatography", Wiley, Toronto (1979).
3. Laub, R. J. and Pecsok, R. L., "Physicochemical Applications of Gas Chromatography", John Wiley & Sons, Inc., New York (1978).
4. Purnell, H., "Gas Chromatography", John Wiley & Sons, Inc., New York (1962).
5. Cantwell, F. F., "Principles of Analytical Gas and Liquid Chromatography", Textbook for Dept. of Chem., Univ. of Alberta, (1986).
6. Levy, A., J. Sci. Instrum, 41, 449 (1964).
7. James, A. T. and Martin, A. J. P., Biochem. J., 50, 679 (1952).
8. Littlewood, A. B., Phillips, C. S. G. and Price, D. T., J. Chem. Soc., 1480 (1955).
9. Lewis, G. N. and Randall, M. (revised by Pitzer, K. S. and Brewer, L.), "Thermodynamics", 2nd ed., McGraw-Hill Book Co. Inc., N. Y., (1961).
10. Klotz I. M. and Rosenberg, R. M., "Introduction to Chemical Thermodynamics", 3rd. ed., The Benjamin/Cummings Publishing Company, (1981)

11. Prausnitz, J. M., Lichtenthaler, R. N. and Gomes de Azevedo, E., "Molecular Thermodynamics of Fluid Phase Equilibria", 2nd ed., Prentice-Hall, Inc., Englewood Cliffs, N. J. (1986).
12. Martire, D. E. and Pollara, L. Z., in "Advances in Chromatography" , J. C. Giddings, and R. A. Keller, eds., V.1, Marcel Dekker, Inc., 335 (1965).
13. Martire, D. E., in "Gas Chromatography", Fowler, L., ed., Academic Press, 33 (1964).
14. Parcher, J. F., Weiner, P. H., Hussey, C. L. and Westlake, T. N., J. Chem. Eng. Data, 20, 145 (1975).
15. Martin, R. L., Anal. Chem., 33, 347 (1961).
16. Martire, D. E., Anal. Chem., 38, 244 (1966).
17. Pecsok, R. L., Yllana, A. de, and Abdul-karim, A., Anal. Chem., 36, 452 (1964).
18. Meyer, E. F. and Ellefson, J., J. Chromatography, 249, 239 (1982).
19. Smith, R. J., Haken, J. K. and Wainwright, M. S., J. Chromatography 334, 95 (1985).
20. Smith, R. J., Haken, J. K., Wainwright, M. S. and Madden, B. G., J. Chromatography, 328, 11 (1985).
21. Wainwright, M. S. and Haken, J. K., J. Chromatography, 184, 1 (1980).

22. Wainwright, M. S., Haken, J. K. and Srisukh, D., J. Chromatography, 179, 160 (1979); 188, 246 (1980).
23. Smith, R. J., Haken, J. K. and Wainwright, M. S., J. Chromatography, 147, 65 (1978).
24. Parcher, J. F., Bell, M. L. and Lin, P. J., in "Advances in Chromatography", Giddings, J. C., Grushka, E., Cazes, J. and Brown, P. R., eds., V. 24, Marcel Dekker, 227 (1984).
25. Sharples, W. E. and Vernon, F., J. Chromatography, 161, 83 (1978).
26. Parcher, J. F. and Johnson, D. M., J. Chromatographic Sci., 18, 267 (1980).
27. Ambrus, L., J. Chromatography, 294, 328 (1984).
28. Riedo, F., Fritz, D., Tarja'n, G. and Kovats E., J. Chromatography, 126, 63 (1976).
29. Peterson, M. L. and Hirsch, J., J. Lipid Res., 1, 132 (1959).
30. Hansen, H. L. and Anderson, K., J. Chromatography, 34, 246 (1968).
31. Gold, H. J., Anal. Chem., 34, 174 (1962).
32. Kaiser, R. E., Chromatographia, 7, 251 (1974).
33. Al-Thamir, W. K., Purnell, J. H., Wellington, C. A. and Laub, R. J., J. Chromatography, 173, 388 (1979).

34. Ettre, L. S. *Chromatographia*, 13, 73 (1980).
35. Parcher, J. F. and Sellm, M. I., *Anal. Chem.*, 51 (13), 2154 (1979).
36. Nakahara, T., Chappellear, P. S. and Kobayashi, R., *Ind. Eng. Chem. Fundam.*, 16, 220 (1977).
37. Lin, P. J. and Parcher, J. F., *J. Chromatographic Sci.*, 20, 33 (1982).
38. Harned, H. S., and Robinson, R. A., *Trans. Faraday Soc.*, 36, 973 (1940).
39. Clarke, E. C. W. and Glew, D. N., *Trans. Faraday Soc.*, 62, 539 (1966).
40. Feates, F. S., and Ives, D. J. G., *J. Chem. Soc.*, 2798 (1956).
41. Ives, D. J. G., and Marsden, P. D., *J. Chem. Soc.*, 649 (1965).
42. Ives, D. J. G., and Moseley, P. G. N., *J. Chem. Soc. Faraday Trans. I*, 72, 1132 (1976).
43. Pitzer, K. S., *J. Am. Chem. Soc.*, 59, 2365 (1937).
44. Everett, D. H. and Wynne-Jones, W. F. K., *Trans. Faraday Soc.*, 35, 1380 (1939).
45. Ramette, G. N., *J. Chem. Educ.*, 54, 280 (1977).
46. Bolton, P. D., *J. Chem. Educ.*, 47, 638 (1970).
47. Timimi, B. A., *Electrochim. Acta*, 19, 149 (1974).

48. Halliwell, H. F. and Strong, L. E., *J. Phys. Chem.*, 89, 4137 (1985).
49. Meyer, E. F. and Baiocchi, F. A., *Anal. Chem.*, 49, 1029 (1977).
50. Meyer, E. F. and Baiocchi, F. A., *J. Chem. Thermodynamics*, 9, 1051 (1977).
51. Ohe, S., "Computer Aided Data Book of Vapor Pressure", Data Book Publishing Company, Tokyo, Japan, 1976.
52. Smith, B. D. and Srivastava, R., "Thermodynamic Data for Pure Compounds", *Physical Sciences Data* 25, Part A and Part B. Elsevier, New York, 1986.
53. Dymond, J. H. and Smith, E. B., "The Virial Coefficients of Pure Gases and Mixtures", Clarendon Press, Oxford, 1980.
54. Lambert, J. D., Roberts, G. A. H., Rowlinson, J. S., and Wilkinson, V. J., *Proc. Roy. Soc.*, A196, 113 (1949).
55. Guggenheim, E. A., and McGlashan, M. L., *Proc. Roy. Soc.*, A206, 448 (1951).
56. Lu, B. C.-Y., Chung, W. K., Adachi, Y. and Boublik, T., *AOSTRA J. Res.*, 2, 139 (1986).
57. Bottomley, G. A., Smith, J. F., Schutte, R. P., and Hepler, L. G., *AOSTRA J. Res.*, 5, 383 (1989).
58. Fu, C.-T., Puttagunta, V. R. and Vilcsak, G., *AOSTRA J. Res.*, 2, 73 (1985).

59. Svrcek, W. Y. and Mehrotra, A. K., J. Can. Petrol. Tech., 21 (4), 31 (1982).
60. Mehrotra, A. K., Svrcek, W. Y., Fu, C.-T., and Puttagunta, V. R., AOSTRA J. Res., 4, 237 (1988).
61. Meyer, E. F. and Baiocchi, F. A., J. Am. Chem. Soc., 99, 6206 (1977).
62. Meyer, E. F., Stec, K. S. and Hotz, R. D., J. Phys. Chem., 77, 2140 (1973).
63. Meyer, E. F. and Baiocchi, F. A., J. Chem. Thermodynamics, 10, 823 (1978)
64. Hoare, M. R. and Purnell, J. H., Trans. Faraday Soc., 52, 222 (1956).
65. Flory, P.J., J. Chem. Phys., 9, 660 (1941).
66. Flory, P.J., J. Chem. Phys., 10, 51 (1942).
67. Huggins, M. L., Ann. N. Y. Acad. Sci., 43, 1 (1942).
68. Guggenheim, E.A., "Mixtures", Chapters X and XI, Oxford University Press, Oxford, (1952)
69. Everett, D. H. and Munn, R. J., Trans. Faraday Soc., 60, 1951 (1964).
70. Hildebrand, J. H. and Scott, R. L., "Regular Solutions", Prentice-Hall, Inc., Englewood Cliffs, New Jersey, (1962).
71. Scatchard, G., Chem. Rev., 8, 321 (1931).

72. Martire, D. E., *Anal. Chem.*, 33, 1143 (1961).
73. Astarita, G., Savage, D. W. and Bisio, A., "Gas Treating With Chemical Solvents", John Wiley & Sons, New York, 1983.
74. Lenoir, J. Y., Renault, P. and Renon, H., *J. Chem. Eng. Data*, 16, 340 (1971).
75. Rivas, O. R. and Prausnitz, J. M., *Ind. Eng. Chem. Fundam.*, 18, 289 (1979).
76. Isaacs, E. E., Otto, F. D. and Mather, A. E., *Can. J. Chem. Eng.*, 55, 751 (1977).
77. Rivas, O. R. and Prausnitz, J. M., *AIChE. J.*, 25, 975 (1979).
78. Sanza, G. J., Klinzing, G. E. and Waiker, R. J., *Can. J. Chem. Eng.*, 62, 565 (1984).
79. Murrieta-Guevara, F., Romero-Martinez, A. and Trejo, J. L., *Fluid Phase Equil.*, 44, 105 (1988).
80. Roberts, B. E. and Mather, A. E., *Can. J. Chem. Eng.*, 67, 519 (1988).
81. Jou, F.-Y., Deshmukh, R. D., Otto, F. D. and Mather, A. E., *J. Chem. Soc. Faraday, Trans 1*, 85, 2675 (1989).
82. Mather, A. E., Unpublished data on solubilities of CO<sub>2</sub> and H<sub>2</sub>S in Selexol.

83. Krichevsky, I. R., and Kasarnovsky, J. S., J. Amer. Chem. Soc., 57, 2168 (1935).
84. Battino, R. and Clever, H. L., Chem. Rev., 66, 395 (1966).
85. Clever, H. L., and Battino, R., In "Solutions and Solubilities", Part 1. Techniques of Chemistry, Vol. viii, Dack, M. R. J., ed., Wiley, New York, 379 (1976).
86. Handa, Y. P. and Benson, G. C., Fluid Phase Equil., 8, 161 (1982).
87. Handa, Y. P., D'arcy, P. J. and Benson, G. C., Fluid Phase Equil., 8, 181 (1982).
88. Horiuti, J., Sci. Pap., Inst. Phys. Chem. Res. (Tokyo), 17, 125 (1931).
89. Wiebe, R., and V. L. Gaddy, J. Am. Chem. Soc., 59, 1984 (1937).
90. Benoit, R. L. and Milanova, E., Can. J. Chem., 57, 1319 (1979).
91. Calvet, E., and Part, H. "Recent Progress in Microcalorimetry". Skinner, H. A.: ed., Pergamon Press, New York (1963).
92. Gravelle, P. C., Adv. Catal., 22, 191 (1972).
93. Handa, Y. P., Hawkins, R. E., and Murray, J. J., J. Chem. Thermodynamics, 16, 623 (1984).
94. Cox, J. D.: ed., "Pure Appl. Chem." 40, 399 (1974).
95. Freeman, R. D.: ed., Bull. Chem. Thermodynamics, 23, 533 (1980).



96. Mraw, S. C., and Naas, D. F., J. Chem. Thermodynamics, 11, 567 (1979).
97. Ditmars, D. A., Ishihara, S., Chang, S. S. and Bernstein, G., J. Res. National Bur. Stds., 87, 159 (1982).
98. Ginnings, D. C., Furukawa, G. T., J. Am. Chem. Soc., 75, 522 (1953).
99. Andrews, J. T. S. and Norton, P. A., J. Chem. Thermodynamics, 10, 949 (1978).
100. Inaba, A., J. Chem. Thermodynamics, 15, 1137 (1983).
101. Eucken, A. and Eigen, M., Zeitschrift fur Electrochemie und Angewandte Physikalische Chemie, 55, 343 (1954).
102. Osborne, N. S., and Van Dusen, M. S., Bull. Nat. Bur. Stds., 14, 397 (1918).
103. Hoge, H. J., J. Res. Nat. Bur. Stds. 36, 111 (1946).
104. Steele, W. V., Chirico, R. D., Knipmeyer, S. E. and Smith, N. K., NIPER-395, U. S. Dept. of Energy (1989)
105. Haar, L., Gallagher, J. S. and Kell, G. S., "NBS/NRC Steam Tables-Thermodynamic and Transport Properties and Computer Programs for Vapor and Liquid States of Water in SI Units", Hemisphere Publishing Corporation (1984).
106. Wexler, A., Hyland, R. and Stewart, R., "Thermodynamic Properties of Dry Air, Moist Air and Water and SI Psychrometric Charts", American Society of Heating, Refrigerating and Air-Conditioning Engineers, Inc., 1986

107. Kirillin, V. A., ed., "Heavy Water—Thermophysical Properties", Israel Program for Scientific Translation (1971).
108. Moynihan, C. T., J. Chem. Educ., 44, 531 (1967).
109. Angell, C. A., and Tucker, J. C., J. Phys. Chem., 78, 278 (1974)
110. Angell, C. A., J. Electrochem. Soc., 112, 1224 (1965).
111. Braunstein, J., J. Phys. Chem., 71, 3402 (1967).
112. a: Braunstein, J. and Braunstein, H., Chem. Comm. 565, (1971)  
b: Braunstein, J. and Braunstein, H., Inorg. Chem., 8, 1558 (1969).
113. Braunstein, H., Braunstein, J., and Hardesty, P. T., J. Phys. Chem. 77, 1907 (1973).
114. Braunstein, H., Braunstein, J., Minano, A. S. and Hagman, R. E., Inorg, Chem. 12, 1407 (1973).
115. Blander, M., J. Chem. Phys., 34, 432 (1961)
116. Angell, C. A., and Moynihan, C. T., in "Molten Salts", Mamantov, G., ed., Marcel Dekker, New York, (1969)
117. Claes, P. and Glibert, J., in "Ionic Liquids", Inman, D. and Lovering, D. G., eds., Plenum Press, N. Y. (1981)
118. Combes, R. in "Ionic Liquids", Inman, D. and Lovering, D. G., eds., Plenum Press, N. Y. (1981)

119. Lovering, D. G. and Oblath, R. M., in "Ionic Liquids", Inman, D. and Lovering, D. G., eds., Plenum Press, N. Y., (1981)
120. Emons, H.-H., *Electrochimica Acta*, 33, 1243 (1988).
121. Emons, H.-H., Voigt, W. and Wollny, F.-W., *Z. Phys. Chem.*, 267, 1 (1986).
122. Guion, J., Sauzade, J. D., and Laugt, M., *Thermochimica Acta*, 67, 167 (1983)
123. Furbo, S. and Svendsen, S., Thermal Insulation Laboratory Report, Den Polytekniske Laereanstalt, Copenhagen, 1977 (cited in reference 122)
124. Chevalier, J. L. and Sallé, H., cited in reference 122
125. Telkes, M., Phase Change Thermal Storage, Monegon Ltd. Reprint, Gaithersburg, MD, 1980
126. Dean, J. A., ed., "Lange's Handbook of Chemistry", McGraw-Hill, N. Y., 12th ed., (1979)
127. Pillai, K. K. and Brinkworth, G. J., *Appl. Energy*, 2, 205 (1976).
128. Weast, R. C., ed., "CRC Handbook of Chemistry and Physics", CRC Press Inc., 58th ed., 1978
129. Lorsch, H. G., Kauffman, K. N. and Denton, J. C., *Energy Convers.*, 15, 1 (1975).
130. Lane, G. A. et. al., Cited in reference 122

131. Cubicciotti, D. and Eding, H., J. Chem. Phys., 40, 978 (1964).
132. Gibbs, J. H. and Dimarzio, E. A., J. Chem. Phys., 28, 373 (1958).
133. Cohen, M. H. and Turnbull, D., J. Chem. Phys., 31, 1164 (1959).
134. Adam, G. and Gibbs, J. H., J. Chem. Phys., 43, 139 (1965).
135. Moynihan, C. T., Balitactac, N., Boone, L., and Litovitz, T. A., J. Chem. Phys., 55, 3013 (1971).
136. Angell, C. A., J. Phys. Chem., 68, 1917 (1964).
137. Angell, C. A. and Sichina, W., Annals of the New York Academy of Sciences, 279, 53 (1976).
138. Angell, C. A., J. Phys. Chem., 69, 2137 (1965).
139. Moynihan, C. T., J. Phys. Chem., 70, 3399 (1966).
140. Angell, C. A., Sare, E. J. and Bressel, R. D., J. Phys. Chem., 71, 2759 (1967).
141. Criss, C. M. and Cobble, J. W., J. Amer. Chem. Soc., 83, 3223 (1961)
142. Sanahuja, A. and Cesari, E., J. Chem. Thermodynamics, 17, 823 (1985)
143. Clarke, E. C. W. and Glew, D. N., J. Phys. Chem. Ref. Data, 14, 489 (1985)

144. Taniewska-Osinska, S. and Palecz B., *Acta Univ. Lodziensis. Folia Chimica*, 4, 79 (1985)
145. Ewing, W. W., *J. Amer. Chem. Soc.*, 49, 1963 (1927)
146. Silvester, L. F., and Pitzer, K. S., *J. Phys. Chem.*, 81, 1822 (1977)
147. Kelley, K. K., "Contributions to the Data on Theoretical Metallurgy XIII. High Temperature Heat-Content, Heat Capacity, and Entropy Data for the Elements and Inorganic Compounds", U. S. Bureau of Mines, Bulletin 584 (1960)

## Appendix A

### Derivation of Relationship between Saturation Two Phase

#### Heat Capacity and Heat Capacity of Saturated Liquid

Consider a mass of liquid,  $M$ , placed in a closed cell with a volume  $V_o$  at initial temperature,  $T_o$ . The liquid is defined as being in equilibrium with its vapor phase. The entropy of the saturated liquid per unit mass is  $S_L$  and the entropy of the saturated vapor per unit mass is  $S_g$ . The total entropy of the system,  $S$ , at temperature  $T_o$  is defined by

$$S = M_L S_L + M_g S_g \quad (A-1)$$

$$= M S_L + M_g (S_g - S_L) \quad (A-1')$$

in which  $M = M_L + M_g$ ,  $M_L$  is the mass of liquid and  $M_g$  is the mass of vapor in the cell, and  $S_g - S_L$  is the entropy of vaporization per unit mass that is given by the following equation:

$$S_g - S_L = \Delta S_{\text{vap}} = \Delta H_{\text{vap}} / T_o \quad (A-2)$$

Substitution of equation (A-2) in equation (A-1') gives

$$S = M S_L + (M_g \Delta H_{\text{vap}} / T_o) \quad (A-3)$$

The second term on the right side of equation (A-3) represents the difference between the entropy of the real liquid plus vapor system and the liquid system without a vapor phase.<sup>103</sup> We redefine this term as  $S'$  so that

$$S = M S_L + S' \quad (A-4)$$

Differentiation of equation (A-4) with respect to T yields

$$dS / dT = M(dS_L / dT) + dS' / dT \quad (A-5)$$

For a reversible absorption of heat  $\delta Q$  with the temperature change of  $dT$ , then the entropy change of the system is

$$dS = \delta Q / T = MC_{II} dT / T \quad (A-6)$$

where  $C_{II}$  is the measured heat capacity per unit mass of the two phase system.

Similarly,

$$dS_L = C_{SL} dT / T \quad (A-6')$$

in which  $C_{SL}$  is the heat capacity per unit mass of saturated liquid. Combination of Equation (A-5) with Equations (A-6) and (A-6') leads to

$$C_{II} = C_{SL} + \frac{T}{M} \frac{dS'}{dT} \quad (A-7)$$

The total volume,  $V$ , of the two phase system is expressed by

$$V = M_L V_L + M_g V_g \quad (A-8)$$

$$= M V_L + M_g (V_g - V_L) \quad (A-8')$$

in which  $V_L$  and  $V_g$  are the specific volumes of the liquid and the vapor, respectively. Rearrangement of equation (A-8') leads us to

$$M_g = \frac{V - M V_L}{V_g - V_L} \quad (A-9)$$

which can be incorporated into the definition of  $S'$  to obtain

$$S' = \frac{V - M V_L}{V_g - V_L} \frac{\Delta H_{vap}}{T_o} \quad (A-10)$$

Combining Equation (A-10) with the Clapeyron equation

$$\frac{dP}{dT} = \frac{\Delta H_{\text{vap}}}{T(V_g - V_L)} \quad (\text{A-11})$$

gives Equation (A-12):

$$S' = \left(\frac{dP}{dT}\right)(V - MV_L) \quad (\text{A-12})$$

Further differentiation of Equation (A-12) with respect to T gives

$$\frac{dS'}{dT} = \left(\frac{d^2P}{dT^2}\right)(V - MV_L) + \left(\frac{dP}{dT}\right)\left[\left(\frac{dV}{dT}\right) - M\left(\frac{dV_L}{dT}\right)\right] \quad (\text{A-13})$$

Substitution of Equation (A-13) into Equation (A-7) leads to

$$C_{II} = C_{SL} + T\left(\frac{d^2P}{dT^2}\right)\left(\frac{V}{M} - V_L\right) + T\left(\frac{dP}{dT}\right)\left[\left(\frac{dV}{dT}\right)\frac{1}{M} - \left(\frac{dV_L}{dT}\right)\right] \quad (\text{A-14})$$

Rearrangement of Equation (A-14) leads to the final equation for calculation of specific heat capacity of saturated liquid,  $C_{SL}$ :

$$C_{SL} = C_{II} + \left(\frac{dP}{dT}\right)\left[T\left(\frac{dV_L}{dT}\right) - \frac{T}{M}\left(\frac{dV}{dT}\right)\right] + \left(\frac{d^2T}{dT^2}\right)\left[V_L T - \frac{VT}{M}\right] \quad (\text{A-15})$$

in this equation  $dp/dT$  and  $d^2p/dT^2$  are the first and second derivatives of vapor pressure with respect to temperature; both terms can be obtained by differentiation of an empirical  $P \sim T$  equation that is obtained by regression of experimental data on vapor pressures. The term  $dV_L/dT$  is the derivative of the specific volume of the liquid with respect to temperature and can be calculated from density values at different temperatures;  $dV/dT$  represents the thermal expansion of the cell. This last quantity can be derived using the linear expansion coefficient of the material from which the experimental cells are



made. The volume of a cell at a temperature  $T_o$  is defined as  $V_o$  and the linear expansion coefficient of the material is  $\epsilon$  so that the volume of the cylinder cell at a new temperature  $T$  is given by

$$V = V_o[1 + \epsilon (T - T_o)]^3 \quad (\text{A-16})$$

Hence, the expansibility of the cell is calculated as

$$\frac{dV}{dT} = 3V_o\epsilon [1 + \epsilon (T - T_o)]^2 \quad (\text{A-17})$$

Equation (A-15) relates the specific heat of saturated liquid to the measured heat capacity of the two phase equilibrium system and other experimental parameters such as  $P$ ,  $V$ ,  $T$ , etc. When the vapor pressures and specific volumes of the liquid over a temperature range are available, the heat capacity of the saturated liquid can be obtained by applying Equation (A-15) to calorimetric values of  $C_{II}$ .

## Appendix B

### Derivation of Relationship between Heat Capacity of Saturated Liquid and Constant Pressure Heat Capacity

Consider a liquid in equilibrium with its vapor, all in a closed system. When the liquid reversibly absorbs a quantity of heat  $\delta Q$  which leads to the temperature change  $dT$ ,  $\delta Q$  can be expressed by the first law as

$$\delta Q = dE + PdV \quad (B-1)$$

We also have

$$dE = dH - PdV - VdP \quad (B-2)$$

Combining (B-1) and (B-2) gives

$$\delta Q = dH - VdP \quad (B-3)$$

We consider  $H$  as a function of  $P$  and  $T$  and write

$$dH = \left(\frac{\partial H}{\partial T}\right)_P dT + \left(\frac{\partial H}{\partial P}\right)_T dP \quad (B-4)$$

This expression for  $dH$  is substituted in Equation (B-3) to give

$$\delta Q = \left(\frac{\partial H}{\partial T}\right)_P dT + \left(\frac{\partial H}{\partial P}\right)_T dP - VdP \quad (B-5)$$

Combining a basic thermodynamic equation

$$dH = TdS + VdP \quad (B-6)$$

with a Maxwell relation

$$\left(\frac{\partial S}{\partial P}\right)_T = -\left(\frac{\partial V}{\partial T}\right)_P \quad (B-7)$$

gives

$$\left(\frac{\partial H}{\partial P}\right)_T = -T\left(\frac{\partial V}{\partial T}\right)_P + V \quad (\text{B-8})$$

which is substituted in equation (B-5) to give

$$\delta Q = \left(\frac{\partial H}{\partial T}\right)_P dT - T\left(\frac{\partial V}{\partial T}\right)_P dP \quad (\text{B-9})$$

Therefore, we obtain

$$\frac{\delta Q}{dT} = \left(\frac{\partial H}{\partial T}\right)_P - T\left(\frac{\partial V}{\partial T}\right)_P \left(\frac{dP}{dT}\right) \quad (\text{B-10})$$

In Equation (B-10), the term  $\delta Q/dT$  represents the heat capacity of saturated liquid  $C_{SL}$  and  $(\partial H/\partial T)_P$  is defined as heat capacity of liquid at constant pressure,

$C_p$ . Therefore Equation (B-10) gives the desired equation

$$C_{SL} = C_p - T\left(\frac{\partial V}{\partial T}\right)_P \left(\frac{dP}{dT}\right) \quad (\text{B-11})$$